DISORDER AT FIRST-ORDER CLASSICAL AND QUANTUM PHASE TRANSITIONS

by

AHMED KHALIL IBRAHIM

A DISSERTATION

Presented to the Graduate Faculty of the

MISSOURI UNIVERSITY OF SCIENCE AND TECHNOLOGY

In Partial Fulfillment of the Requirements for the Degree

DOCTOR OF PHILOSOPHY

in

PHYSICS

2018

Approved by

Dr. Thomas Vojta, Advisor
Dr. Gerald Wilemski
Dr. Paul E. Parris
Dr. Aleksandr Chernatynskiy
Dr. José A. Hoyos

PUBLICATION DISSERTATION OPTION

This dissertation has been prepared in the form of four papers:

Paper I, Pages 35–64, has been published as *Enhanced rare-region effects in the contact process with long-range correlated disorder*, published in Physical Review E 90, 042132 (2014) with Hatem Barghathi and Thomas Vojta.

Paper II, Pages 65–81, has been published as *Emerging critical behavior at a first-order phase transition rounded by disorder*, published in Fortschritte der Physik 65, 1600018 (2017) with Thomas Vojta.

Paper III, Pages 82–106, has been published as *Monte Carlo simulations of the disordered three-color quantum Ashkin-Teller chain*, published in Physical Review B 95, 054403 (2017) with Thomas Vojta.

Paper IV, Pages 107–127, is a manuscript ready to be published as *Numerical investigation of a disordered superconductor-metal quantum phase transition* (2018) with Thomas Vojta.

In addition, the dissertation contains an introductory section (Sec. 1) and a brief summary (Sec. 2).

ABSTRACT

This dissertation studies the effects of quenched disorder on classical, quantum and nonequilibrium phase transitions. After a short introduction which covers the basic concepts of phase transitions, finite-size scaling and random disorder, the dissertation focuses on four separate but related projects. First, we investigate the influence of quenched disorder with long-range spatial correlations on the nonequilibrium phase transitions in the contact process. We show that the long-range correlations increase the probability to find rare atypical regions in the sample. This leads to enhanced Griffiths singularities and changes the universality class of the transition.

Project 2 and 3 focus on disorder at first-order phase transitions. In project 2, we analyze the phase transitions of a classical Ashkin-Teller magnet. We demonstrate that the first-order classical phase transition is destroyed by disorder, and the resulting continuous transition belongs to the clean two-dimensional Ising universality class with logarithmic corrections.

Project 3 investigates the fate of the first-order quantum phase transition in the quantum Ashkin-Teller model by large-scale Monte Carlo simulations. We find that disorder rounds the first-order quantum phase transition just as in the classical case. The resulting critical behavior depends on the strength of the inter-color coupling in the quantum Ashkin-Teller model. This leads to two different regimes, the weak and strong coupling regimes, both of which feature infinite-randomness critical behavior but in different universality classes.

Finally, we study the quantum phase transition of a disordered nanowire from superconductor to metallic behavior. We show that the critical behavior is of infinite-random type and belongs to the random transverse-field Ising universality class as predicted by strong disorder renormalization group results.

ACKNOWLEDGMENTS

First of all, I would like to express my deepest thanks and gratitude to my advisor Dr. Thomas Vojta, for his patience and dedication in supporting and guiding me throughout the PhD study period and writing my dissertation. I believe this work would not have been possible without his assistance and support. Thank you, Dr. Vojta.

I am greatly indebted to all my advisory committee members, Dr. Gerald Wilemski, Dr. Paul Parris, Dr. Aleksandr Chernatynskiy, and Dr. José A. Hoyos, for their valuable discussions and accessibility.

I would like to thank our former chairman, Dr. George D. Waddill, our graduate coordinator, Dr. Jerry Peacher, and also the staff in the Physics Department, Pamela J. Crabtree, Janice Gargus, Russell L. Summers, Ronald Woody, and Andy Stubbs, for their help. I am very thankful to the Higher Committee for Education Development (HCED) in Iraq for granting me a PhD scholarship.

I would like especially to give my thanks to my friend, Dr. Hatem Barghathi. Thank you for your help and support.

A special thanks to my family, my parents, my brothers, and my sister. Thank you for your love, support, and encouragement.

Finally, I would like to express my gratitude to my beloved wife, Raghdaa "Um Raneem", and my wonderful daughters, Raneem, Rafeef, and Taleen. Thank you, for all your patience, care, and support.

TABLE OF CONTENTS

Page

LIST OF ILLUSTRATIONS

Figure Page

SECTION

PAPER I

LIST OF TABLES

SECTION

1. INTRODUCTION

1.1. THERMAL AND QUANTUM PHASE TRANSITIONS

What is a phase? A phase is a state of matter whose properties are uniform in space (at a macroscopic level) and time-independent. Moreover, its qualitative characteristics do not change upon trivial (infinitesimal) changes of external parameters such as pressure, temperature, magnetic field, and chemical composition. Simple examples of phases are the three phases of water: solid, liquid and gas. Which phase (solid, liquid or gas) water exists in depends on the values of the external (control) parameters (pressure and temperature) as shown in the phase diagram in Fig. 1.1. The lines separating unique phases are called phase boundaries. Crossing one of these lines, i.e., changing from one phase to another is called a *phase transition*.

A phase transition is therefore a qualitative change in the state of a system in response to changes of one or more of the control parameters of the system. In thermodynamic equilibrium systems, it corresponds to a nonanalyticity of the free energy as function of the control parameters. Phase transitions can be divided into two different kinds: first-order and continuous (second-order) transitions. In Fig. 1.1, when tuning temperature and/or pressure, the transitions between the various phases of water involve phase coexistence. This means that the two distinct phases coexist at the phase boundary. Such transitions generally involve absorbtion or release of a nonzero amount of energy, called the *latent heat*, that is necessary to transform one phase into the other. Transitions with phase coexistence and latent heat are called first-order (discontinuous) phase transitions. The transitions of water are all of first-order, except for one single point, the so-called *critical*

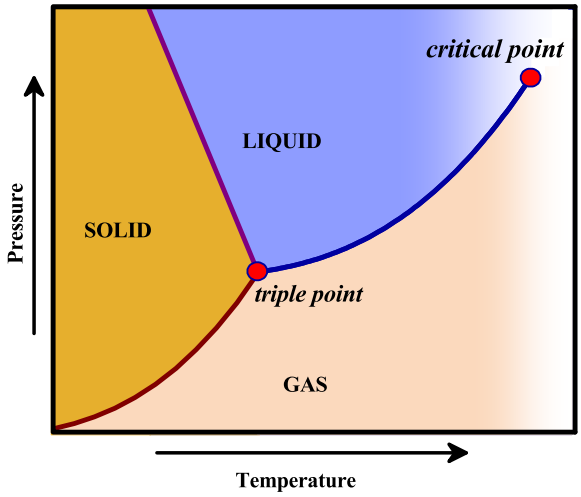

Fig. 1.1. Schematic phase diagram of water. The solid lines indicate first-order phase transitions. The gas-liquid phase boundary ends in a critical point at which the phase transition is continuous. The intersection of three lines is referred to as the triple point at which all three phases coexist.

point. At this point, the boundary between the gas and liquid phases ends and the gas and liquid phases become indistinguishable. Transitions occurring at such a critical point are called continuous (second-order) phase transitions; they do not display phase coexistence or latent heat [1].

1.1.1. Landau Theory of Phase Transitions. One of the earliest theories developed to understand and describe phase transformations is Landau theory. Landau [2, 3, 4, 5] suggested a series of postulates to approximate the free energy F_L of a system. He proposed that the free energy can be described as a function of the *order parameter*, which is a macroscopic thermodynamic observable that has a nonzero value in one phase (the ordered phase) and vanishes in the other phase (the disordered phase). For example, for the ferromagnetic phase transition, the order parameter is the total magnetization m, which has a non-zero value in the ferromagnetic phase (ordered phase) and is zero in the paramagnetic phase (disordered phase), as shown in Fig. 1.2.

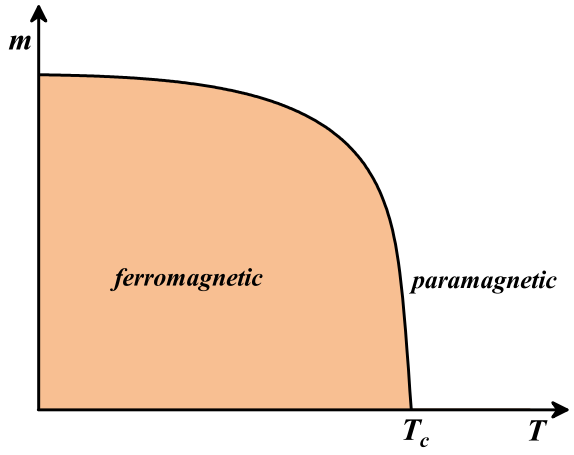

Fig. 1.2. Schematic of magnetization m vs. temperature T at a ferromagnetic phase transition. If the temperature T is below the critical temperature T_c, the substance has a finite (non-zero) value of the magnetization m (ferromagnetic phase). When $T > T_c$, then the magnetization m vanishes (paramagnetic phase).

According to Landau's postulate, the free energy F_L close to the transition can be expanded as a power series of the order parameter m

$$F_L(m) = F_L(0) - hm + rm^2 + km^3 + um^4 + O(m^5), \tag{1.1}$$

where h is the external field. The values of the coefficients r, k, and u depend only on the external parameters (pressure, temperature, etc.), but not on the order parameter m itself. The correct physical value of the order parameter m can be obtained by minimizing the free energy. Landau theory can describe both first-order and continuous transitions, based on the values of the coefficients. If the external field vanishes ($h = 0$) and $k = 0$ as well as $u > 0$, the system undergoes a continuous phase transition. Fig. 1.3 shows the free energy as a function of m for several values of the coefficient r. For $r < 0$, the free energy has two minima which are located at (ignoring high-order terms)

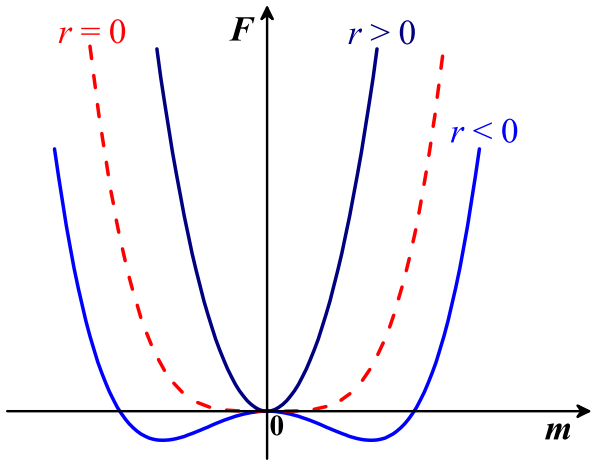

Fig. 1.3. Schematic of the Landau free energy F_L as a function of the order parameter m for various value of r.

$$m = \pm\sqrt{\frac{-r}{2u}}, \tag{1.2}$$

putting the system into the ferromagnetic (ordered) phase (i.e., $m \neq 0$). If $r > 0$, the minimum of the free energy is at $m = 0$, i.e., the system is in the paramagnetic (disordered) phase.

The phase transition between these phases occurs at $r = 0$. Consequently, r can be considered as a measure of the distance from the transition point. Because the order parameter m in Eq. (1.2) is a continuous function of r, the transition is a continuous one. The critical exponent β of the order parameter of a phase transition is generally defined as

$$m \sim (-r)^{\beta}\,. \tag{1.3}$$

According to Eq. (1.2), Landau theory predicts the value $\beta = \frac{1}{2}$ identical to the value in simple mean-field theories [6, 7]. Other exponents can be found analogously and also take mean-field values, as presented in Table 1.1. If $k \neq 0$, Landau theory characterizes a first-order transition, where the order parameter m changes suddenly (discontinuously) from $m = 0$ to a non-zero m at the transition point.

In Landau theory, the fluctuations of the order parameter about its mean are neglected. Is this justified close to the critical point? In general, fluctuations of the order parameter increase with decreasing dimensionality d of the system. Thus, the fluctuations lead to two different critical dimensionalities, the upper (d_c^+) and lower (d_c^-) critical dimensions. Landau theory is valid for high dimensions, i.e., $d \geq d_c^+$. Here the fluctuations are insignificant, and the critical exponents become independent of d and take their mean-field values. However, Landau theory breaks down below d_c^+. For $d_c^+ > d > d_c^-$, the fluctuations can change the critical behavior of the phase transition from Landau's predictions, but the phase transition itself survives. If $d \leq d_c^-$, the fluctuations become extremely strong, and therefore destroy the phase transition.

The failure of Landau theory below d_c^+ due to the fluctuations of order parameter can be overcome by writing the partition function as a path integral

$$Z = \int D[\phi(\vec{x})] e^{-F_{LGW}}, \tag{1.4}$$

Table 1.1. Critical exponents in Landau theory

	exponent	definition	value
Specific heat	α	$C \propto \lvert r\rvert^{-\alpha}$	$\alpha = 0$
Susceptibility	γ	$\chi \propto \lvert r\rvert^{-\gamma}$	$\gamma = 1$
Order parameter	β	$m \propto (-r)^{\beta}$	$\beta = \frac{1}{2}$
Critical isotherm	δ	$h \propto \lvert m\rvert^{\delta} sgn(m)$	$\delta = 3$
Correlation length	ν	$\xi \propto \lvert r\rvert^{-\nu}$	$\nu = \frac{1}{2}$
Correlation function	η	$G(x) \propto \lvert x\rvert^{-d+2-\eta}$	$\eta = 0$

where F_{LGW} is the Landau-Ginzburg-Wilson free energy which is a functional of the fluctuating field $\phi(\vec{x})$

$$F_{LGW}[(\phi(\vec{x})] = \int d^d\vec{x}\{-h\phi(\vec{x}) + r\phi^2(\vec{x}) + k\phi^3(\vec{x}) + u\phi^4(\vec{x}) + [\nabla\phi(\vec{x})]^2\}\,. \tag{1.5}$$

The average $\langle\phi(\vec{x})\rangle$ equals the order parameter m

$$m = \langle\phi(\vec{x})\rangle = \frac{1}{Z}\int D[\varphi(\vec{x})]\varphi(\vec{x})e^{-F_{LGW}}\,. \tag{1.6}$$

In contrast to Landau theory, the Eqs. (1.4) and (1.5) are not exactly solved. However, they can be studied by sophisticated modern techniques, such as renormalization group methods.

1.1.2. The Scaling Hypothesis and Renormalization Group. Singular behavior of thermodynamic quantities close to the critical point is characterized by a set of critical exponents $(\alpha, \gamma, \beta, ...)$, see Table 1.1. These power-law relations are indicative of scaling behavior and are an important part of critical phenomena. How can one understand scaling? The critical point ($r = 0$) of a continuous phase transition is characterized by a diverging order parameter correlation length, $\xi \to \infty$, for $r \to 0$

$$\xi \sim |r|^{-\nu}\,. \tag{1.7}$$

Here, ν is the correlation length critical exponent. Based on the scaling hypothesis, the only relevant length scale in the vicinity of a critical point is the correlation length ξ [8]. Thus, if all lengths in the system are rescaled by an arbitrary factor b and, at the same time, the external parameters are adjusted such that ξ retains its value, this does not lead to changes of the physical properties. According to the scaling hypothesis, this can be achieved by rescaling the distance from criticality r as rb^{y_r} and the field h as hb^{y_h}, where b is an arbitrary length scale factor, and y_r and y_h are further critical exponents. Rescaling

by the scale factor b therefore leads to the homogeneity formula

$$f(r,h) = b^{-d} f(rb^{y_r}, hb^{y_h}), \tag{1.8}$$

where the free energy density f changes by a volume factor b^d. Similarly, the correlation length rescales by a factor b^{-1}[9]

$$\xi(r,h) = b\xi(rb^{y_r}, hb^{y_h}). \tag{1.9}$$

By choosing the scale factor to be $b = r^{-1/y_r}$, and substituting it in Eqs. (1.8) and (1.9), we obtain scaling relations for the free energy and the correlation length

$$f(r,h) = r^{d/y_r} f_S(hr^{-y_h/y_r}), \tag{1.10}$$

$$\xi(r,h) = r^{-1/y_r} \xi_S(hr^{-y_h/y_r}), \tag{1.11}$$

where f_S and ξ_S are scaling functions. In the absence of a field ($h = 0$), Eqs. (1.10) and (1.11) lead to

$$f \sim |r|^{d/y_r}, \tag{1.12}$$

$$\xi \sim |r|^{-1/y_r} \sim |r|^{-\nu}. \tag{1.13}$$

Thus, the exponent ν is equal to $1/y_r$.

By taking the appropriate derivatives of the free energy (Eq. 1.8), other observables, for instance, the order parameter m, susceptibility χ and specific heat C, can be found. The order parameter m fulfills the homogeneity relation

$$m(r,h) = -(\partial f/\partial h) = b^{y_h-d} m(rb^{1/\nu}, hb^{y_h}), \tag{1.14}$$

the susceptibility χ reads

$$\chi(r,h) = (\partial m/\partial h) = b^{2y_h-d} \chi(rb^{1/\nu}, hb^{y_h}), \tag{1.15}$$

and the specific heat C fulfills

$$C(r,h) = -T(\partial^2 f/\partial^2 r) = b^{2/\nu-d} C(rb^{1/\nu}, hb^{y_h}). \tag{1.16}$$

Determining the thermodynamic critical exponents for the above observables is possible. By setting the scale factor to $b = r^{-\nu}$ and the field to zero ($h = 0$), the magnetization leads to

$$m \sim r^{(d-y_h)\nu} \sim r^{\beta}, \tag{1.17}$$

where $\beta = (d - y_h)\nu$ is the order parameter critical exponent. Analogously, by setting $b = h^{-1/y_h}$ at the criticality ($r = 0$), the magnetization reads

$$m \sim h^{(d-y_h)/y_h} \sim h^{1/\delta}, \tag{1.18}$$

where $\delta = \dfrac{y_h}{d - y_h}$ is the critical isotherm exponent. Similarly, applying the corresponding conditions, one obtains the exponents of susceptibility γ and the specific heat α

$$\chi \sim r^{(d-2y_h)\nu} \sim r^{-\gamma}, \tag{1.19}$$

$$C \sim r^{d\nu-2} \sim r^{-\alpha}\,, \tag{1.20}$$

where $\gamma = (2y_h - d)\nu$ which is called Fisher's scaling relation [10], and $\alpha = 2 - d\nu$ which is known as Josephson's identity [11].

Also, by combining these scaling relations for the critical exponents, one can derive other scaling laws,viz., Widom's and Rusbrook's scaling relations, respectively [9, 12]

$$\gamma = 2 - \alpha - 2\beta\,, \tag{1.21}$$

$$\gamma = \beta(\delta - 1)\,. \tag{1.22}$$

These relations imply that there are only two independent exponents.

Scaling relations are very useful for determining the transition point of a system within a computer simulation. For example, the Binder cumulant g is defined as

$$g = 1 - \frac{\langle m^4 \rangle}{3\langle m^2 \rangle^2}\,. \tag{1.23}$$

This quantity has (scale) dimension zero, which results in the scaling form

$$g(r, h) = g(rb^{1/\nu}, hb^{y_h})\,. \tag{1.24}$$

(Note that the power of b in front of g on the r.h.s. is zero). More details about employing this quantity to analyze the critical behavior will be given in Sec. 1.3.

Critical phenomena feature the concept of *universality classes*. This means that the critical exponents are identical for entire classes of phase transitions. In other words, the critical exponents depend only on the dimensionality of the system and the symmetry of the order parameter, but not on microscopic details.

As discussed previously, the physics close to a continuous phase transition is dominated by fluctuations on large length scales. A systematic approach to analyze the long-distance and long-time behavior is provided by the renormalization group method (RG) [13, 14]. This approach essentially eliminates or integrates out the microscopic short-distance degrees of freedom that are irrelevant to the critical behavior, but keeps the long-distance fluctuations. The critical point is characterized by the RG method as a *fixed point* of this scale transformation. By analyzing these fixed points, precise predictions for the critical exponents of various thermodynamic quantities close to the critical point can be obtained. Moreover, the renormalization group method can be applied to confirm the scaling hypothesis and to explain the concept of universality classes for the critical exponents [1].

1.1.3. Quantum Phase Transitions. All phase transitions that have been discussed in the previous sections occur at nonzero temperatures, and they are often driven by changes in the temperature. A different class of phase transition can exist at the absolute zero of temperature due to the variation of non-thermal external parameters like pressure or magnetic field. This kind of transitions is usually called *quantum phase transitions* (QPT) [15] because they are governed by quantum fluctuations due to Heisenberg's uncertainty principle, rather than by thermal (classical) fluctuations. Quantum phase transition have attracted great interest in the last decades by both experimentalists and theorists in condensed matter physics.

Consider the quantum Ising model (transverse-field Ising model) as an example. It consists of a lattice occupied by $S = \frac{1}{2}$ spins with Hamiltonian

$$H = -J \sum_{\langle ij \rangle} \sigma_i^z \sigma_j^z - h \sum_i \sigma_i^x , \tag{1.25}$$

where σ_i^x and σ_i^z are the Pauli matrices of the x and z spin operator components at site i. The first term is the nearest-neighbor interaction which prefers ferromagnetic order in the z-direction, and a transverse magnetic field in the x-direction is contained in the second term. Since σ_i^x can decomposed into the spin-flip operators

$$\sigma_i^x = \sigma_i^- + \sigma_i^+ , \tag{1.26}$$

the transverse magnetic field leads to random flipping of the spins. These spin flips can destroy the ferromagnetic phase when the transverse magnetic field is sufficiently high, even if the temperature is zero ($T = 0$). The transition between the ferromagnetic and paramagnetic phases at zero temperature is thus characterized by quantum fluctuations while thermal fluctuations are absent. In other words, at zero temperature, quantum mechanics plays a significant role for the critical behavior. In contrast, it does not play any role if the transitions occur at nonzero temperature. In this case, thermal fluctuations become dominant for the critical behavior of the system [16].

Similar to classical (thermal) phase transitions, quantum phase transitions can be split into first-order and continuous (second-order) phase transitions. In second-order quantum phase transitions, the correlation length ξ and the correlation time ξ_t diverge as

$$\xi \sim r^{-\nu} , \tag{1.27}$$

$$\xi_t \sim \xi^z , \tag{1.28}$$

when the critical point is approached. Here, z is the dynamical critical exponent. A schematic phase diagram of a system close to a quantum critical point (QCP) is shown in Fig. 1.4. One needs to distinguish two different types of fluctuations: thermal and quantum fluctuations. At zero temperature, quantum fluctuations are dominant, because the quantum energy is greater than the thermal energy, i.e., $\hbar\omega_c \gg k_B T$. In the opposite case, $\hbar\omega_c \ll k_B T$, the fluctuations are of thermal character. Because the divergence of ξ_t at the critical point leads to a vanishing frequency scale $\omega_c \sim \xi_t^{-1}$ (and with it, a vanishing energy scale $\hbar\omega_c$), thermal fluctuations dominate the critical behavior at any nonzero T.

Consequently, all continuous transitions that occur at any non-zero temperatures are governed entirely by thermal fluctuations. Thus all these transitions are classical phase transitions. On the other hand, at precisely zero-temperature, only quantum fluctuations are present, leading to quantum phase transitions.

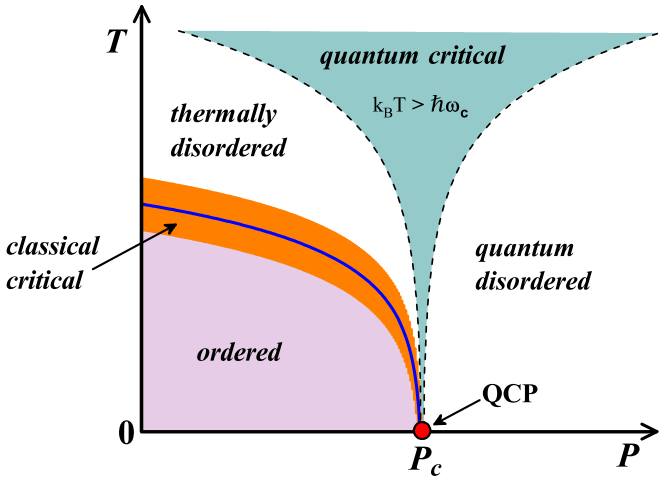

Fig. 1.4. Schematic phase diagram in the vicinity of a quantum critical point (QCP) located at P_c. The horizontal axis is the non-thermal control parameter P which can changes the system by means of the zero-temperature (quantum) phase transition, while the vertical axis is the temperature T. The solid line is the boundary between finite-temperature phases, near to this line the critical behavior is classical. The dashed lines are the borders of the quantum critical region then are given by $k_B T \sim \hbar w_c$.

In Fig. 1.4, the ordered region is destroyed by thermal fluctuations at high temperatures; quantum mechanics is unimportant at such transitions. In contrast, quantum mechanics is relevant at zero temperature when the quantum fluctuations destroy the long-range order. Therefore, the quantum disordered region appears at the disordered side of the quantum critical point at low temperatures where the thermal influences are insignificant. Above the quantum critical point ($p \approx p_c$) is the region known as the quantum critical region, which is bounded by crossover lines $k_B T \sim \hbar\omega_c$. Here, the system is critical with respect to p, and the critical singularities are cut off by the temperature.

What is the relation between quantum and classical critical behavior? This question can be answered by the concept known as the *quantum-classical mapping*. To understand this, the main starting point is the partition function

$$Z = \mathrm{Tr} e^{-(H_{kin}+H_{pot})/k_B T} . \tag{1.29}$$

In classical statistical mechanics, the kinetic (H_{kin}) and potential (H_{pot}) parts of the Hamiltonian $H = H_{kin} + H_{pot}$ of the system commute, so the partition function factorizes, i.e., $Z = Z_{kin} Z_{pot}$. Because the contribution of kinetic part of the Hamiltonian to the free energy derives from a product of simple Gaussian integrals which do not display any singularity, classical phase transitions can be studied by using time-independent theories such as Landau-Ginzburg-Wilson theory (Eq. 1.5), which generally exists in d space dimensions.

However, in quantum mechanics, the kinetic and potential parts of the Hamiltonian usually do not commute. Thus, the partition function does not factorize ($Z \neq Z_{kin} Z_{pot}$). Consequently, theories of quantum phase transitions must treat space and time at the same footing. The canonical density operator $e^{-\beta H}$ is identical to a time-evolution operator in imaginary time τ when $\beta = \tau = it/\hbar$, where $\beta = 1/k_B T$ is the inverse temperature, and t denotes the real time. Using the Trotter formula [17], the partition function can be written as a path integral over space and time dependent fields . For instance, a quantum version of

the Landau-Ginzburg-Wilson functional (Eq. 1.5) can be expressed as

$$F_{LGW}[\phi] = \int \int_0^\beta d\tau d^d x \{-h\phi(x,\tau) + r\phi^2(x,\tau) + k\phi^3(x,\tau) + u\phi^4(x,\tau) + [\nabla\phi(x,\tau)]^2 + [\partial_\tau\phi(x,\tau)]^2\}. \quad (1.30)$$

The imaginary time τ therefore acts like an extra space dimension with infinite extension at zero temperature. Thus, a quantum phase transition in d space dimensions is equivalent to a classical phase transition in $d + 1$ dimensions. This is usually known as *quantum-classical mapping*. An explicit example of such a mapping from the 1-dimensional transverse-field Ising model to 2-dimensional classical Ising model is shown in next section.

The quantum-classical mapping also allows us to generalize the scaling hypothesis to QPTs. According to Eq. (1.28), time scales as length to the power of z. Thus, in the quantum case, the homogeneity relation (1.8) for the free energy density generalizes to

$$f(r,h) = b^{-(d+z)} f(rb^{y_r}, hb^{y_h}). \quad (1.31)$$

Moreover, we can add the temperature as a parameter in the quantum free energy. Temperature scales like an energy which scales like an inverse time. The quantum homogeneity relation (1.31) can therefore be generalized to finite temperatures as

$$f(r,h,T) = b^{-(d+z)} f(rb^{y_r}, hb^{y_h}, Tb^z). \quad (1.32)$$

Analogously, correlation length (1.9), magnetization (1.14), and susceptibility (1.15) can be generalized to the quantum case as

$$\xi(r,h,T) = b\xi(rb^{y_r}, hb^{y_h}, Tb^z), \quad (1.33)$$

$$m(r,h,T) = b^{y_h-(d+z)} m(rb^{1/\nu}, hb^{y_h}, Tb^z)\,, \tag{1.34}$$

$$\chi(r,h,T) = b^{2y_h-(d+z)} \chi(rb^{1/\nu}, hb^{y_h}, Tb^z)\,. \tag{1.35}$$

1.1.4. Transverse-Field Ising Model. To explain the procedures of the quantum-classical mapping, let us take the one-dimensional quantum Ising model in a transverse field and map it to the two-dimensional classical one (the procedure is similar to Feynman's path integral [18]). The Hamiltonian of the one-dimensional transverse-field Ising model reads (see Eq. 1.25)

$$H = -J \sum_{\langle i \rangle} \sigma_i^z \sigma_{i+1}^z - h \sum_i \sigma_i^x\,, \tag{1.36}$$

where J is the ferromagnetic interaction between nearest-neighbor spins in the z-direction, and h is the transverse magnetic field in the x-direction. The ground state of the system (ferromagnetic or paramagnetic behavior) depends on the values of the J and h in the Hamiltonian. For $J \ll h$, the system is a paramagnet. However, the system is in a ferromagnetic state with nonzero z-magnetization when $J \gg h$. Thus, the paramagnetic and ferromagnetic phases must be separated by a quantum phase transition at $J \sim h$.

As we mentioned in the previous section, the starting point to map the system from quantum to classical is the partition function (Eq. 1.29). Because the partition function can not be factorized into interaction and transverse field parts, we employ the Trotter decomposition [17], i.e., $e^{\Phi+\Psi} = \lim_{N\to\infty} \left(e^{\Phi/N} e^{\Psi/N}\right)^N$ to write the partition function as

$$Z = \mathrm{Tr} \lim_{N\to\infty} \left[e^{\delta_\tau J \sum\limits_{\langle ij \rangle} \sigma_i^z \sigma_j^z} e^{\delta_\tau h \sum\limits_i \sigma_i^x} \right]^N\,, \tag{1.37}$$

where $\delta_\tau = \frac{\beta}{N}$. We now insert complete-sets of σ^x and σ^z eigenstates (between the factors). After some algebra, we can express the partition function as

$$Z = \lim_{N\to\infty} \sum_{S_{i,n}} e^{\delta_\tau J \sum\limits_{\langle ij\rangle,n} S_{i,n}S_{j,n}} e^{K^\tau \sum\limits_{i,n} S_{i,n}S_{i,n+1}}, \tag{1.38}$$

where $S_{i,n}$ is the σ^z eigenvalue of the spin at site i and imaginary time index n, and $K^\tau = \frac{1}{2}\ln[\coth(\delta_\tau h)]$ is the interaction in the imaginary time direction. Eq. (1.38) is a representation of the partition function of the quantum Ising model that is identical to a classical Ising model in 1+1 dimensions. Thus, the quantum Hamiltonian (Eq. 1.36) is mapped to a classical one, with two interaction parameters: $\delta_\tau J$ in the space dimension and K^τ in the time-like dimension as

$$\frac{H_{classical}}{T_{classical}} = -\delta_\tau J \sum_{\langle ij\rangle,n} S_{i,n}S_{j,n} - K^\tau \sum_{i,n} S_{i,n}S_{i,n+1}\,, \tag{1.39}$$

where $T_{classical}$ is the temperature of the mapped classical system. The critical behavior of the classical two-dimensional Ising Hamiltonian is well known. It was solved exactly by L. Onsager [19]. Thus, the universality class of the quantum phase transition of one-dimensional transverse-field Ising model is identical to that of the two-dimensional classical Ising model.

1.2. NON-EQUILIBRIUM PHASE TRANSITIONS

So far, we have discussed phase transitions in equilibrium systems. However, many phenomena happening in our lives (such as weather behavior or spreading of an epidemic) cannot be described as equilibrium patterns. Transitions can occur during the time evolution between different nonequilibrium steady states. Such transitions are called *non-equilibrium phase transitions* [20, 21, 22].

Although there are many differences between equilibrium and non-equilibrium systems, some characteristics are shared including scaling and critical behavior near a critical point. One of the prototypical models introduced to study non-equilibrium phase transitions is the *contact process* by Harris [23].

The contact process (Fig. 1.5) is defined on d-dimensional hypercubic lattice. It can be comprehended as a model for the spreading of a disease. Any site in the lattice can be associated with either the active (infected) or the inactive (healthy) state. The time evolution of the contact process is a *Markov process* [24] in continuous time. For each active (infected) site, there are two possible processes: (i) Active site can spontaneously heal (becoming inactive (healthy)) with healing rate μ. Or, (ii) active site can infect a healthy (inactive) neighbor site, which is converted to an active site with infection rate λ. The parameters μ and λ are the control parameters of the contact process.

Depending on the values of λ and μ, the behavior of the contact process can be determined. For large λ, i.e., $\lambda/\mu \gg 1$, the infection processes take control, and there is a high probability for many sites to be in the active state. In this phase (active phase), the density of active sites remains nonzero in the long-time limit, $\lim_{t\to\infty} \rho(t) = \rho_s > 0$. In contrast, for small λ ($\lambda/\mu \ll 1$), the annihilation is the dominating processes of the system. All sites will eventually reach the inactive state. Thus the steady-state density $\rho_s = 0$. This phase, the inactive phase, is an absorbing phase, because the system cannot leave it anymore. The transition between the active and inactive phases which occurs at a critical value λ_c of the infection rate is therefore called an absorbing state phase transition. Close to the critical point λ_c, the order parameter ρ_s for the contact process displays a power-law relation

$$\rho_s \sim |\lambda - \lambda_c|^{\beta}, \tag{1.40}$$

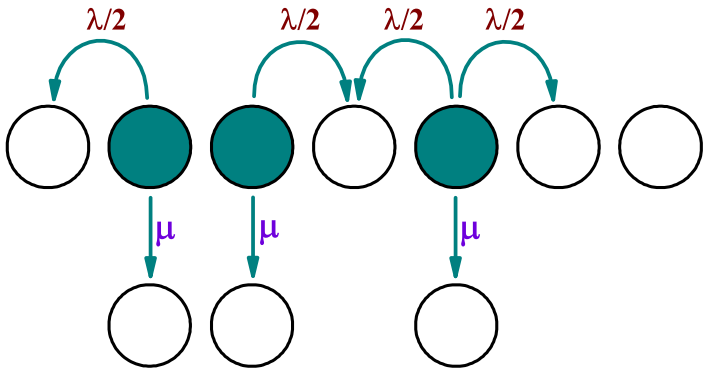

Fig. 1.5. Schematic of contact process in one-dimension. Infected (active) sites infect their neighbors at rate $\lambda/2$. Active sites can spontaneously become inactive (healthy) with healing rate μ.

where β is the exponent of the order parameter. Similar to equilibrium phase transitions, the correlation length ξ increases as a power of the distance from criticality

$$\xi \sim |\lambda - \lambda_c|^{-\nu}, \tag{1.41}$$

where ν is the correlation length exponent. Analogously, the correlation time ξ_t behaves as

$$\xi_t \sim |\lambda - \lambda_c|^{z}, \tag{1.42}$$

where z is the dynamical critical exponent. By finding these three exponents (β, ν and z), we can determine the universality class of the phase transition in the contact process [25, 26]*.

*General non-equilibrium phase transitions have four independent exponents [22], but the universality class of the contact process (directed percolation) has only three.

1.3. FINITE-SIZE SCALING

When studying any macroscopic system by computer simulations to analyze the critical behavior, invariably one must make an approximation and simulate a small model system. This introduces systematic errors known as *finite-size effects*. How important are these finite-size effect for a continuous phase transition point? A real phase transition (singularity in free energy) can only exist in infinite systems, i.e., $L \to \infty$. As a result, in finite systems, peaks in observables are rounded rather than having divergences. These peaks shift, narrow and increase in height with increasing L. A systematic way of dealing with finite-size effects is provided by finite-size scaling theory [27, 28, 29]. This theory supposes the inverse linear system size L^{-1} can be introduced as additional system parameter that takes the system away from the transition point (which corresponds to $L \to \infty$). Close to a critical point, the only relevant length scale is the correlation length of infinite system ξ_∞. Therefore the finite-size effects must be governed only by the ratio $\frac{L}{\xi_\infty}$. Now, the classical free energy density relation (1.8) can be generalized in terms of the system size L as

$$f(r, h, L) = b^{-d} f(r b^{\frac{1}{\nu}}, h b^{y_h}, L b^{-1}) . \tag{1.43}$$

Analogously, the quantum homogeneity free energy relation (1.32) can be generalized to

$$f(r, h, T, L) = b^{-(d+z)} f(r b^{\frac{1}{\nu}}, h b^{y_h}, T b^{z}, L b^{-1}) . \tag{1.44}$$

The scaling form of the classical free energy density (1.43) can be used to derive finite-size scaling forms of different observables by adjusting the arbitrary scale factor b. Setting $b = L$ and $h = 0$, this leads to the scaling form

$$f(r, L) = L^{-d} \Phi_f(r L^{\frac{1}{\nu}}), \tag{1.45}$$

where $\Phi_f(rL^{\frac{1}{\nu}})$ is a dimensionless scaling function which can be used to find how the critical point shifts as a function of the system size L. For finite systems, the critical point corresponds to a feature in Φ_f at some nonzero argument $x_c = r_c L^{\frac{1}{\nu}}$, so the transition temperature $T_c(L)$ is shifted from the bulk value $T_c^0(L \to \infty)$ through

$$T_c(L) - T_c^0 \sim r_c = x_c L^{-\frac{1}{\nu}} . \tag{1.46}$$

Moreover, the scaling form of Binder cumulant (1.24) also can be generalized to finite-size scaling as

$$g(r, L) = g(rL^{\frac{1}{\nu}}) . \tag{1.47}$$

The finite-size scaling form of Binder cumulant is a very important relation to determine the critical point in many isotropic systems. Because g has scale dimension zero, its curves for various L cross at critical temperature T_c, see Fig. 1.6

$$g(0, L) = g(0), \tag{1.48}$$

because at the critical temperature $r = \frac{T - T_c}{T_c} = 0$. In anisotropic systems (where not all directions are equivalent), for example those arising from the quantum-classical mapping, the situation is more complicated. In some systems, the finite-size scaling of Binder cumulant is given by conventional scaling

$$g(r, L, L_\tau) = g(rL^{\frac{1}{\nu}}, L_\tau / L^z) . \tag{1.49}$$

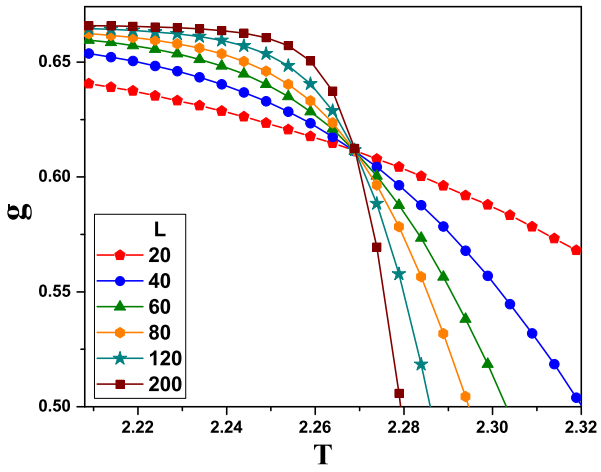

Fig. 1.6. Schematic of Binder cumulant g vs. temperature T for different system size L in classical Ising model. All curves cross at the same temperature that corresponds to a critical temperature T_c.

Other systems show activated scaling

$$g(r, L, L_\tau) = g(rL^{\frac{1}{\nu}}, \ln(L_\tau)/L^{\psi}), \tag{1.50}$$

where L and L_τ are the linear system sizes in the space and time-like directions, respectively. These two scaling forms are very useful to study the critical behavior in many quantum systems. Fig. 1.7 compares the behavior of Binder cumulant with conventional and activated scaling. For fixed L and T, the Binder cumulant g has a maximum (peak) as a function of L_τ at position L_τ^{max}. The position of the peak yields the optimal sample shape. Thus, at the critical temperature, peaks of Binder cumulant should have the same value which is independent of L as shown in Fig. 1.7a.

For conventional power-law dynamic scaling, the curves of Binder cumulant for different L should collapse onto each other when it plotted as a function of L_τ/L_τ^{max}. However, for activated scaling the Binder cumulant curves should collapse when plotted as a function of $\ln(L_\tau)/\ln(L_\tau^{max})$. Fig. 1.7b shows that the random quantum Ising model follows the activated scaling rather than conventional scaling.

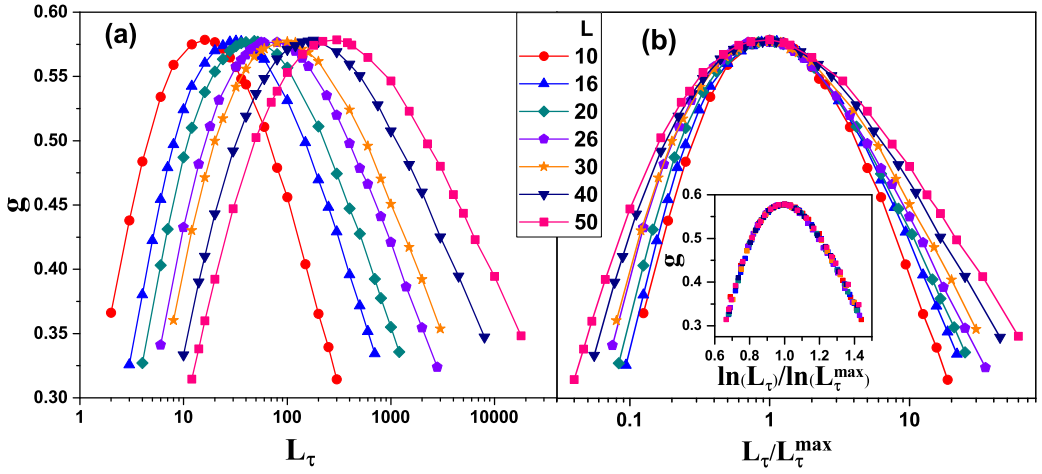

Fig. 1.7. Behavior of Binder cumulant in the random quantum Ising model. (a) Binder cumulant as a function of L_τ for several L at the critical temperature. (b) Scaling plot of the Binder cumulant at T_c. Main panel: Power-law scaling g vs L_τ/L_τ^{max}. Inset: Activated scaling g vs $\ln(L_\tau)/\ln(L_\tau^{max})$.

Finite-size scaling theory plays an important role in studying and analyzing the computer simulation data of phase transitions. Critical exponents of the system can be determined by fitting the data from the simulations to finite-size scaling forms. Thus, the critical behavior becomes easy to determine.

1.4. DISORDERED PHASE TRANSITIONS

In condensed matter physics, the expressions "order" and "disorder" are used in two different meanings. On the one hand, following Landau, an ordered state is a state with a spontaneously broken symmetry that is usually found at low temperatures. Upon heating, the system undergoes a phase transition into a less ordered phase that restores the symmetry. For instance, the melting of ice restores the translational symmetry that is broken by the crystal lattice, and the demagnetization of a metal by heating restores the broken spin rotation symmetry, see Figs. (1.1) and (1.2).

On the other hand, the terms "order" and "disorder" refer to clean (pure) and dirty systems, respectively. The latter kind of disorder can have many different origins including vacancies, impurity atoms, crystal defect, or other kinds of imperfections. Based on the time dependence, the disorder can be classified into two types: quenched (time-independent) and annealed (time-dependent) disorder [30]. This work focuses only on the effects of time-independent disorder. What are the influences of such disorder on phase transitions?

1.4.1. Quenched Disorder. The influence of quenched disorder on the behavior of phase transitions and critical points has attracted considerable attention [31, 32, 33]. The simplest, most straightforward type of disorder is random-mass (random-T_c) disorder. It does not alter the symmetries of the bulk phases. Instead, it locally changes the tendency towards one or the other phase, i.e., it changes the location of the local "critical point". Technically, random-T_c disorder can be applied to a clean system by changing the distance from the criticality r to a random functional of real space position,

$$r = r_0 + \delta r(\vec{x})\,. \tag{1.51}$$

For example, the Landau-Ginzburg-Wilson functional (Eq. 1.5) in the presence of random-T_c disorder can be written as

$$F_{LGW}[(\phi(\vec{x})] = \int d^d\vec{x}\{-h\phi(\vec{x}) + [r_0 + \delta r(\vec{x})]\phi^2(\vec{x}) + k\phi^3(\vec{x}) + u\phi^4(\vec{x}) + [\nabla\phi(\vec{x})]^2\}\,. \tag{1.52}$$

Adding quenched disorder to a clean system that undergoes a phase transition raises many questions concerning the stability of the transition, the order of the transition, and its critical behavior. Criteria addressing these questions will be discussed in the next sections.

1.4.2. Imry-Ma Criterion. In the presence of quenched disorder, does a first-order phase transition survive and remain sharp? Imry and Ma [34] introduced the answer to this question by developing a heuristic argument to test the stability of phase coexistence against domain formation in the presence of random-mass disorder. To understand this argument, consider a single d-dimensional domain of the ferromagnetic phase with linear size L embedded in a larger paramagnetic phase, as shown in Fig. 1.8. Right at a clean first-order phase transition, the bulk free energies of the two phases agree.

Let us now introduce random-mass disorder. Based on Imry and Ma, one needs to compare two different free energies, the free energy gain from the quenched disorder which can be estimated from the central limit theorem

$$E_{dis} \sim L^{d/2}, \tag{1.53}$$

and the free energy loss due to the formation of the domain wall

$$E_{dw} \sim L^{d-1}. \tag{1.54}$$

According to the Imry-Ma argument, the ferromagnetic state will be stable against domain formation if $E_{dis} < E_{dw}$. This is possible only if the dimension of the system $d > 2$. In this case the formation of the domain wall becomes unfavorable, and thus, macroscopic phase coexistence is stable against weak random-mass disorder. In contrast, quenched disorder destroys a first-order phase transition if $d \leq 2$ because the system prefers domain formation which prevents the macroscopic phase coexistence [35].

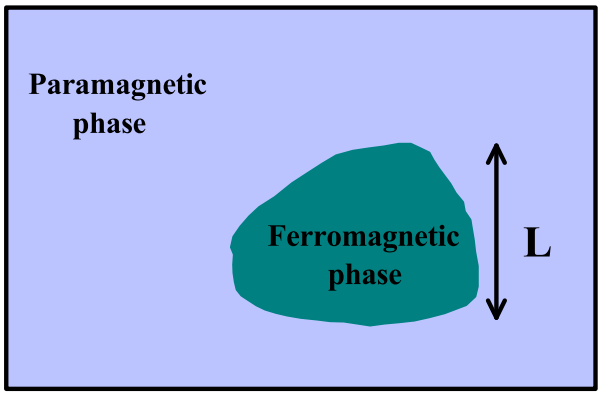

Fig. 1.8. Schematic of the Imry-Ma criterian.

Moreover, Aizenman and Wehr [36] proved a rigorous theorem for the existence of domains in all dimensions $d \leq 2$. Thus, the first-order phase transition can not survive in the presence of quenched disorder. The criterion does not resolve the fate of transitions that are destroyed by randomness. In Papers II and III, this question is studied for classical and quantum Ashkin-Teller models.

1.4.3. Harris Criterion. In the previous section, the effects of quenched disorder on a first-order phase transition were determined by comparing how different energies scale with respect to the dimension of the system. However, what are the effects on a second-order phase transition? Harris [37] addressed this inquiry by developing a criterion to test the stability of a clean critical point of a continuous phase transition against random-T_c disorder. He derived this criterion by considering that the system can be divided into blocks which are independent of one another if their linear dimension is the correlation length ξ (see Fig. 1.9). Each block j has its own local critical temperature T_c^j, which depends on the local distace from criticality, $r + \delta r(\vec{x})$ averaged over the volume ξ^d. These local critical temperatures have a typical variation ΔT_c from block to block.

By comparing ΔT_c with the distance from criticality $r = |T - T_c|$, Harris's argument compares two cases: If $\Delta T_c > |T - T_c|$, some blocks will be in one phase and some will exist in the other phase. Thus, a uniform transition between these phases is impossible.

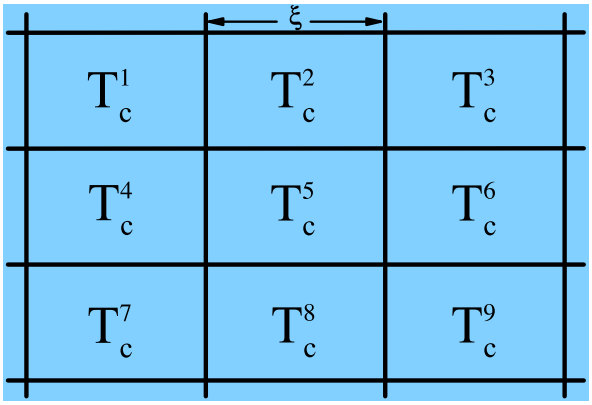

Fig. 1.9. Schematic of Harris criterian.

However, the transition can be uniform when $\Delta T_c < |T - T_c|$, where almost all the blocks are in the same phase. Based on this argument, the condition for the stability of the clean critical point against quenched disorder should be

$$\Delta T_c \ll |T - T_c| \,. \tag{1.55}$$

The variation of the local critical temperatures ΔT_c decreases with increasing correlation length ξ. It can be estimated from the central limit theorem as

$$\Delta T_c \sim \xi^{-d/2} \,. \tag{1.56}$$

According to Eq. 1.13, the correlation length ξ depends on the distance from the critical temperature as

$$\xi \sim |T - T_c|^{-\nu} \,. \tag{1.57}$$

By combining Eqs. (1.56) and (1.57), we get

$$\Delta T_c \sim |T - T_c|^{d\nu/2} \,. \tag{1.58}$$

Thus, the clean critical point cannot be stable against randomness if the condition

$$d\nu > 2, \tag{1.59}$$

is violated. This is known as the Harris criterion for the stability of continuous phase transitions in presence of quenched disorder.

1.4.4. Strong-Disorder Renormalization Group Theory and Infinite Randomness Critical Point. Traditional renormalization group (RG) methods to predict the critical behavior of systems that undergo a phase transition often do not work for strongly disordered systems. A very different type of RG was suggested by Ma, Dasgupta, and Hu [38, 39] who studied random antiferromagnets. This lead to the development of the method now known as the strong-disorder renormalization group (SDRG)[40].

The strategy of the SDRG is to decrease the number of degrees of freedom and reduce the local energy scale by finding the strongest coupling in a system (the largest local energy) and its the corresponding ground state of the Hamiltonian. The excited states associated with the strong couplings are eliminated, and weaker effective couplings are generated. This is repeated ad infinitum.

As a prototypical example, the strong-disorder renormalization group was applied by Fisher [41, 42] to the random transverse-field Ising chain. The Hamiltonian of this model is given by

$$H = -\sum_i J_i \sigma_i^z \sigma_{i+1}^z - \sum_i h_i \sigma_i^x, \tag{1.60}$$

where σ_i^x and σ_i^z are Pauli matrices representing the spin operator at site i. The nearest-neighbor interactions J_i and transverse fields h_i are both independent random variables with probability distributions $P(J_i)$ and $R(h_i)$, respectively. This model has two phases that are separated by a quantum phase transition when the typical values h and J of these variables

agree, ($\langle \ln J \rangle = \langle \ln h \rangle$) [43]. If $h \gg J$, the ground state is a polarized paramagnetic state in the field direction (x-direction). In contrast, for $h \ll J$, the system is ferromagnetic in the z-direction.

Based on the idea of the SDRG, we first look for the strongest coupling Ω in the entire system as

$$\Omega = \max\{J_i, h_i\} . \tag{1.61}$$

This coupling could be either an interaction between nearest neighbor sites or a transverse field at one site.

If $\Omega = h_i$, i.e., the strongest coupling is a transverse field, the spin σ_i is pinned in the field direction. It does not make any contribution to the magnetization in the z-direction and can be eliminated from the system. Nevertheless, the excited state of spin σ_i gives a weak effective coupling $\tilde{J}$ between the nearest neighbor spins.

The effective coupling $\tilde{J}$ can be estimated in perturbation theory by considering the unperturbed part of the Hamiltonian ($H = H_0 + H_1$) as

$$H_0 = -h_i \sigma_i^x , \tag{1.62}$$

while the rest of the local Hamiltonian

$$H_1 = -J_{i-1} \sigma_{i-1}^z \sigma_i^z - J_i \sigma_i^z \sigma_{i+1}^z , \tag{1.63}$$

is treated in second-order perturbation theory, yielding an effective interaction

$$H_{eff} = -\tilde{J} \sigma_{i-1}^z \sigma_{i+1}^z \qquad \text{with} \qquad \tilde{J} = \frac{J_{i-1} J_i}{h_i} . \tag{1.64}$$

Fig. 1.10 illustrate the steps of the strong-disorder renormalization group when $\Omega = h_i$.

In contrast, if the largest coupling is an interaction J_i between the spins at site i and $i+1$, then the transverse fields h_i and h_{i+1} can be considered as a perturbation to the unperturbed term $(-J_i\sigma_i^z\sigma_{i+1}^z)$ in the local Hamiltonian. The two spins σ_i and σ_{i+1} are joined together into a spin cluster $\tilde{\sigma}$ with an effective transverse field $\tilde{h}$ and an effective magnetic moment $\tilde{\mu}$

$$\tilde{\mu} = \mu_i + \mu_{i+1}\,, \tag{1.65}$$

where μ_i and μ_{i+1} are the moments associated with σ_i and σ_{i+1}. Analogously, we can find the expression of $\tilde{h}$ by writing the local Hamiltonian as $H = H_0 + H_1$ where

$$H_0 = -J_i\sigma_i^z\sigma_{i+1}^z\,, \tag{1.66}$$

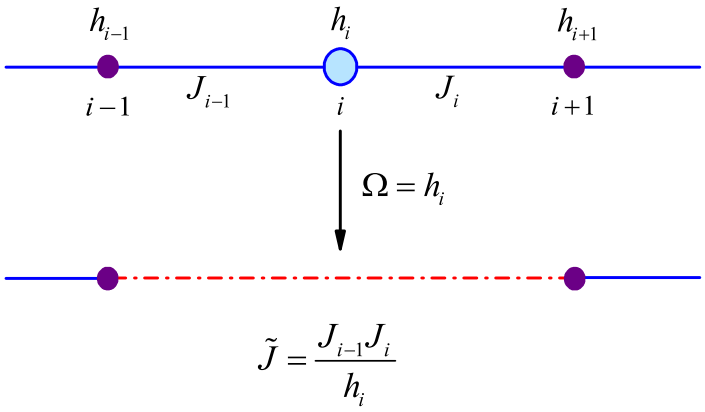

Fig. 1.10. Schematic of the strong-disorder renormalization group step for decimating a field.

and

$$H_1 = -h_i\sigma_i^x - h_{i+1}\sigma_{i+1}^x \,. \tag{1.67}$$

By using second-order perturbation theory, we get the effective transverse field

$$H_{eff} = -\tilde{h}\tilde{\sigma}^x \qquad \text{with} \qquad \tilde{h} = \frac{h_i h_{i+1}}{J_i} \,. \tag{1.68}$$

The procedure of this renormalization group step is explained schematically in Fig. 1.11.

The concept of the strong-disorder renormalization group is based on iteration. By repeating the steps of the SDRG above, the strongest energy in the system gradually decreases, $\Omega \to 0$. The interactions J_i and the transverse fields h_i are independent random variables at each stage of the strong-disorder renormalization group, and their probability distributions $P(J;\Omega)$ and $R(h;\Omega)$ evolve during the process of the SDRG. Fisher [42] studied the critical behavior of the Hamiltonian (1.60) of the random transverse-field Ising model and derived the SDRG flow equations of these distributions.

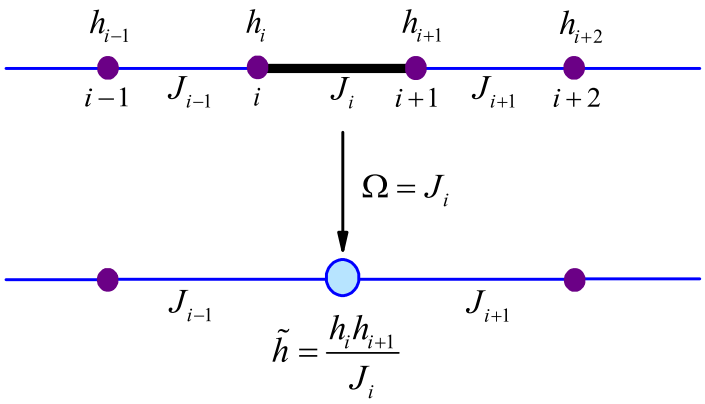

Fig. 1.11. Schematic of the strong-disorder renormalization group step for decimating an interaction.

At the critical point ($\langle \ln h \rangle = \langle \ln J \rangle$), Fisher found the solutions of the flow equations by introducing a logarithmic variable $\Gamma = \ln(\Omega_0/\Omega)$, where Ω_0 is the initial strongest energy in the system. The probability distribution of the interactions takes the form

$$P(J;\Omega) = \frac{1}{\Gamma J}\left(\frac{J}{\Omega}\right)^{1/\Gamma}, \tag{1.69}$$

and the distribution of the transverse fields is

$$R(h;\Omega) = \frac{1}{\Gamma h}\left(\frac{h}{\Omega}\right)^{1/\Gamma}. \tag{1.70}$$

In the low-energy limit, the relative widths of the probability distribution Eqs. (1.69) and (1.70) become larger and larger with decreasing Ω ($\Omega \to 0$). This implies that the effects of randomness (disorder) get stronger and stronger without bound. Thus, the system is dominated by a critical fixed point of the so-called *infinite-randomness type*. At such critical points, the dynamic scaling of the system is logarithmic (activated) scaling rather than power-law scaling (i.e., length scales like logarithm of time).

When the infinite-randomness critical point is approached, the behavior is characterized by a set of independent critical exponents including the tunneling critical exponent $\psi = 1/2$, which controls the relation between the typical length of a cluster L and Ω

$$L \sim \left[\ln\left(\frac{\Omega_0}{\Omega}\right)\right]^{1/\psi}. \tag{1.71}$$

Also, the exponent $\phi = (\sqrt{5}+1)/2$ wich equals the golden ratio, is the critical exponent of the magnetic moment μ of a cluster

$$\mu \sim \left[\ln\left(\frac{\Omega_0}{\Omega}\right)\right]^{\phi}. \tag{1.72}$$

These two expressions introduce the unusual scaling behavior (activated scaling instead of conventional scaling) of observables at this kind of critical point. Activated scaling also appears in many quantum phase transitions in disordered metals, for example in the superconducting nanowires studied in Paper IV.

1.4.5. Rare-Regions and Griffiths Effects. Disorder does not only affect the phase transition itself but also the behavior close to the transition. For definiteness, assume that disorder changes the transition point to T_c from its clean (bulk) value T_c^0. Interesting effects arise in the region between the clean critical point and the disordered transition point, i.e., the range of temperatures $T_c < T < T_c^0$, which is known as the *Griffiths region* or *Griffiths phase*. It is caused by rare strong disordered fluctuations and the spatial regions where they occur.

The effects of rare regions on a phase transition range from changing the properties of a phase transition to completely destroying it. In 1969, Griffiths [44] proved the existence of a singularity in the free energy of the system in the entire interval of temperatures $T_c < T < T_c^0$. This singularity can be attributed to rare regions. Thus, the effects of rare regions on phase transitions are also called the *Griffiths effects* [45].

To explain the Griffiths effects, consider in Fig. 1.12, a diluted classical ferromagnetic system. Dilution favors the paramagnetic state, and thus the critical temperature T_c^0 reduces to T_c. There can be large spatial regions (rare-regions) in the range $T_c < T < T_c^0$ which are devoid of any impurities (vacancies). Such regions have slow dynamics and make large contributions to the thermodynamics. A Griffiths region also exists in the ordered phase. There, the rare regions are clusters inside holes in the ferromagnetic order.

How large is the rare-region contributions to the thermodynamic behavior of a system close to a phase transition? The probability P for finding a rare-region as function of its size L_{RR} is

$$P(L_{RR}) \sim \exp(-AL_{RR}^d), \tag{1.73}$$

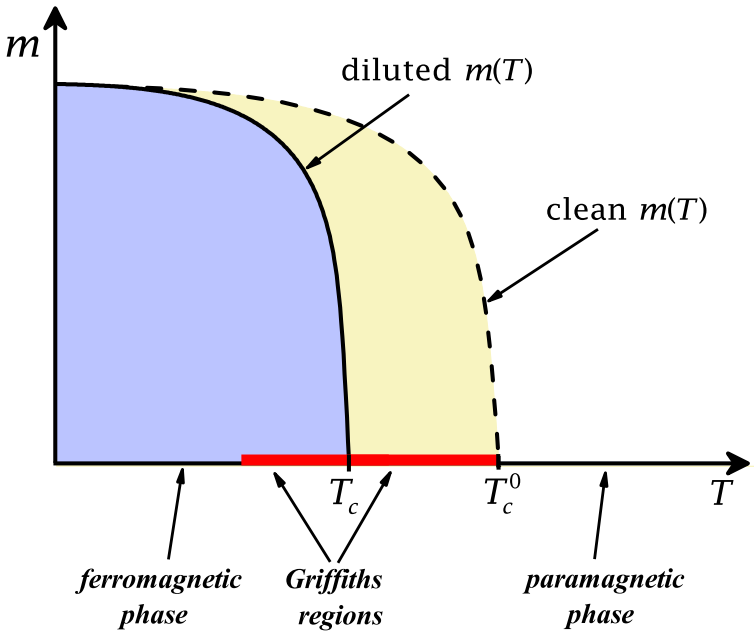

Fig. 1.12. Schematic of Griffiths-regions on both sides of T_c in the plot of magnetization m as a function of temperature T.

where A is a constant. The influences of the rare regions on the system now depend on how large a contribution each rare region can make. This is controlled by the effective dimensions d_{RR} of the rare region and its relation to the lower critical dimensionality d_c^- of the system. Thus, three cases can be compared [20, 46, 47]:

i. If $d_{RR} < d_c^-$, it is impossible that the rare region undergoes the phase transition without contributions from the entire system. The contribution of the rare region scales as a power of its size, which isn't able to defeat the exponential decay in the rare region probability (Eq. 1.73). Therefore, the effects of the Griffiths phase in this case will be exponentially weak (conventional critical point with power-law dynamic scaling).

ii. If $d_{RR} = d_c^-$, the rare region is exactly at the lower critical dimension. In this case, the rare region still cannot undergo the phase transition by itself (independently), but the contributions of the rare region to observables lead to strong exponential behavior that overcomes the decreasing of the rare region probability. Thus, the Griffith effects lead to infinite-randomness critical points with non-conventional dynamic scaling.

iii. The last case consists of rare regions above the lower critical dimension, $d_{RR} > d_c^-$. In this case, the rare region can undergo the phase transition independently from the bulk system. This leads to the destruction of the sharp phase transition of the system by smearing.

Case (i) implies that, in a classical system with short-range correlated disorder, the Griffiths singularities in the free energy are only essential ones [48, 49, 50], resulting in very weak thermodynamic Griffith effects. In contrast, the rare region effects become more important and influential for long-range correlated disordered systems, see Paper I.

PAPER

I. ENHANCED RARE-REGION EFFECTS IN THE CONTACT PROCESS WITH LONG-RANGE CORRELATED DISORDER

Ahmed K. Ibrahim, Hatem Barghathi, and Thomas Vojta

Department of Physics, Missouri University of Science and Technology, Rolla, MO 65409, USA

ABSTRACT[†]

We investigate the nonequilibrium phase transition in the disordered contact process in the presence of long-range spatial disorder correlations. These correlations greatly increase the probability for finding rare regions that are locally in the active phase while the bulk system is still in the inactive phase. Specifically, if the correlations decay as a power of the distance, the rare region probability is a stretched exponential of the rare region size rather than a simple exponential as is the case for uncorrelated disorder. As a result, the Griffiths singularities are enhanced and take a non-power-law form. The critical point itself is of infinite-randomness type but with critical exponent values that differ from the uncorrelated case. We report large-scale Monte-Carlo simulations that verify and illustrate our theory. We also discuss generalizations to higher dimensions and applications to other systems such as the random transverse-field Ising model, itinerant magnets and the superconductor-metal transition.

[†]Published in Physical Review E 90, 042132 (2014).

1. INTRODUCTION

The effects of quenched spatial disorder on phase transitions have been a topic of great interest for several decades. Initially, research concentrated on classical (thermal) transitions for which many results can be obtained by using perturbative methods adapted from the theory of phase transitions in clean systems (see, e.g., Ref. [1]).

Later, it became clear, however, that many transitions are dominated by the non-perturbative effects of strong, rare disorder fluctuations and the rare spatial regions that support them. Such rare regions can be locally in one phase while the bulk system is in the other. The resulting slow dynamics leads to thermodynamic singularities, now known as the Griffiths singularities [2, 3], not just at the transition point but in an entire parameter region around it. Griffiths singularities at generic classical (thermal) phase transitions are very weak and probably unobservable in experiment [4]. In contrast, at many quantum and nonequilibrium phase transitions, the rare regions lead to strong Griffiths effects characterized by non-universal power-law singularities of various observables. The critical point itself is of exotic infinite-randomness type and characterized by activated rather than power-law dynamical scaling. This was first demonstrated in the random-transverse field Ising chain using a strong-disorder renormalization group [5, 6] as well as heuristic optimal fluctuation arguments and computer simulations [7, 8, 9]. Similar power-law Griffiths singularities were also found at the nonequilibrium transition of the disordered contact process [10, 11, 12] and at many other quantum and nonequilibrium transitions. In some systems, the rare region effects are even stronger and destroy the sharp phase transition by smearing [13]. Recent reviews and a classification of rare region effects can be found, e.g., in Refs. [14].

The majority of the literature on rare regions and Griffiths singularities focuses on uncorrelated disorder. In many physical situations, we can expect, however, that the disorder is correlated in space, for example if it caused by charged impurities. It is intuitively clear that sufficiently long-ranged spatial disorder correlations must enhance the rare region

effects because they greatly increase the probability for finding large atypical rare regions. Rieger and Igloi [15] studied a random transverse-field Ising chain with power-law disorder correlations. They indeed found that sufficiently long-ranged correlations change the universality class of the transition. They also predicted that the Griffiths singularities take the same power-law form as in the case of uncorrelated disorder, but with changed exponents.

In this paper, we investigate the nonequilibrium phase transition in the disordered one-dimensional contact process with power-law disorder correlations by means of optimal fluctuation theory and computer simulations. Our paper is organized as follows. We define the contact process with correlated disorder in Sec. 2. In Sec. 3, we develop our theory of the nonequilibrium phase transition and the accompanying Griffiths phase. Specifically, we show that the probability of finding a large rare region is a stretched exponential of its size rather than a simple exponential as for uncorrelated disorder. As a result, the Griffiths singularities are enhanced and take a non-power-law form. The critical point itself is of infinite-randomness type but its exponents differ from the uncorrelated case. Sec. 4 is devoted to Monte-Carlo simulations that verify and illustrate our theory. In Sec. 5, we generalize our results to higher dimensions and other physical systems. We also discuss the relation between the present work and Ref. [15]. We conclude in Sec. 6.

2. CONTACT PROCESS WITH CORRELATED DISORDER

The contact process [16] is a prototypical nonequilibrium many-particle system which can be understood as a model for the spreading of an epidemic. Consider a one-dimensional regular lattice of L sites. Each site can be in one of two states, either inactive (healthy) or active (infected). The time evolution of the contact process is given by a continuous-time Markov process during which active lattice sites infect their nearest neighbors or heal spontaneously. Specifically, an active site becomes inactive at rate μ, while an inactive site becomes active at rate $n\lambda/2$ where n is the number of its active nearest

neighbors. The healing rate μ and the infection rate λ are the external control parameters of the contact process. Without loss of generality, μ can be set to unity, thereby fixing the unit of time.

The qualitative behavior of the contact process is easily understood. If healing dominates over infection, $\mu \gg \lambda$, the epidemic eventually dies out completely, i.e., all lattices sites become inactive. At this point, the system is in a fluctuationless state that it can never leave. This absorbing state constitutes the inactive phase of the contact process. In the opposite limit, $\mu \ll \lambda$, the infection never dies out (in the thermodynamic limit $L \to \infty$). The system eventually reaches a steady state in which a nonzero fraction of lattices sites is active. This fluctuating steady state constitutes the active phase of the contact process. The active and inactive phases are separated by a nonequilibrium phase transition in the directed percolation universality class [17, 18, 19]. The order parameter of this absorbing-state transition is given by the steady state density $\rho_{\rm stat} = \lim_{t\to\infty} \rho(t)$ which is the long-time limit of the density of infected sites at time t,

$$\rho(t) = \frac{1}{L} \sum_i \langle n_i(t) \rangle \ . \tag{1}$$

Here, $n_i(t)$ is the occupation of site i at time t, i.e., $n_i(t) = 1$ if the site is infected and $n_i(t) = 0$ if it is healthy. $\langle \ldots \rangle$ denotes the average over all realizations of the Markov process.

So far, we have discussed the clean contact process for which λ and μ are spatially uniform. Quenched spatial disorder is introduced by making the infection rate λ_i of site i and/or its healing rate μ_i random variables. The correlations of the randomness can be characterized by the correlation function

$$G_\lambda(i,j) = [\lambda_i \lambda_j]_{\rm dis} - [\lambda_i]_{\rm dis}\,[\lambda_j]_{\rm dis} \tag{2}$$

where $[\ldots]_{\rm dis}$ denotes the disorder average. The correlation function G_μ of the healing rates μ_i can be defined analogously. The existing literature on the disordered contact process mostly considered the case of uncorrelated disorder, $G_\lambda(i,j) \sim G_\mu(i,j) \sim \delta_{ij}$. In the present paper, we are interested in long-range correlations whose correlation function decays as a power of the distance r_{ij} between the two sites,

$$G_\lambda(i,j) \sim G_\mu(i,j) \sim r_{ij}^{-\gamma}\,, \tag{3}$$

for large r_{ij}. For our analytical calculations we will often use a correlated Gaussian distribution

$$P_G(\lambda_1,\ldots,\lambda_L) \sim \exp\left[-\frac{1}{2}\sum_{i,j}(\lambda_i-\bar\lambda)A_{ij}(\lambda_j-\bar\lambda)\right] \tag{4}$$

of average $\bar\lambda = [\lambda_i]_{\rm dis}$ and covariance matrix $(A^{-1})_{ij} = G_\lambda(i,j)$ [20]. Alternatively, we will also use a correlated binary distribution in which λ_i can take values λ and $c\lambda$ with overall probabilities $(1-p)$ and p, respectively. Here, p and c are constants between 0 and 1.

3. THEORY

3.1. RARE-REGION PROBABILITY. The Griffiths phase in the disordered contact process is caused by rare large spatial regions whose effective infection rate is larger than the bulk average $\bar\lambda$. For weak disorder and outside the asymptotic critical region, the effective infection rate can be approximated by

$$\lambda_{RR} \approx \frac{1}{L_{RR}}\sum_{i\in RR}\lambda_i \tag{5}$$

To estimate how the probability distribution of λ_{RR} depends on the rare region size L_{RR}, we start from the correlated Gaussian (4), introduce λ_{RR} as a new variable and then integrate out all other random variables. For large L_{RR} and up to subleading boundary terms, this

leads to the distribution

$$P(\lambda_{RR}, L_{RR}) \sim \exp\left[-\frac{L_{RR}}{2\tilde{G}(L_{RR})}(\lambda_{RR} - \bar{\lambda})^2\right] \tag{6}$$

where $\tilde{G}(L_{RR})$ is the sum over the correlation function

$$\tilde{G}(L_{RR}) \sim \sum_{j=0}^{L_{RR}/2} G_\lambda(0, j) \; . \tag{7}$$

Two cases need to be distinguished, depending on the value of the decay exponent γ in the correlation function (3). If $\gamma > 1$, the sum $\tilde{G}(L_{RR})$ converges in the limit $L_{RR} \to \infty$. The probability distribution of the effective infection rate λ_{RR} thus takes the asymptotic form

$$P(\lambda_{RR}, L_{RR}) \sim \exp\left[-\frac{1}{2b^2} L_{RR} (\lambda_{RR} - \bar{\lambda})^2\right] \tag{8}$$

where b is a constant. This form is identical to the result for uncorrelated or short-range correlated disorder (and agrees with the prediction of the central limit theorem). For $0 < \gamma < 1$, in contrast, the sum $\tilde{G}(L_{RR})$ behaves as $L_{RR}^{1-\gamma}$ for large L_{RR}. Consequently, the probability distribution of λ_{RR} reads

$$P(\lambda_{RR}, L_{RR}) \sim \exp\left[-\frac{1}{2b^2} L_{RR}^{\gamma} (\lambda_{RR} - \bar{\lambda})^2\right] \; . \tag{9}$$

This is a stretched exponential decay in L_{RR} rather than the simple exponential obtained in (8). In other words, for $0 < \gamma < 1$, the probability for finding a large deviation of λ_{RR} from the average $\bar{\lambda}$ decays much more slowly with rare region size than in the uncorrelated case.

We have also considered a correlated binary disorder distribution instead of the Gaussian (4). In this case, rare regions can be defined as regions of L_{RR} consecutive sites having the larger of the two infection rates. For uncorrelated disorder, the probability for finding such a region decays as a simple exponential of its size L_{RR}. We have confirmed

numerically that the corresponding probability for the power-law correlations (3) with $0 < \gamma < 1$ follows a stretched exponential

$$w(L_{RR}) \sim \exp(-cL_{RR}^{\gamma}) \tag{10}$$

with the same exponent γ as in Eq. (9).

3.2. GRIFFITHS PHASE. We now use the results of Sec. 3.1 to analyze the time evolution of the density of active sites $\rho(t)$ in the Griffiths phase on the inactive side of the nonequilibrium transition. This calculation is a generalization to the case of correlated disorder of the approach of Refs. [21, 22].

The rare region contribution to $\rho(t)$ can be obtained by summing over all regions that are locally in the active phase, ie., all regions having $\lambda_{RR} > \lambda_c$. For the correlated Gaussian distribution (4), $\rho(t)$ reads

$$\begin{aligned}\rho(t) \quad \sim \quad & \int_{\lambda_c}^{\infty} d\lambda_{RR} \int_0^{\infty} dL_{RR}\, P(\lambda_{RR}, L_{RR}) \times \\ & \times L_{RR} \exp[-t/\tau(\lambda_{RR}, L_{RR})]\end{aligned} \tag{11}$$

Here, $P(\lambda_{RR}, L_{RR})$ is the rare region distribution (8) or (9), depending on the value of γ; and $\tau(\lambda_{RR}, L_{RR})$ denotes the lifetime of the rare region. It can be estimated as follows. As the rare region is locally in the active phase, $\lambda_{RR} > \lambda_c$, it can only decay via an atypical coherent fluctuation of all its sites. The probability for this to happen is exponentially small in the rare region size [10], resulting in an exponentially large life time

$$\tau(\lambda_{RR}, L_{RR}) = t_0 \exp\left[aL_{RR}\right] \tag{12}$$

where t_0 is a microscopic time scale. The coefficient a vanishes at $\lambda_{RR} = \lambda_c$ and increases with increasing λ_{RR}, i.e., the deeper the region is in the active phase, the larger a becomes. Because a has the dimension of an inverse length, it scales as $\xi_{\perp}^{-1}$ (where $\xi_{\perp}$ is the correlation

length) according to finite-size scaling [23],

$$a = a'(\lambda_{RR} - \lambda_c)^{\nu_{0\perp}} \,. \tag{13}$$

Note that $\nu_{0\perp}$ is the *clean* correlation length exponent unless the rare region is very close to criticality (inside the narrow asymptotic critical region) [24].

In the long-time limit $t \gg t_0$, the integral (11) can be solved in saddle-point approximation. The saddle point equations read

$$\frac{\partial}{\partial L_{RR}} \left[\frac{L_{RR}^{\gamma}}{2b^2}(\lambda_{RR} - \bar{\lambda})^2 + \frac{t}{t_0} e^{-a'(\lambda_{RR}-\lambda_c)^{\nu_{0\perp}} L_{RR}} \right] = 0 \,, \tag{14}$$

$$\frac{\partial}{\partial \lambda_{RR}} \left[\frac{L_{RR}^{\gamma}}{2b^2}(\lambda_{RR} - \bar{\lambda})^2 + \frac{t}{t_0} e^{-a'(\lambda_{RR}-\lambda_c)^{\nu_{0\perp}} L_{RR}} \right] = 0 \,, \tag{15}$$

and yield the saddle point values

$$\lambda_{sp} - \lambda_c = \frac{\gamma \nu_{0\perp}}{2 - \gamma \nu_{0\perp}} (\lambda_c - \bar{\lambda}) \,, \tag{16}$$

$$L_{sp} \sim (\lambda_c - \bar{\lambda})^{-\nu_{0\perp}} \ln(t/t_0) \,. \tag{17}$$

Eqs. (14) to (17) apply to the long-range correlated case $\gamma < 1$; the corresponding relations for the short-range correlated case follow by formally setting $\gamma = 1$.

For the method to be valid, λ_{sp} must be within the integration range of the integral (11). The bulk system is in the inactive phase implying $\bar{\lambda} < \lambda_c$. Moreover, the clean correlation length exponent of the one-dimensional contact process takes the value $\nu_{0\perp} \approx 1.097$ [25]. Consequently, the saddle-point value λ_{sp} is larger than λ_c, as required. Inserting the saddle-point values into the integrand yields

$$\rho(t) \sim \exp\left[-\frac{1}{z'} \left(\ln \frac{t}{t_0} \right)^{\gamma} \right] \tag{18}$$

where

$$z' \sim (\lambda_c - \bar{\lambda})^{\gamma\nu_{0\perp}-2} \tag{19}$$

plays the role of a dynamical exponent in the Griffiths phase. In the short-range correlated case, γ is formally 1. Thus, Eq. (18) reproduces the well-known power-law Griffiths singularity of density in this case [10, 11, 12]. In contrast, in the long-range correlated case, $\gamma < 1$, the decay of the density is slower than any power. Long-range disorder correlations thus lead to a qualitatively enhanced Griffiths singularity.

The above derivation started from the correlated Gaussian distribution (4). However, an analogous calculation can be performed for a correlated binary distribution by combining the rare region probability (10) with the rare region life time (12). Solving the resulting integral over L_{RR} in saddle-point approximation leads to the same functional form (18) of the Griffiths singularity, with

$$z' = a^\gamma / c \ . \tag{20}$$

If the rare regions are not in the active phase but right a the critical point, their decay time depends on their size via the power law $\tau(\lambda_c, L_{RR}) \sim L_{RR}^{z_0}$ rather than the exponential (12). Here, $z_0 \approx 1.581$ is the clean dynamical exponent. For a correlated binary disorder distribution, this can be achieved by tuning the stronger of the two infection rates to the clean critical value. Repeating the saddle-point integration for this case gives a stretched exponential density decay

$$\ln \rho(t) \sim -t^{\gamma/(\gamma+z_0)} \ . \tag{21}$$

As before, the short-range correlated case is recovered by formally setting $\gamma = 1$.

Griffiths singularities in other quantities can be derived in an analogous manner. Consider, for example, systems that start from a single active site in an otherwise inactive lattice. In this situation, the central quantity is the survival probability $P_s(t)$ that measures how likely the system is to be still active (i.e., to contain at least one active site) at time

t. For directed percolation problems such as the contact process, the survival probability behaves in the same way as the density of active sites [17]. Thus, the time-dependencies (18) and (21) derived for $\rho(t)$ also hold for $P_s(t)$.

We emphasize that the dependencies of the Griffiths dynamical exponent z' on the distance from criticality given in (19) and (20) hold outside the asymptotic critical region of the disordered contact process. The analysis of the critical region itself requires more sophisticated methods that will be discussed in the next section.

3.3. CRITICAL POINT. After discussing the Griffiths phase, we now turn to the critical point of the disordered contact process itself. The contact process with spatially *uncorrelated* disorder features an exotic infinite-randomness critical point in the universality class of the (uncorrelated) random transverse-field Ising chain [11, 12]. Is this critical point stable or unstable against the long-range power-law disorder correlations (3)? According to Weinrib and Halperin's generalization [26] of the Harris criterion, power-law disorder correlations are irrelevant if the decay exponent γ fulfills the inequality

$$\gamma > 2/\nu_\perp^{unc} \tag{22}$$

where $\nu_\perp^{unc}$ is the correlation length exponent for uncorrelated disorder. If this inequality is violated, the correlations are relevant, and the critical behavior must change. The correlation length exponent of the contact process with uncorrelated disorder takes the value $\nu_\perp^{unc} = 2$ [5, 11]. The long-range correlations are thus irrelevant if $\gamma > 1$ and relevant if $\gamma < 1$. Interestingly, this is the same criterion as we derived for the Griffiths phase in Secs. 3.1 and 3.2.

What is the fate of the transition in the long-range correlated case $\gamma < 1$? As long-range correlations tend to further enhance the disorder effects, we expect the critical behavior to be of infinite-randomness type, but with modified critical exponents that produce stronger singularities. In the strong-disorder regime close to criticality, the behavior of the contact

process is identical to that of a random transverse-field Ising chain as both are governed by the same strong-disorder renormalization group recursion relations [5, 11]. Note that the application of these recursion is justified even in the presence of disorder correlations provided that the distributions of the *logarithms* of μ and λ become infinitely broad. The transverse-field Ising chain with long-range correlated disorder was solved by Rieger and Igloi [15] who mapped the problem onto fractional Brownian motion. They found an exact result for the tunneling exponent ψ which relates correlation length $\xi_\perp$ and correlation time ξ_t via $\ln(\xi_t/t_0) \sim \xi_\perp^\psi$. For $\gamma > 1$, it takes the uncorrelated value $\psi = 1/2$ while it is given by $\psi = 1 - \gamma/2$ for $\gamma < 1$. The correlation length exponent $\nu_\perp$ takes the value 2 for $\gamma > 1$ as for uncorrelated disorder. For $\gamma < 1$, it reads $\nu_\perp = 2/\gamma$ in agreement with general arguments by Weinrib and Halperin [26]. A third exponent is necessary to define a complete set; Rieger and Igloi numerically calculated the scale dimension $\beta/\nu_\perp$ of the order parameter and found it to decay continuously from its uncorrelated value $(3 - \sqrt{5})/4$ (taken for all $\gamma > 1$) to 0 (for $\gamma = 0$).

A qualitative understanding of these results in the context of the contact process can be obtained from simple arguments based on the strong-disorder recursion relations [11] even though a closed form solution of the renormalization group does not exist for the case of long-range correlated disorder [27]. Imagine performing a (large) number of strong-disorder renormalization group steps, iteratively removing the largest decay rates μ_i and infection rates λ_i. The resulting chain will consist of surviving sites (representing clusters of original sites) whose effective decay rate can be estimated as

$$\mu_{\text{eff}} = C_\mu \frac{\mu_1 \dots \mu_L}{\lambda_1 \dots \lambda_{L-1}} \tag{23}$$

and long bonds with effective infection rates

$$\lambda_{\text{eff}} = C_\lambda \frac{\lambda_1 \dots \lambda_L}{\mu_1 \dots \mu_{L-1}} \tag{24}$$

where L is the size of the cluster or bond. In the strong-disorder limit, the prefactors C_μ and C_λ provide subleading corrections only. $\ln \mu_{\text{eff}}$ and $\ln \lambda_{\text{eff}}$ can thus be understood as the displacements of correlated random walks

$$\ln \mu_{\text{eff}} \sim \sum_{i=1}^{L-1} \ln(\mu_i/\lambda_i)\,, \qquad \ln \lambda_{\text{eff}} \sim \sum_{i=1}^{L-1} \ln(\lambda_i/\mu_i)\,. \tag{25}$$

Right at criticality, these random walks have to be (asymptotically) unbiased because healing and infection remain competing in the limit $L \to \infty$. The typical values $\ln \mu_{\text{typ}}$ and $\ln \lambda_{\text{typ}}$ of the cluster healing and infection rates can be estimated from the variance of the random walk displacements giving

$$|\ln \mu_{\text{typ}}| \sim |\ln \lambda_{\text{typ}}| \sim \sqrt{L\,\tilde{G}(L)} \sim \begin{cases} L^{1/2} & (\gamma > 1) \\ L^{1-\gamma/2} & (\gamma < 1) \end{cases} \tag{26}$$

for large L. Here, $\tilde{G}(L)$ is the sum over the disorder correlation function defined in Eq. (7). This estimate thus reproduces the values of ψ quoted above [28].

Moving away from criticality introduces a bias into the random walks. The crossover from critical to off-critical behavior occurs when the displacement due to the bias becomes larger than the displacement (26) due to the randomness. The bias term scales as $|\lambda - \lambda_c|L$. We thus obtain a crossover length

$$L_x \sim \begin{cases} |\lambda - \lambda_c|^{-2} & (\gamma > 1) \\ |\lambda - \lambda_c|^{-2/\gamma} & (\gamma < 1) \end{cases} \tag{27}$$

in agreement with the quoted values of $\nu_\perp$.

4. MONTE-CARLO SIMULATIONS

4.1. OVERVIEW. We now turn to large-scale Monte-Carlo simulations of the one-dimensional contact process with power-law correlated disorder. We use the same numerical implementation of the contact process as in earlier studies with uncorrelated disorder in one, two, three, and five dimensions in Refs. [12, 22, 29, 30]. It is based on an algorithm suggested by Dickman [31]: The simulation starts at time $t = 0$ from an initial configuration of active and inactive sites and consists of a sequence of events. During each event an active site i is chosen at random from a list of all N_a active sites. Then a process is selected, either infection of a neighbor with probability $\lambda_i/(1 + \lambda_i)$ or healing with probability $1/(1 + \lambda_i)$. For infection, either the left or the right neighbor are chosen with probability 1/2. The infection succeeds if this neighbor is inactive. The time is then incremented by $1/N_a$.

Using this algorithm, we have simulated long chains for times up to $t = 10^7$. All production runs use $L = 2^{20} \approx 10^6$ sites with periodic boundary conditions, and the results are averages over large numbers of disorder configurations; precise data will be given below.

The random infection rates λ_i are drawn from a correlated binary distribution in which λ_i can take values λ and $c\lambda$ with overall probabilities $(1 - p)$ and p, respectively. Here, p and c are constants between 0 and 1. To generate these correlated random variables, we employ the Fourier-filtering method [32]. It starts from uncorrelated Gaussian random numbers u_i and turns them into correlated Gaussian random numbers v_i characterized by the (translationally invariant) correlation function $G_\lambda(i, j)$. This is achieved by transforming the Fourier components $\tilde{u}_q$ of the uncorrelated random numbers according to

$$\tilde{v}_q = \left[\tilde{G}(L, q)\right]^{1/2} \tilde{u}_q, \tag{28}$$

where $\tilde{G}(L, q)$ is the Fourier transform of $G_\lambda(i, j)$. We parameterize our long-range correlations by the function

$$G_\lambda(i, j) = \left[1 + (i - j)^2\right]^{-\gamma/2} \tag{29}$$

with periodic boundary conditions using the minimum image convention. Simulations are performed for $\gamma = 1.5, 0.8, 0.6$ and 0.4. To arrive at binary random variables, the correlated Gaussian random numbers v_i then undergo binary projection: the infection rate λ_i takes the value λ ("strong site") if v_i is greater than a composition-dependent threshold and the value $c\lambda$ with $0 < c < 1$ ("weak site") if v_i is less than the threshold. We chose a concentration $p = 0.8$ of weak sites and a strength $c = 0.2$ in all simulations. While the binary projection changes the details of the disorder correlations, the functional form of the long-distance tail remains unchanged.

Most of our simulations are spreading runs that start from a single active site in an otherwise inactive lattice; we monitor the survival probability $P_s(t)$, the number of sites $N_s(t)$ of the active cluster, and its (mean-square) radius $R(t)$. Within the activated scaling scenario [11, 12] associated with an infinite-randomness critical point, these quantities are expected to display logarithmic time dependencies,

$$P_s \sim [\ln(t/t_0)]^{-\bar{\delta}}, \tag{30}$$

$$N_s \sim [\ln(t/t_0)]^{\bar{\Theta}}, \tag{31}$$

$$R \sim [\ln(t/t_0)]^{1/\psi}. \tag{32}$$

The exponents $\bar{\delta}$ and $\bar{\Theta}$ can be expressed in terms of the scale dimension $\beta/\nu_\perp$ of the order parameter and the tunneling exponent ψ as $\bar{\delta} = \beta/(\nu_\perp\psi)$ and $\bar{\Theta} = 1/\psi - 2\bar{\delta}$ [12].

4.2. RESULTS: CRITICAL BEHAVIOR. We start be considering the case $\gamma = 1.5$. According to the theory laid out in Sec. 3, the power-law disorder correlations are irrelevant for $\gamma > 1$. We therefore expect the critical behavior for $\gamma = 1.5$ to be identical to that of the random contact process with uncorrelated disorder which features an infinite-

randomness critical point in the universality class of the (uncorrelated) random transverse-field Ising chain [11, 12]. Its critical exponents are known exactly, their numerical values read $\beta = 0.38197$, $\nu_\perp = 2$, $\psi = 0.5$, $\bar{\delta} = 0.38197$, and $\bar{\Theta} = 1.2360$ [5, 6].

To test these predictions, we analyze the time evolution of P_s, N_s and R in Fig. 1. Specifically, the figure presents plots of $P_s^{-1/\bar{\delta}}$, $N_s^{1/\bar{\Theta}}$ and R^ψ vs. $\ln(t)$ using the theoretically predicted exponent values. In such plots, the critical time dependencies (30) to (32) correspond to straight lines independent of the unknown value of the microscopic time scale t_0. The plots show that the data for infection rate $\lambda = 11.44$ follow the predicted time dependencies (30) to (32) over more than four orders of magnitude in time. We thus identify $\lambda_c = 11.44(6)$ as the critical infection rate (the number in brackets is an estimate of the error of the last digit); and we conclude that the critical behavior for $\gamma = 1.5$ is indeed identical to that of the contact process with uncorrelated disorder.

We now turn to $\gamma < 1$, for which the long-range correlations are expected to change the critical behavior. A complete set of exponents is not known analytically in this case; the data analysis is therefore more complicated than for $\gamma > 1$. As we do have an analytical value for the tunneling exponent, $\psi = 1 - \gamma/2$, we can graph R^ψ vs. $\ln(t)$, to find the critical point. Fig. 2 shows the corresponding plot for $\gamma = 0.4$. The data at $\lambda = 11.6$ follow the predicted time dependence (32) for more than three orders of magnitude in time. We thus identify $\lambda_c = 11.6(2)$ as the critical infection rate. Analogous plots for $\gamma = 0.8$ and 0.6 give infection rates of $\lambda_c = 11.3(2)$ and $\lambda_c = 11.4(2)$, respectively.

Alternatively, we can employ a version of the method used in Refs. [29, 30] that allows us to eliminate the unknown microscopic time scale t_0 from the analysis. It is based on the observation that t_0 takes the same value in all of the quantities (because it is related to the basic energy scale of the underlying renormalization group). Thus, if we plot $N_s(t)$ versus $P_s(t)$, the critical point corresponds to power-law behavior, and t_0 drops out. The same is true for other combinations of observables. Specifically, by combining Eqs. (30), (31) and (32), we see that $N_s/P_s^2 \propto R$ at criticality. Thus, identifying straight lines in

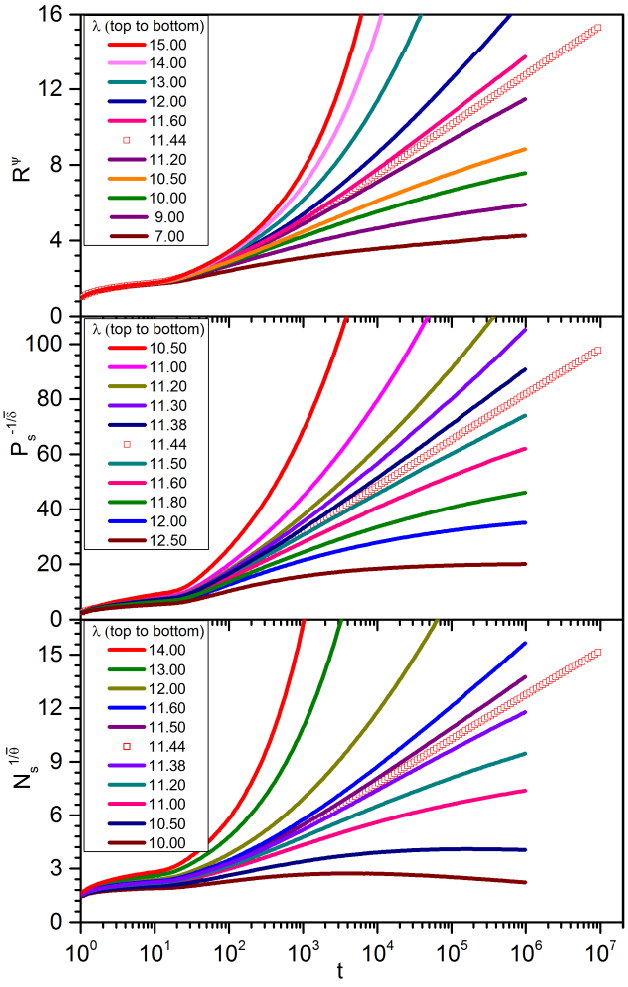

Fig. 1. Time evolution of the number of active sites N_s, the survival probability P_s, and the radius of the active cloud R for the disordered contact process with power-law disorder correlations characterized by a decay exponent $\gamma = 1.5$. The data are averages over up to 40000 samples with 100 individual runs per sample. The critical exponents are fixed at their uncorrelated values $\psi = 0.5$, $\bar{\delta} = 0.38197$, and $\bar{\Theta} = 1.2360$.

plots of N_s/P_s^2 versus R allows us to find the critical point without needing a value for t_0. Fig. 3 shows such a plot for $\gamma = 0.8$; and we have created analogous plots of $\gamma = 0.6$ and 0.4. They give the same critical infection rates, $\lambda_c = 11.3(2)$ (for $\gamma = 0.8$), $\lambda_c = 11.4(2)$ (for $\gamma = 0.6$), and $\lambda_c = 11.6(2)$ (for $\gamma = 0.4$) as the plots of R^ψ vs. $\ln(t)$. Interestingly, within their numerical errors, λ_c does not depend on the decay exponent γ of the disorder correlations.

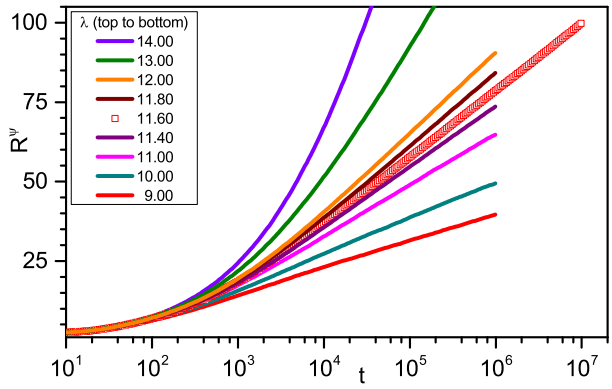

Fig. 2. Time evolution of the radius of the active cloud R for $\gamma = 0.4$. The data are averages over about 30000 samples with 100 individual runs per sample. The tunneling exponent is set to its analytical value $\psi = 1 - \gamma/2 = 0.8$.

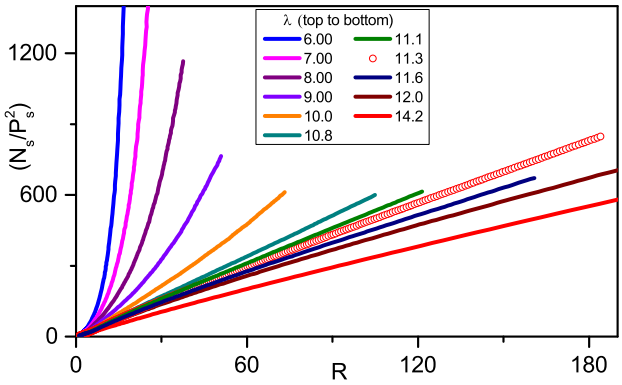

Fig. 3. N_s/P_s^2 vs. R for a correlation decay exponent $\gamma = 0.8$. The data are averages over about 20000 samples with 100 individual runs per sample. The maximum time is 10^6 for all curves except the critical one, $\lambda = 11.3$, for which it is 10^7.

Once the critical point is identified, we can verify and/or find critical exponents by analyzing the time evolutions of P_s, N_s and R. Fig. 4 displays $P_s^{-1/\bar{\delta}}$, $N_s^{1/\bar{\Theta}}$ and R^{ψ} versus $\ln(t)$ at criticality for $\gamma = 0.8$. The tunneling exponent ψ is set to its theoretical value $1 - \gamma/2$ while $\bar{\delta}$ and $\bar{\Theta}$ are determined from the data by requiring that the corresponding curves become straight lines for large times. The data follow the predicted logarithmic time dependencies (30), (31) and (32) over about four orders of magnitude in time. This not only

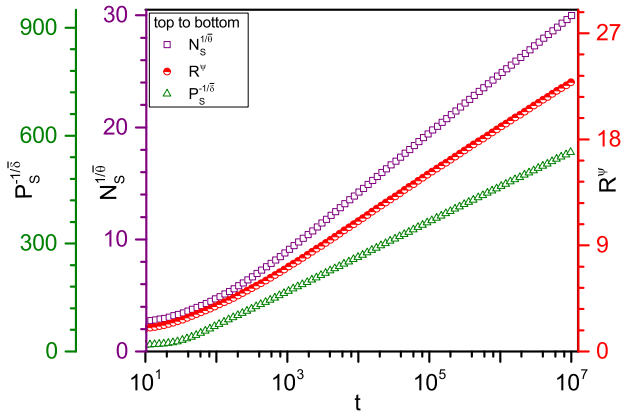

Fig. 4. $N_s^{1/\bar{\Theta}}$, $P_s^{-1/\bar{\delta}}$, and R^{ψ} versus $\ln(t)$ at criticality for a correlation decay exponent $\gamma = 0.8$. Here, $\psi = 0.6$ is set to its theoretical value while $\bar{\delta} = 0.269$ and $\bar{\Theta} = 0.982$ are determined from the data by requiring that the corresponding curves become straight lines for large times.

confirms the theoretical value of ψ, it also allows us to extract estimates the scale dimension $\beta/\nu_\perp$ of the order parameter from both $\bar{\delta}$ and $\bar{\Theta}$. We have performed the same analysis also for $\gamma = 0.6$ and $\gamma = 0.4$.

The resulting exponent values are summarized in Table 1. The uncertainty of $\bar{\delta}$ and $\bar{\Theta}$ can be roughly estimated from the hyperscaling relation $\bar{\Theta} + 2\bar{\delta} = 1/\psi$. The exponents for $\gamma = 0.6$ and $\gamma = 0.4$ fulfill this relation in good approximation (less than 4% difference between the left and the right sides). For $\gamma = 0.8$, the agreement is not quite as good. As $\gamma = 0.8$ is close to the marginal value of 1, this may be caused by a slow crossover from the short-range correlated fixed point to the long-range correlated one.

The values of the scale dimension of the order parameter, $\beta/\nu_\perp$, are in reasonable agreement with those calculated by Rieger and Igloi from the average persistence of a Sinai random walker (see inset of Fig. 1 of Ref. [15]).

To obtain a complete set of exponents, we also analyze off-critical data. Fig. 5 shows a double-logarithmic plot of P_s vs. R for decay exponent $\gamma = 0.8$.

Table 1. Critical exponents of the one-dimensional contact process with power-law correlated disorder. The exponents $\nu_\perp$ and ψ (above the horizontal line) are known analytically, as are all exponents in the short-range case $\gamma > 1$. The exponents $\bar{\delta}$ and $\bar{\Theta}$ for $\gamma < 1$ stem from fits of our data. The scale dimension $\beta/\nu_\perp$ of the order parameter can be extracted from both $\bar{\delta}$ and $\bar{\Theta}$, the data in the table are averages of the two values.

exponent	$\gamma > 1$	$\gamma = 0.8$	$\gamma = 0.6$	$\gamma = 0.4$
$\nu_\perp$	2	2.5	3.33	5
ψ	0.5	0.6	0.7	0.8
$\bar{\delta}$	0.3820	0.27	0.20	0.13
$\bar{\Theta}$	1.2360	0.98	0.98	1.01
$\beta/\nu_\perp$	0.1910	0.18	0.14	0.10

The plot allows us to determine the crossover radius R_x at which the survival probability of slightly off-critical curves has dropped to half of its critical value. According to scaling, the crossover radius must depend on the distance from criticality via $R_x \sim |\lambda - \lambda_c|^{-\nu_\perp}$. The inset of Fig. 5 shows that our data indeed follow this power law with the predicted exponent $\nu_\perp = 2/\gamma = 2.5$.

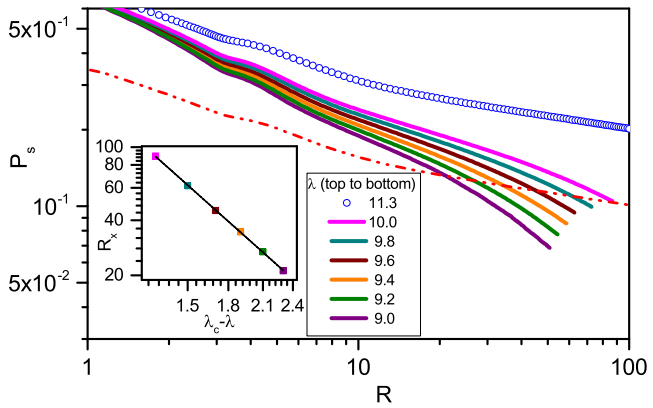

Fig. 5. Double-log plot of P_s vs. R for decay exponent $\gamma = 0.8$ and several infection rates λ at and below the critical rate $\lambda_c = 11.3$. The dash-dotted line shows $P_s/2$ for $\lambda = \lambda_c$. The crossing points of the dash-dotted line with the off-critical data determines the crossover radius R_x. Inset: R_x vs. $|\lambda - \lambda_c|$. The solid line is a power-law fit to $R_x \sim |\lambda - \lambda_c|^{-\nu_\perp}$ with an exponent $\nu_\perp = 2.5$.

4.3. RESULTS: GRIFFITHS PHASE. We now turn to the Griffiths phase $\lambda_{c0} \leq \lambda < \lambda_c$ where $\lambda_{c0} \approx 3.298$ is the critical infection rate of the clean contact process containing only "strong" sites ($p = 0$).

Right at the clean critical point, $\lambda = \lambda_{c0}$, the time evolution of the survival probability is predicted to follow the stretched exponential (21) in the long-time limit. Our corresponding data for $\gamma = 0.8$, 0.6, and 0.4 are plotted in Fig. 6. For all γ, the data indeed follow stretched exponentials over more than six orders of magnitude in P_s. The exponent y decreases with decreasing γ, as predicted in (21). The actual numerical values of y are somewhat larger than the prediction $y = \gamma/(\gamma + z_0)$. We attribute this to the fact that, due to the rapid decay of P_s, the data are taken at rather short times ($t \lessapprox 10^3$). Thus, they probably have not reached the true asymptotic regime, yet.

We now move into the bulk of the Griffiths phase, $\lambda_{c0} < \lambda < \lambda_c$. Here, we wish to contrast the conventional power-law Griffiths singularity with the unusual non-power-law form (18). Fig. 7 shows the survival probability as a function of time for a decay exponent $\gamma = 1.5$ and several infection rates inside the Griffiths phase. After initial transients, all

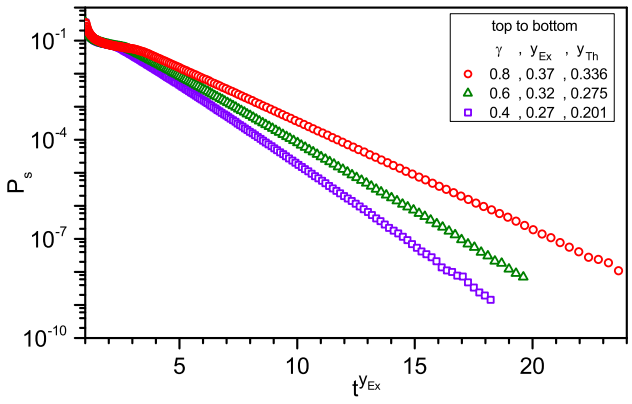

Fig. 6. Time evolution of the survival probability P_s at the clean critical infection rate $\lambda_{c0} = 3.298$ for decay exponents $\gamma = 0.8$, 0.6, and 0.4. The data are averages over 2×10^4 to 10^5 samples with at least 10^4 individual runs per sample. The experimental values y_{Ex} are determined by requiring that the respective curves become straight lines for large times, implying a stretched exponential time dependence, $\ln P_s \sim t^y$. The theoretical values follow from Eq. (21) which gives $y_{Th} = \gamma/(\gamma + z_0)$.

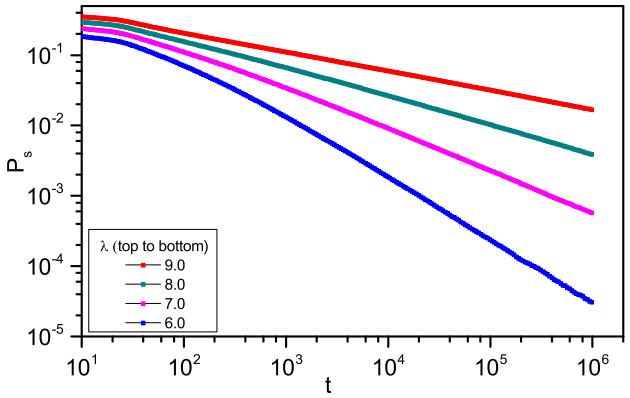

Fig. 7. Double-log plot of the survival probability P_s vs. time t for decay exponent $\gamma = 1.5$ at several infection rates inside the Griffiths phase, $\lambda_{c0} < \lambda < \lambda_c$. The data are averages over up to 40000 samples with 100 individual runs per sample.

data follow power laws (represented by straight lines) over serval orders of magnitude in P_s and/or t. For $\gamma = 1.5$, we thus find the same type of power-law Griffiths singularity as in the case of uncorrelated or short-range correlated disorder.In the long-range correlated regime, $\gamma < 1$, we expect the survival probability to follow Eq. (18) rather than a power-law. This prediction is tested in Fig. 8 which shows of P_s vs. t for decay exponent $\gamma = 0.4$.

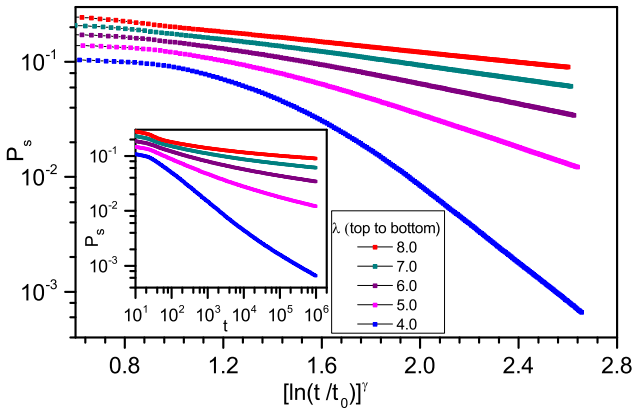

Fig. 8. Survival probability P_s vs. time t for decay exponent $\gamma = 0.4$ at several infection rates inside the Griffiths phase, $\lambda_{c0} < \lambda < \lambda_c$, plotted such that Eq. (18) yields straight lines (the values of t_0 are fit parameters). The data are averages over up to 20000 samples with 100 individual runs per sample. Inset: Double-log plot of the same data to test for power-law behavior.

In the double-logarithmic plot in the inset, all data show pronounced upward curvatures rather than the straight lines expected for power laws. In contrast, when plotted as $\ln P_s$ vs. $[\ln(t/t_0)]^\gamma$ (where t_0 is a fit parameter) in the main panel of the figure, all curves become straight for sufficiently long times implying that the long-time behavior of P_s indeed follows Eq. (18).

We have produced analogous plots for decay exponents $\gamma = 0.6$ and 0.8. As γ decreases from 1 towards 0, the upward curvature in the double-logarithmic plots becomes bigger, reflecting stronger and stronger deviations from power-law behavior, as expected. In contrast, Eq. (18) describes the long-time behavior of all data very well, confirming our theory.

5. GENERALIZATIONS

5.1. HIGHER DIMENSIONS. It this section, we generalize our results to the contact process in higher dimensions $d > 1$. The theory of Sec. 3.1 can be easily adapted, yielding the rare-region distribution

$$P(\lambda_{RR}, L_{RR}) \sim \begin{cases} \exp\left[-\dfrac{1}{2b^2}\, L_{RR}^d\, (\lambda_{RR} - \bar{\lambda})^2\right] & (\gamma > d) \\ \exp\left[-\dfrac{1}{2b^2}\, L_{RR}^\gamma\, (\lambda_{RR} - \bar{\lambda})^2\right] & (\gamma < d) \end{cases} . \tag{33}$$

This means that the functional form of the rare-region distribution is identical to the case of uncorrelated disorder as long as $\gamma > d$. For $\gamma < d$, the probability for finding a rare-region decays more slowly with its size. In terms of the volume L_{RR}^d, it is given by a stretched exponential rather than a simple one.

Using this result, we now repeat the calculation of Sec. 3.2 for general d. For $\gamma < d$, the resulting long-time behavior of the density of active sites in the Griffiths phase reads

$$\rho(t) \sim \exp\left[-\frac{d}{z'}\left(\ln\frac{t}{t_0}\right)^{\gamma/d}\right] \tag{34}$$

with

$$z' \sim d(\lambda_c - \bar{\lambda})^{\gamma\nu_{0\perp}-2} \tag{35}$$

As in one dimension, the decay described by Eq. (34) is slower than any power. For $\gamma > d$, in contrast, we find the usual power-law behavior. Eq. (34) also holds for a correlated binary distribution with $z' = d\, a^{\gamma/d}/c$. The behavior right at the boundary of the Griffiths phase (when the stronger of the two infection rates of the binary distribution is tuned to the clean critical value) takes the form (21) for all dimensions.

The behavior of the critical point itself will again be of infinite-randomness type, but for a sufficiently small correlation decay exponent $\gamma < 2/\nu_\perp^{unc}$, the critical exponents will differ from those of the contact process with uncorrelated disorder (which were found numerically in Ref. [29] for two dimensions and in Ref. [30] for three dimensions). The correlation length exponent will take the value $\nu_\perp = 2/\gamma$ [26]; other exponents need to be found numerically [15].

It is interesting to compare the relevance criteria of the long-range correlations in the Griffiths phase and at the critical point. In one dimension, the long-range correlations become relevant for $\gamma < 1$ both in the Griffiths phase and at criticality (because the correlation length exponent of the one-dimensional contact process with uncorrelated disorder has the value $\nu_\perp^{unc} = 2$, saturating the Harris criterion). In dimensions $d > 1$, the two criteria differ. The uncorrelated correlation length exponent is larger than $2/d$ [29, 30]. Thus, the long-range correlations do not become relevant for $\gamma < d$ but only if $\gamma < 2/\nu_\perp^{unc} < d$. In contrast, the long-range correlations become relevant for $\gamma < d$ in the Griffiths phase. Consequently, for $d > 1$, we expect a (narrow) range of decay exponents γ for which the long-range correlations are relevant in the Griffiths phase but irrelevant at criticality. The fate of the system in this subtle regime remains a task for the future.

5.2. OTHER SYSTEM. The theory of Secs. 3.1 and 3.2 and its generalization to higher dimensions have produced enhanced *non-power-law* Griffiths singularities for sufficiently long-ranged disorder correlations. Are these results restricted to the contact

process or do they apply to other systems as well? In this section, we show that they hold for a broad class of systems in which the charateristic energy or inverse time scale of a rare region depends exponentially on its volume (class B of the rare region classification of Refs. [14, 33]). In addition to the contact process, this class contains, e.g., the random transverse-field Ising model, Hertz' model of the itinerant antiferromagnetic quantum phase transition, and the pair-breaking superconductor-metal quantum phase transition.

To demonstrate the enhanced Griffiths singularities, we generalize the calculation of the rare region density of states developed in Ref. [21] to the case of our power-law correlated disorder. Consider a disordered system with rare regions whose characteristic energy ϵ depends on their volume via

$$\epsilon(\lambda_{RR}, L_{RR}) = \epsilon_0 \exp[-a L_{RR}^d] \; . \tag{36}$$

Here, ϵ_0 is a microscopic energy scale, and $a = a'(\lambda_{RR} - \lambda_c)^{d\nu_{0\perp}}$ with λ representing the parameter that tunes the system through the phase transition. In the contact process, $\epsilon = 1/\tau$ is the inverse life time of a rare region; in the transverse-field Ising model, it represents its energy gap. We can derive a rare-region density of states by summing over all values of λ_{RR} and L_{RR},

$$\tilde{\rho}(\epsilon) \sim \int_{\lambda_c}^{\infty} \int_0^{\infty} dL_{RR}\, P(\lambda_{RR}, L_{RR})\, \delta[\epsilon - \epsilon(\lambda_{RR}, L_{RR})] \tag{37}$$

with the Gaussian rare-region probability $P(\lambda_{RR}, L_{RR})$ from Eq. (33). After carrying out the integral over L_{RR} with the help of the δ function, the remaining λ_{RR}-integral can be performed in saddle-point approximation in the limit $\epsilon \to 0$. For $\gamma < d$, the resulting density of states takes the form

$$\tilde{\rho}(\epsilon) \sim \frac{1}{\epsilon} \exp\left[-\frac{d}{z'}\left(\ln\frac{\epsilon_0}{\epsilon}\right)^{\gamma/d}\right] \tag{38}$$

with z' given by Eq. (35). For $\gamma > d$, in contrast, we recover the usual power-law behavior $\tilde{\rho}(\epsilon) \sim \epsilon^{d/z'-1}$. If we start from correlated binary disorder rather than a Gaussian distribution, we arrive at the same expression (38) for the density of states with $z' = da^{\gamma/d}/c$. Eq. (38) shows that the Griffiths singularities are qualitatively enhanced for $\gamma < d$ as the density of states diverges as $1/\epsilon$ times a function that is slower than any power law.

Griffiths singularities in other observables can be calculated from appropriate integrals of $\tilde{\rho}(\epsilon)$. For example, our results for the density of active sites in the contact process can be reproduced by $\rho(t) \sim \int d\epsilon\, \tilde{\rho}(\epsilon) \exp(-\epsilon t)$. In the case of the random transverse-field Ising model, we can calculate (see, e.g., Ref. [14]) the temperature dependence of observables such as the entropy $S(T) \sim \int_0^T d\epsilon \tilde{\rho}(\epsilon)$, the specific heat $C(T) = T(\partial S/\partial T)$, and the susceptibility $\chi(T) \sim (1/T) \int_0^T d\epsilon \tilde{\rho}(\epsilon)$. For $\gamma < d$, we find

$$S(T) \sim C(T) \sim T\chi(T) \sim \exp\left[-\frac{d}{z'}\left(\ln\frac{\epsilon_0}{T}\right)^{\gamma/d}\right] . \tag{39}$$

Analogously, the magnetization in a longitudinal field H scales as

$$M(H) \sim \exp\left[-\frac{d}{z'}\left(\ln\frac{\epsilon_0}{H}\right)^{\gamma/d}\right] . \tag{40}$$

Let us compare these results with those obtained in Ref. [15]. Eq. (38), (39), and (40) yield Griffiths singularities that are qualitatively stronger than power laws. In contrast, Rieger and Igloi obtained the usual power-law Griffiths singularities, albeit with changed exponents. We believe that this discrepancy arises from the fact that Rieger and Igloi assumed that the probability for finding a strongly coupled cluster of size L_{RR} in d dimensions takes the same functional form, $\exp(-cL_{RR}^d)$, as for uncorrelated disorder. Our calculations show that this assumption is justified for $\gamma > d$. For $\gamma < d$, however, the rare region probability decays as $\exp(-cL_{RR}^\gamma)$, i.e., more slowly than in the uncorrelated case.

6. CONCLUSIONS

To summarize, we have studied the effects of long-range spatial disorder correlations on the critical behavior and the Griffiths singularities in the disordered one-dimensional contact process. As long as the correlations decay faster as $1/r_{ij}$ with the distance r_{ij} between the sites, the correlations are irrelevant both at criticality and in the Griffiths phase. This means that both the critical and the Griffiths singularities are identical to those of the contact process with uncorrelated disorder. If the correlations decay more slowly than $1/r_{ij}$, the universality class of the critical point changes, and the Griffiths singularities take an enhanced, non-power-law form.

What is the reason for the enhanced singularities? As positive spatial correlations imply that neighboring sites have similar infection rates, it is intuitively clear that sufficiently long-ranged correlations must increase the probability for finding large atypical regions. This is borne out in our calculations in Sec. 3.1: If the disorder correlations decay more slowly than $1/r_{ij}$, the probability for finding a rare region behaves as a stretched exponential of its size (rather than the simple exponential found for uncorrelated and short-range correlated disorder). Note that similar stretched exponentials have also been found in the distributions of rare events in long-range correlated time series [34, 35].

Our theory of the Griffiths phase is easily generalized to higher dimensions. In general dimension d, the rare-region probability decays exponentially with the rare-region volume as long as the disorder correlations decay faster than $1/r_{ij}^d$. As a result, the Griffiths singularities take the usual power-law form. For correlations decaying slower than $1/r_{ij}^d$, the rare region probability becomes a stretched exponential of the volume, leading to enhanced, non-power-law Griffiths singularities.

Moreover, as shown in Sec. 5.2, the theory is not restricted to the contact process. It holds for all systems for which the characteristic energy (or inverse time) of a rare region depends exponentially on its volume, i.e., for all systems in class B of the rare region classification of Refs. [14, 33]. The random transverse-field Ising model is a prototypical

example in the class. Our theory predicts that the character of its Griffiths singularities changes from the usual power-law behavior for correlations decaying faster than $1/r_{ij}^d$ to the enhanced non-power-law forms (39) and (40) for correlations decaying slower than $1/r_{ij}^d$.

What about systems in the other classes, class A and class C, of the rare region classification of Refs. [14, 33]? The rare regions in systems belonging to class A have characteristic energies that decrease as a power of their sizes. Using this power-law dependence rather than the exponential (36) in the calculation of Sec. 5.2 yields an exponentially small density of states. We conclude that rare regions effects in class A remain very weak, even in the presence of long-range disorder correlations. Rare regions in systems belonging to class C can undergo the phase transition by themselves, independently from the bulk system. This results in a smearing of the global phase transition. Svoboda et al. [36] considered the effects of spatial disorder correlations on such smeared phase transitions. They found that even short-range correlations can have dramatic effects and qualitatively change the behavior of observable quantities compared to the uncorrelated case. This phenomenon may have been observed in $Sr_{1-x}Ca_xRuO_3$ [37].

ACKNOWLEDGEMENTS

This work was supported by the NSF under Grant Nos. DMR-1205803 and PHYS-1066293. We acknowledge the hospitality of the Aspen Center for Physics.

REFERENCES

[1] G. Grinstein. Phases and phase transitions of quneched disordered systems. In E. G. D. Cohen, editor, *Fundamental Problems in Statistical Mechanics VI*, page 147. Elsevier, New York, 1985.

[2] R. B. Griffiths. Nonanalytic behavior above the critical point in a random Ising ferromagnet. *Phys. Rev. Lett.*, 23:17, 1969.

[3] B. M. McCoy. Incompleteness of the critical exponent description for ferromagnetic systems containing random impurities. *Phys. Rev. Lett.*, 23:383, 1969.

[4] Y. Imry. Griffiths singularity in finite macroscopically large dilute Ising models. *Phys. Rev. B*, 15:4448, 1977.

[5] D. S. Fisher. Random transverse field Ising spin chains. *Phys. Rev. Lett.*, 69:534, 1992.

[6] D. S. Fisher. Critical behavior of random transverse-field Ising spin chains. *Phys. Rev. B*, 51:6411, 1995.

[7] M. Thill and D. A. Huse. Equilibrium behaviour of quantum Ising spin glass. *Physica A*, 214:321, 1995.

[8] A. P. Young and H. Rieger. Numerical study of the random transverse-field Ising spin chain. *Phys. Rev. B*, 53:8486, 1996.

[9] Partial results on the related McCoy-Wu model had already been obtained much earlier [38, 39] but they were only fully understood after Fisher's strong-disorder renormalization group calculation [5, 6].

[10] A. J. Noest. New universality for spatially disordered cellular automata and directed percolation. *Phys. Rev. Lett.*, 57:90, 1986; Power-law relaxation of spatially disordered stochastic automata and directed percolation. *Phys. Rev. B*, 38:2715, 1988.

[11] J. Hooyberghs, F. Iglói, and C. Vanderzande. Strong-disorder fixed point in absorbing-state phase transitions. *Phys. Rev. Lett.*, 90:100601, 2003; Absorbing state phase transitions with quenched disorder. *Phys. Rev. E*, 69:066140, 2004.

[12] T. Vojta and M. Dickison. Critical behavior and Griffiths effects in the disordered contact process. *Phys. Rev. E*, 72:036126, 2005.

[13] T. Vojta. Disorder-induced rounding of certain quantum phase transitions. *Phys. Rev. Lett.*, 90:107202, 2003; Smearing of the phase transition in Ising systems with planar defects. *J. Phys. A*, 36:10921, 2003; Broadening of a nonequilibrium phase transition by extended structural defects. *Phys. Rev. E*, 70:026108, 2004.

[14] T. Vojta. Rare region effects at classical, quantum, and non-equilibrium phase transitions. *J. Phys. A*, 39:R143, 2006; Quantum Griffiths effects and smeared phase transitions in metals: theory and experiment. *J. Low Temp. Phys.*, 161:299, 2010.

[15] H. Rieger and F. Igloi. Random quantum magnets with long-range correlated disorder: Enhancement of critical and Griffiths-McCoy singularities. *Phys. Rev. Lett.*, 83:3741, 1999.

[16] T. E. Harris. Contact interactions on a lattice. *Ann. Prob.*, 2:969, 1974.

[17] P. Grassberger and A. de la Torre. *Ann. Phys. (NY)*, 122:373, 1979.

[18] H. K. Janssen. *Z. Phys. B*, 42:151, 1981.

[19] P. Grassberger. *Z. Phys. B*, 47:365, 1982.

[20] The negative tail of the Gaussian has to be truncated appropriately because the infection rate λ_i must be positive.

[21] Thomas Vojta and José A. Hoyos. Criticality and quenched disorder: Harris criterion versus rare regions. *Phys. Rev. Lett.*, 112:075702, Feb 2014.

[22] Thomas Vojta, John Igo, and José A. Hoyos. Rare regions and griffiths singularities at a clean critical point: The five-dimensional disordered contact process. *Phys. Rev. E*, 90:012139, Jul 2014.

[23] M. N. Barber. Finite-size scaling. In C. Domb and J. L. Lebowitz, editors, *Phase Transitions and Critical Phenomena*, volume 8, pages 145–266. Academic, New York, 1983.

[24] The scaling behavior of a also follows from the fact that the term aL_{RR} in the exponent of (12) represents the number $(L_{RR}/\xi_\perp)$ of independent correlation volumes that need to decay coherently.

[25] I. Jensen. Low-density series expansions for directed percolation: I. a new efficient algorithm with applications to the square lattice. *J. Phys. A*, 32:5233, 1999.

[26] Abel Weinrib and B. I. Halperin. Critical phenomena in systems with long-range-correlated quenched disorder. *Phys. Rev. B*, 27:413–427, Jan 1983.

[27] This mainly stems from the fact that the strong-disorder renormalization group cannot be formulated in terms of single-site distributions if the disorder is long-range correlated.

[28] Note that this argument is not rigorous as it neglects the subtle correlations involved in picking which μ_i or λ_i to decimate in the strong-disorder renormalization group step.

[29] T. Vojta, A. Farquhar, and J. Mast. Infinite-randomness critical point in the two-dimensional disordered contact process. *Phys. Rev. E*, 79:011111, 2009.

[30] Thomas Vojta. Monte carlo simulations of the clean and disordered contact process in three dimensions. *Phys. Rev. E*, 86:051137, Nov 2012.

[31] R. Dickman. Reweighting in nonequilibrium simulations. *Phys. Rev. E*, 60:R2441, 1999.

[32] H. A. Makse, S. Havlin, M. Schwartz, and H. E. Stanley. Method for generating long-range correlations for large systems. *Phys. Rev. E*, 53:5445–5449, 1996.

[33] T. Vojta and J. Schmalian. Quantum Griffiths effects in itinerant Heisenberg magnets. *Phys. Rev. B*, 72:045438, 2005.

[34] Armin Bunde, Jan F. Eichner, Jan W. Kantelhardt, and Shlomo Havlin. Long-term memory: A natural mechanism for the clustering of extreme events and anomalous residual times in climate records. *Phys. Rev. Lett.*, 94:048701, Jan 2005.

[35] Eduardo G. Altmann and Holger Kantz. Recurrence time analysis, long-term correlations, and extreme events. *Phys. Rev. E*, 71:056106, May 2005.

[36] C. Svoboda, D. Nozadze, F. Hrahsheh, and T. Vojta. Disorder correlations at smeared phase transitions. *EPL (Europhysics Letters)*, 97(2):20007, 2012.

[37] L. Demkó, S. Bordács, T. Vojta, D. Nozadze, F. Hrahsheh, C. Svoboda, B. Dóra, H. Yamada, M. Kawasaki, Y. Tokura, and I. Kézsmárki. Disorder promotes ferromagnetism: Rounding of the quantum phase transition in $Sr_{1-x}Ca_xRuO_3$. *Phys. Rev. Lett.*, 108:185701, May 2012.

[38] B. M. McCoy and T. T. Wu. Random impurities as the cause of smooth specific heats near the critical temperature. *Phys. Rev. Lett.*, 21:549, 1968.

[39] B. M. McCoy and T. T. Wu. Theory of a two-dimensional Ising model with random impurities. i. thermodynamics. *Phys. Rev.*, 176:631, 1968.

II. EMERGING CRITICAL BEHAVIOR AT A FIRST-ORDER PHASE TRANSITION ROUNDED BY DISORDER

Ahmed K. Ibrahim and Thomas Vojta

Department of Physics, Missouri University of Science and Technology, Rolla, MO 65409, USA

ABSTRACT[*]

We investigate the two-dimensional four-color Ashkin-Teller model by means of large-scale Monte-Carlo simulations. We demonstrate that the first-order phase transition of the clean system is destroyed by random disorder introduced via site dilution. The critical behavior of the emerging continuous transition belongs to the clean two-dimensional Ising universality class, apart from logarithmic corrections. These results confirm perturbative renormalization-group predictions; they also agree with recent findings for the three-color case, indicating that the critical behavior is universal.

[*]Published in Fortschritte der Physik 65, 1600018 (2017).

1. INTRODUCTION

At a first-order phase transition, two distinct thermodynamic phases have the same free energy density and thus coexist macroscopically. Is such phase coexistence still possible if the system contains random disorder that locally favors one phase over the other (so-called random-T_c or random-mass disorder)? Building on earlier work for random fields [1], Imry and Wortis [2] compared the possible free-energy gain from forming a domain that takes advantage of the disorder with the free-energy cost of its domain wall. They found that the formation of finite-size domains is favored in dimensions $d \leq 2$, even for arbitrarily weak disorder. (If the randomness breaks a continuous symmetry, the marginal dimension is $d = 4$.) This destroys the macroscopic phase coexistence and with it the first-order phase transition. After further work [3], this result was rigorously proven by Aizenman and Wehr [4].

What happens to a system whose first-order phase transition is unstable against disorder? Is there an intermediate phase? Is the transition completely destroyed by smearing; or does it become continuous? If the latter, in what universality class is the emerging critical point?

The effects of disorder on first-order phase transitions have received less attention than the corresponding effects on continuous transitions (see, e.g., Refs. [5, 6] for reviews). As a result, the above questions are still being debated even for simple model systems such as the two-dimensional Ashkin-Teller model. The classical N-color Ashkin-Teller model [7, 8, 9, 10] is made up of N Ising models that are coupled via four-spin interactions. For more than two colors ($N > 2$), the clean Ashkin-Teller model undergoes a first-order phase transition from a magnetically ordered phase at low temperatures to a paramagnetic phase at high temperatures.

In two dimensions, the first-order transition cannot survive in the presence of disorder; the two-dimensional N-color Ashkin-Teller model is thus a prototypical system for studying the questions posed above. Perturbative renormalization group calculations

[11, 12, 13] predict that disorder rounds the first-order transition of the clean-Ashkin-Teller model to a continuous one which, somewhat surprisingly, is in the *clean* Ising universality class with additional logarithmic corrections to scaling. Early numerical simulations [14, 15] of small systems reported nonuniversal critical behavior. However, a recent high-accuracy study [16] of the disordered three-color Ashkin-Teller model provided strong evidence in favor of the scenario predicted by the perturbative renormalization group [11, 12, 13].

In the present paper, we test the universality of the emerging critical behavior in the disordered Ashkin-Teller model by studying the four-color case and comparing it to the existing simulations for three colors as well as the renormalization group findings. Specifically, we report results of large-scale Monte Carlo simulations of the site-diluted two-dimensional four-color Ashkin-Teller model with up to 2240^2 sites. The paper is organized as follows. In Sec. 2, we introduce the model and summarize the predictions of the perturbative renormalization group. Sec. 3 is devoted to the Monte-Carlo simulation results. We summarize and conclude in Sec. 4.

2. DILUTED ASHKIN-TELLER MODEL

The two-dimensional N-color Ashkin-Teller model [8, 9, 10] is defined on a square lattice of L^2 sites. Each lattice site i contains N Ising spins $S_i^\alpha = \pm 1$, distinguished by the "color"-index $\alpha = 1 \ldots N$. In the absence of disorder, the Hamiltonian reads

$$H = -J \sum_{\alpha=1}^{N} \sum_{\langle ij \rangle} S_i^\alpha S_j^\alpha - \epsilon J \sum_{\alpha<\beta} \sum_{\langle ij \rangle} S_i^\alpha S_j^\alpha S_i^\beta S_j^\beta \ . \tag{1}$$

It can be understood as N identical Ising models that are coupled via their energy densities. $\langle ij \rangle$ denotes the sum over pairs of nearest neighbor sites on the lattice; $J > 0$ is a ferromagnetic interaction; and $\epsilon \geq 0$ parameterizes the strength of the inter-color coupling. The clean two-color model (the original model proposed by Ashkin and Teller [7]) undergoes a

continuous phase transition from a magnetically ordered (Baxter) phase at low temperatures to a paramagnetic phase at high temperatures. In the Baxter phase, the spins of each color order ferromagnetically w.r.t. each other but the relative orientation of the colors is arbitrary (see, e.g., Ref. [17]). The critical behavior of the two-color model is nonuniversal, i.e., the critical exponents change continuously with ϵ. We are interested in the case of three or more colors for which the phase transition between the paramagnetic and Baxter phases is of first order [8, 9, 10].

We introduce quenched disorder into the Hamiltonian (1) by means of site dilution. This means, a fraction p of the lattice sites are randomly replaced by vacancies on which the spins S_i^α for all colors are removed. Site dilution is a microscopic realization of random-T_c or random mass disorder, i.e., disorder that locally favors one phase over the other but does not break any of the spin symmetries.

Murthy [11] and Cardy [12, 13] studied the phase transition of the N-color Ashkin-Teller model with random-T_c disorder by means of a perturbative renormalization group. They found that the renormalization group flow on the critical (ϵ, Δ)-surface asymptotically approaches the clean Ising fixed point $\epsilon = 0, \Delta = 0$. (Here, Δ is a measure of the disorder strength.) This implies a continuous transition that is, surprisingly, in the clean 2D Ising universality class, apart from logarithmic corrections analogous to those occurring in the disordered Ising model [18, 19, 20, 21]. The following finite-size scaling behavior has been derived [22, 23, 24]. At criticality ($T = T_c$), the specific heat shows a characteristic double-logarithmic dependence on the system size,

$$C \sim \ln \ln L \, . \tag{2}$$

Magnetization and susceptibility at T_c (averaged over all N colors) behave as

$$M \sim L^{-\beta/\nu} \left(1 + b_M / \ln L\right), \tag{3}$$

$$\chi \sim L^{\gamma/\nu}\,(1 + b_\chi/\ln L)\,, \tag{4}$$

where $\gamma/\nu = 7/4$ and $\beta/\nu = 1/8$ as in the clean Ising model, and b_M and b_χ are constant. Any quantity R of scale dimension zero behaves as

$$R = R^*\,(1 + b_R/\ln L)\,, \tag{5}$$

$$dR/dT \sim L^{1/\nu}(\ln L)^{-1/2}\,[1 + O(1/(\ln L))] \tag{6}$$

with the clean Ising exponent $\nu = 1$. The finite-size scaling forms (5) and (6) hold for the Binder cumulants

$$g_{\rm av} = \left[1 - \frac{\langle m^4\rangle}{3\langle m^2\rangle^2}\right]_{\rm dis}\,, \quad g_{\rm gl} = 1 - \frac{[\langle m^4\rangle]_{\rm dis}}{3[\langle m^2\rangle]^2_{\rm dis}}\,. \tag{7}$$

Here, $\langle\ldots\rangle$ denotes the thermodynamic (Monte-Carlo) average while $[\ldots]_{\rm dis}$ stands for the disorder average. We need to distinguish average and "global" versions of this quantity, depending on when the disorder average is performed. The scaling forms (5) and (6) also hold for the correlation length ratios $\xi_{\rm av}/L$ and $\xi_{\rm gl}/L$. In our simulations, the correlation lengths are computed from the second moment of the spin correlation function $G(\mathbf{r}) = (1/L^2)\sum_{i,j,\alpha}\langle S_i^\alpha S_j^\alpha\rangle\delta(\mathbf{r}-\mathbf{r}_{ij})$ [25, 26, 27]. They can be obtained efficiently from the Fourier transform $\tilde{G}(q)$ of the correlation function:

$$\xi_{\rm av} = \left[\left(\frac{\tilde{G}(0) - \tilde{G}(q_{\rm min})}{q^2_{\rm min}\tilde{G}(q_{\rm min})}\right)^{1/2}\right]_{\rm dis}\,, \tag{8}$$

$$\xi_{\rm gl} = \left(\frac{[\tilde{G}(0) - \tilde{G}(q_{\rm min})]_{\rm dis}}{q^2_{\rm min}[\tilde{G}(q_{\rm min})]_{\rm dis}}\right)^{1/2}\,. \tag{9}$$

Here, $q_{\rm min} = 2\pi/L$ is the minimum wave number that fits into a system of linear size L.

3. MONTE CARLO SIMULATIONS

3.1. METHOD AND OVERVIEW. To simulate the thermodynamics of the four-color Ashkin-Teller model (1), we employ an embedding algorithm analogous to that used in Refs. [16, 28]. It is based on a simple observation. If the spins of colors $\alpha = 2, 3$ and 4 are fixed, the Hamiltonian (1) is equivalent to an Ising model for the spins $S_i^{(1)}$ with effective interactions $J_{ij}^{\text{eff}} = J + \epsilon J(S_i^{(2)}S_j^{(2)} + S_i^{(3)}S_j^{(3)} + S_i^{(4)}S_j^{(4)})$. This (embedded) Ising model can be simulated using any valid Monte-Carlo method. Analogous embedded Ising models can be constructed for the spins $S_i^{(2)}$, $S_i^{(3)}$, and $S_i^{(4)}$. By combining Monte-Carlo updates for all four embedded Ising models we obtain a valid Monte-Carlo method for the entire Ashkin-Teller Hamiltonian.

Using this algorithm, we simulate systems with sizes from 35^2 to 2240^2 sites with periodic boundary conditions and dilution $p = 0.3$. All results are averaged over a large number of disorder configurations (10,000 to 500,000), details will be given below. We combine Wolff single-cluster updates [29] with Swendsen-Wang multi-cluster updates [30]. The latter help equilibrating small isolated clusters of sites that occur for larger dilutions. Specifically, each full Monte Carlo sweep consists of a Swendsen-Wang sweep for each color and a Wolff sweep (a number of single-cluster flips such that the total number of flipped spins for each color equals the number of lattice sites). We use 100 full Monte Carlo sweeps for equilibrating each sample (disorder configuration) and 200 sweeps for measuring observables (one measurement per sweep). The actual equilibration times are much shorter [16]. Biases in the observables due to the short measurement periods are overcome by using improved estimators [16].

The Wolff and Swendsen-Wang algorithms are only valid as long as all effective interactions of the embedded Ising models, $J_{ij}^{\text{eff}} = J + \epsilon J(S_i^{(2)}S_j^{(2)} + S_i^{(3)}S_j^{(3)} + S_i^{(4)}S_j^{(4)})$, are not negative. In the worst case, the term in parenthesis can take the value -3. The coupling constant ϵ therefore must not exceed $1/3$. In the production runs, we use the largest possible value, $\epsilon = 1/3$, because this leads to a strong first-order transition in the clean case.

3.2. RESULTS. To find the phase transition of the four-color Ashkin-Teller model with coupling $\epsilon = 1/3$ and dilution $p = 0.3$ we perform a series of simulation runs using linear system sizes $L = 35$ to 2240. The number of disorder realizations ranges from 500,000 for the smallest systems to 10,000 for the largest ones. As usual, the critical temperature T_c can be determined from the crossings of the Binder cumulant vs. temperature curves for different system sizes (and analogously from the crossings of the reduced correlation length curves ξ/L vs. T).

The Binder cumulant g_{gl} as a function of temperature T is shown in Fig. 1, and Fig. 2 presents the reduced correlation length ξ_{gl}/L as a function of temperature T. Similar graphs can be created for the quantities g_{av} and ξ_{av}/L. In all cases, the crossing points of their curves for different L move with increasing L. This indicates that corrections to the leading scaling behavior are important for the studied system sizes. To find the true, asymptotic value of the critical temperature, we therefore need to extrapolate the crossing points to infinite system size. To do so, we find the crossing temperature $T_x(L/2, L)$ of the

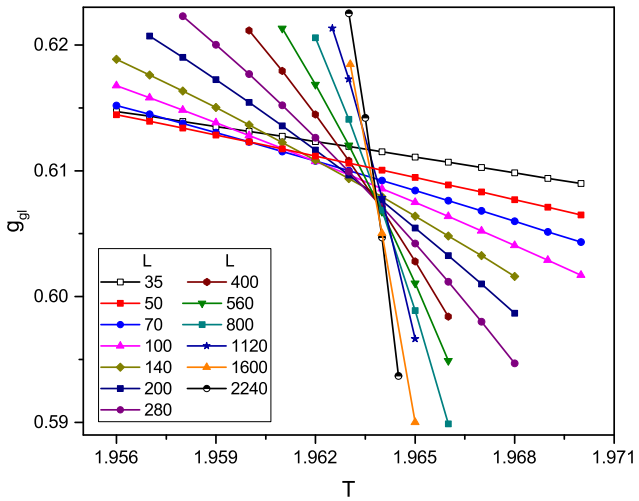

Fig. 1. Binder cumulant g_{gl} vs. temperature T of the site-diluted two-dimensional four-color Ashkin-Teller model with $p = 0.3$ and $\epsilon = 1/3$ for different linear system sizes L. The shift towards higher temperatures of the crossing point with increasing L is caused by corrections to scaling.

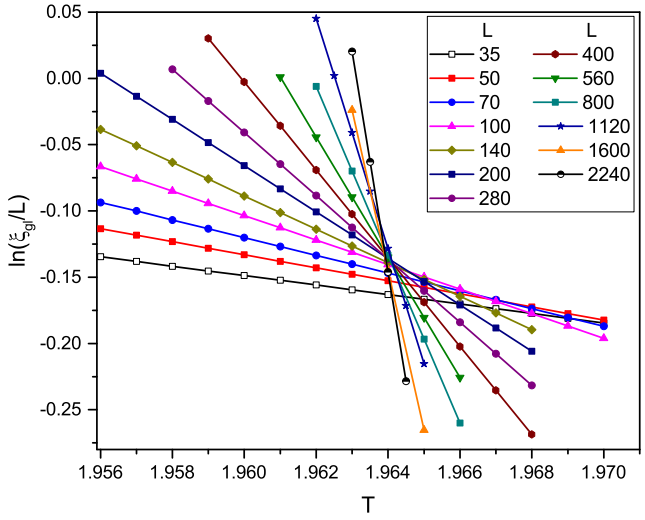

Fig. 2. Reduced correlation length $\xi_{\rm gl}/L$ vs. temperature T for different linear system sizes L. With increasing L, the crossings move to lower T, again indicating corrections to scaling.

$g_{\rm gl}$ vs. T curves for system sizes $L/2$ and L as well as the analogous crossing temperatures for $g_{\rm av}$, $\xi_{\rm gl}/L$, and $\xi_{\rm av}/L$. The resulting dependence of the crossing temperatures on the system size is presented in Fig. 3. The figure shows that all crossings approach the same temperature as L increases. Fits to the heuristic relation $T_x(L/2, L) = T_c + aL^{-b}$ yield a critical temperature of $T_c = 1.9639(3)$ (the number in parentheses is an estimate of the error of the last digits).

To determine the critical behavior, we now analyze the finite-size scaling properties of various observables right at T_c. The data analysis follows Ref. [16] and is based on the finite-size scaling forms (2) to (6). Fig. 4 presents a double-logarithmic plot of specific heat C vs. system size L. The specific heat increases more slowly than a power law with L, as indicated by the downward curvature of the graph. In agreement with the prediction (2), the data can be fitted well to the form $a\ln[b\ln(cL)]$ over the entire size range. The fit is of high quality, giving a reduced error sum $\bar{\chi}^2 \approx 0.8$. (The reduced error sum of a fit of n data points (x_i, y_i) to a function $f(x)$ having q fit parameters is defined as $\bar{\chi}^2 = 1/(n-q)\sum_i[y_i - f(x_i)]^2/\sigma_i^2$ where σ_i is the standard deviation of y_i.) For comparison, we have also attempted to fit the specific heat to the simple logarithmic form $a\ln(bL)$ and to

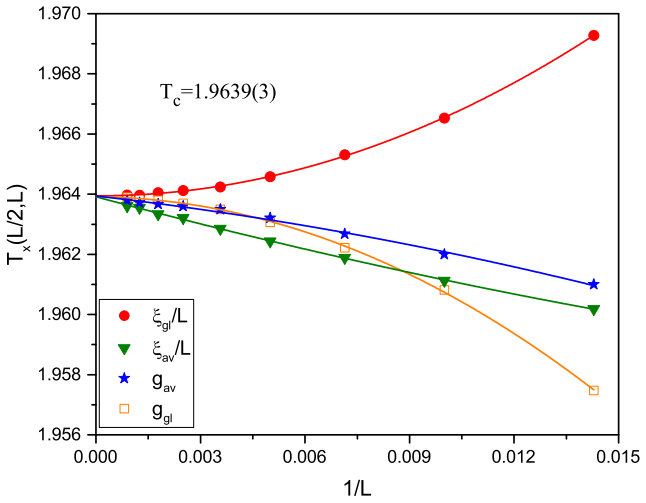

Fig. 3. Crossing temperatures $T_x(L/2, L)$ vs. inverse system size $1/L$. The solid lines are fits to $T_x(L/2, L) = T_c + aL^{-b}$ yielding $T_c = 1.9639(3)$. The error bars of T_x are about a symbol size for the smallest L, they become much smaller with increasing L.

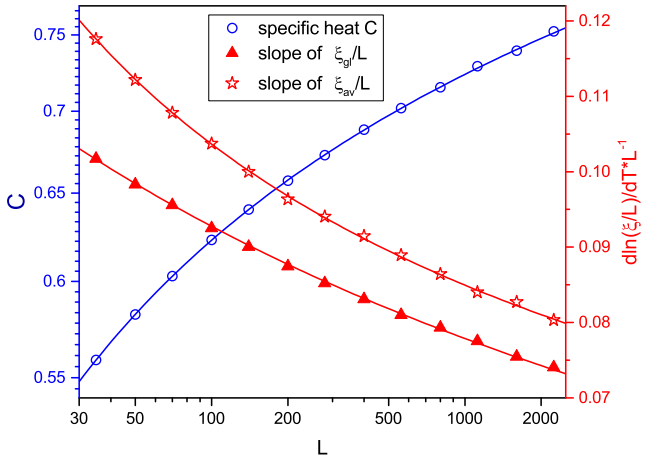

Fig. 4. Double-logarithmic plots of the specific heat C and the slopes $L^{-1}d\ln(\xi_{\rm gl}/L)/dT$ and $L^{-1}d\ln(\xi_{\rm av}/L)/dT$ vs. system size L at the critical temperature of $T_c = 1.9639$. The error bars are smaller than the symbol sizes. The solid lines are fits to $a\ln[b\ln(cL)]$ for C and $a[\ln(bL)]^{-1/2}$ for the slopes.

$C_\infty - aL^{-b}$. The latter function corresponds to power-law scaling with a negative finite-size scaling exponent $\alpha/\nu = -b$. The power-law fit is of poor quality with a reduced error sum $\bar{\chi}^2 \approx 4.3$, and the simple logarithmic fit is completely off, giving $\bar{\chi}^2 \approx 420$.

Fig. 4 also presents the slopes $d\ln(\xi_{\rm gl}/L)/dT$ and $d\ln(\xi_{\rm av}/L)/dT$ of the normalized correlation lengths vs. temperature curves at T_c. We have divided out the power law $d\ln(\xi/L)/dT \sim L$ of the clean Ising universality class to make the corrections predicted in eq. (6) more easily visible. The figure demonstrates that these corrections are not of power-law type, instead the data can be fitted well by the predicted logarithmic form $a[\ln(bL)]^{-1/2}$, yielding reduced error sums $\bar{\chi}^2$ of about 0.3 for $\xi_{\rm av}$ and 0.9 for $\xi_{\rm gl}$.

In addition, we study the system size dependence of the magnetization and the magnetic susceptibility at the critical temperature. According to eqs. (3) and (4), these quantities are predicted to follow the clean Ising power laws with additive logarithmic corrections. We again divide out the clean Ising power laws and plot the resulting quantities, viz., $M\,L^{1/8}$ and $\chi\,L^{-7/4}$ in Fig. 5. The figure demonstrates that the corrections to the Ising universality class are not of power-law form. Moreover, they are very weak, in particular for the magnetization where they change the value by less than 1% over the entire system size range. To capture this small correction, we had to increase the number of disorder

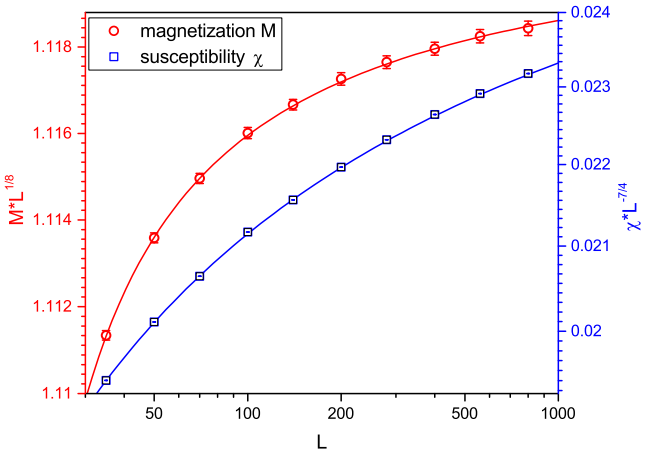

Fig. 5. Double-logarithmic plots of $M\,L^{1/8}$ and $\chi\,L^{-7/4}$ vs. L at the critical temperature of $T_c = 1.9639$. The solid lines are fits to $a[1 + b/\ln(cL)]$, as suggested by eqs. (3) and (4).

configurations significantly (500,000 for all system sizes) to reduce the error bars. The larger numerical effort limits these simulations to system sizes between $L = 35$ and 800. Both $M\,L^{1/8}$ and $\chi\,L^{-7/4}$ can be fitted well to the function $a[1 + b/\ln(cL)]$ predicted by the renormalization group results (3) and (4). The reduced error sums $\bar{\chi}^2$ are approximately 0.4 for the susceptibility and 0.3 for the magnetization.

4. SUMMARY AND CONCLUSIONS

In summary, we have carried out large-scale Monte Carlo simulations of the site-diluted two-dimensional four-color Ashkin-Teller model. Our results confirm that the first-order phase transition occurring in the undiluted (clean) model is rounded by the disorder, as required by the Aizenman-Wehr theorem [4].

We have used finite-size scaling of the magnetization, magnetic susceptibility, specific heat and correlation length to determine the universality class of the emerging continuous phase transition. All our data agree very well with the results of the perturbative renormalization group [11, 12, 13] which predicts critical behavior in the clean two-dimensional Ising universality class, but with logarithmic corrections similar to those occurring in the two-dimensional disordered Ising model. These findings agree with those of extensive high-accuracy simulations of the three-color case [16]. Consequently, they provide strong evidence for the universality of the critical behavior of the disordered Ashkin-Teller model.

Possible reasons for the discrepancies between our results (Ref. [16] and the present paper) and those of the earlier simulations [14, 15] were discussed in detail in Ref. [16]. Here, we just reiterate the main points: Our systems are much larger, up to 2240^2 sites (compared to just 32^2 sites in Ref. [14] and 128^2 sites in Ref. [15]). This suggests that the earlier simulations were not in the asymptotic regime, especially for weak disorder where the crossover from the clean first-order transition to the disordered continuous one is slow. Note, however, that a discrepancy exists already for the *clean* three-color model. The clean

phase diagram of Ref. [16], which was determined and verified using three independent Monte Carlo algorithms, coincides with older results by Grest and Widom [8] but disagrees with Ref. [14].

From a more general point of view, the renormalization groups results for the random-T_c Ising [18, 19, 20, 21] and Ashkin-Teller [12] models suggested a kind of "super-universality" of critical points in two-dimensional disordered systems. This idea was initially supported by computer simulations of disordered Ising[31, 32], Ashkin-Teller[28], and Potts[28, 33] models as well as interface arguments [34]. Numerical sudies of the disordered q-state Potts model[35, 36] showed, however, that the finite-size scaling exponent β/ν differs from the Ising value and varies with q. Moreover, the phase transition in the random-bond Blume-Capel model was also found to display complex non-Ising behavior, at least for strong disorder [37, 38, 39].

Recently, the disordered quantum Ashkin-Teller spin chain has attracted lots of interest because it serves as a paradigmatic model for studying disorder effects at first-order *quantum* phase transitions. As a quantum version of the Aizenman-Wehr theorem has been proven [40], the first-order character of the transition in the clean problem must change upon the introduction of disorder. Recent strong-disorder renormalization group approaches predict continuous transitions governed by infinite-randomness critical points in different universality classes, depending on the coupling strength ϵ [41, 42, 43]. Furthermore, in the case of two colors an exotic strong-disorder infinite-coupling phase [44] is predicted to appear for large ϵ. These predictions can be tested by generalizations of our Monte Carlo method to the (1 + 1)-dimensional quantum case. Some work along these lines is already in progress.

It may also be interesting to investigate the Ashkin-Teller model defined on a topologically disordered lattice such as the random Voronoi-Delaunay lattice (see, e.g., [45]). Recent work [46] has shown that the Imry-Ma argument does not hold for these lattices

because a topological constraint suppresses the disorder fluctuations. This leaves open the possibility that the first-order phase transition survives in the presence of such topological disorder.

ACKNOWLEDGEMENTS

This work was supported in part by the NSF under Grant Nos. DMR-1205803 and DMR-1506152.

REFERENCES

[1] Yoseph Imry and Shang-keng Ma. Random-field instability of the ordered state of continuous symmetry. *Phys. Rev. Lett.*, 35:1399–1401, Nov 1975.

[2] Yoseph Imry and Michael Wortis. Influence of quenched impurities on first-order phase transitions. *Phys. Rev. B*, 19:3580–3585, Apr 1979.

[3] Kenneth Hui and A. Nihat Berker. Random-field mechanism in random-bond multicritical systems. *Phys. Rev. Lett.*, 62:2507–2510, May 1989.

[4] Michael Aizenman and Jan Wehr. Rounding of first-order phase transitions in systems with quenched disorder. *Phys. Rev. Lett.*, 62:2503–2506, May 1989.

[5] T. Vojta. Rare region effects at classical, quantum, and non-equilibrium phase transitions. *J. Phys. A*, 39:R143, 2006.

[6] T. Vojta. Quantum Griffiths effects and smeared phase transitions in metals: theory and experiment. *J. Low Temp. Phys.*, 161:299, 2010.

[7] J. Ashkin and E. Teller. Statistics of two-dimensional lattices with four components. *Phys. Rev.*, 64:178–184, Sep 1943.

[8] Gary S. Grest and Michael Widom. N-color Ashkin-Teller model. *Phys. Rev. B*, 24:6508–6515, Dec 1981.

[9] Eduardo Fradkin. N-color Ashkin-Teller model in two dimensions: Solution in the large-N limit. *Phys. Rev. Lett.*, 53:1967–1970, Nov 1984.

[10] R. Shankar. Ashkin-Teller and Gross-Neveu models: New relations and results. *Phys. Rev. Lett.*, 55:453–456, Jul 1985.

[11] Ganpathy N. Murthy. Critical behavior of the n-component ashkin-teller model with bond impurities. *Phys. Rev. B*, 36:7166–7168, Nov 1987.

[12] John Cardy. Effect of random impurities on fluctuation-driven first-order transitions. *J. Phys. A*, 29:1897, 1996.

[13] John Cardy. Quenched randomness at first-order transitions. *Physica A*, 263:215, 1999.

[14] Arash Bellafard, Helmut G. Katzgraber, Matthias Troyer, and Sudip Chakravarty. Bond disorder induced criticality of the three-color Ashkin-Teller model. *Phys. Rev. Lett.*, 109:155701, Oct 2012.

[15] Arash Bellafard, Sudip Chakravarty, Matthias Troyer, and Helmut G. Katzgraber. The effect of quenched bond disorder on first-order phase transitions. *Ann. Phys.*, 357:66, 2015.

[16] Qiong Zhu, Xin Wan, Rajesh Narayanan, José A. Hoyos, and Thomas Vojta. Emerging criticality in the disordered three-color ashkin-teller model. *Phys. Rev. B*, 91:224201, Jun 2015.

[17] R.J. Baxter. *Exactly Solved Models in Statistical Mechanics*. Academic Press, New York, 1982.

[18] Viktor S. Dotsenko and Vladimir S. Dotsenko. Critical behaviour of the phase transition in the 2d ising model with impurities. *Adv. Phys.*, 32(2):129–172, 1983.

[19] B. N. Shalaev. *Fiz. Tverd. Tela (Leningrad)*, 36:3002, 1984. [Sov. Phys.– Solid State **26**, 1811 (1984)].

[20] R. Shankar. Exact critical behavior of a random bond two-dimensional ising model. *Phys. Rev. Lett.*, 58:2466–2469, Jun 1987.

[21] Andreas W. W. Ludwig. Comment on "exact critical behavior of a random-bond two-dimensional ising model". *Phys. Rev. Lett.*, 61:2388–2388, Nov 1988.

[22] Giorgio Mazzeo and Reimer Kühn. Critical behavior of the two-dimensional spin-diluted ising model via the equilibrium ensemble approach. *Phys. Rev. E*, 60:3823–3836, Oct 1999.

[23] Martin Hasenbusch, Francesco Parisen Toldin, Andrea Pelissetto, and Ettore Vicari. Universal dependence on disorder of two-dimensional randomly diluted and random-bond $\pm j$ ising models. *Phys. Rev. E*, 78:011110, Jul 2008.

[24] R. Kenna and J. J. Ruiz-Lorenzo. Scaling analysis of the site-diluted ising model in two dimensions. *Phys. Rev. E*, 78:031134, Sep 2008.

[25] F. Cooper, B. Freedman, and D. Preston. Solving ϕ^4 field theory with Monte-carlo. *Nucl. Phys. B*, 210:210, 1982.

[26] J. K. Kim. Application of finite size scaling to Monte-Carlo simulations. *Phys. Rev. Lett.*, 70:1735, 1993.

[27] S. Caracciolo, A. Gambassi, M. Gubinelli, and A. Pelissetto. Finite-size correlation length and violations of finite-size scaling. *Eur. Phys. J. B*, 20:255, 2001.

[28] Shai Wiseman and Eytan Domany. Critical behavior of the random-bond ashkin-teller model: A monte carlo study. *Phys. Rev. E*, 51:3074–3086, Apr 1995.

[29] U. Wolff. Collective Monte-Carlo updating for spin systems. *Phys. Rev. Lett.*, 62:361, 1989.

[30] Robert H. Swendsen and Jian-Sheng Wang. Nonuniversal critical dynamics in monte carlo simulations. *Phys. Rev. Lett.*, 58:86–88, Jan 1987.

[31] V.B. Andreichenko, Vl.S. Dotsenko, W. Selke, and J.-S. Wang. Monte carlo study of the 2d ising model with impurities. *Nucl. Phys. B*, 344(3):531 – 556, 1990.

[32] J. S. Wang, W. Selke, Vl S. Dotsenko, and V. B. Andreichenko. The two-dimensional random bond ising model at criticality – a monte carlo study. *EPL (Europhysics Letters)*, 11(4):301, 1990.

[33] S. Chen, Alan M. Ferrenberg, and D. P. Landau. Monte carlo simulation of phase transitions in a two-dimensional random-bond potts model. *Phys. Rev. E*, 52:1377–1386, Aug 1995.

[34] Mehran Kardar, Attilio L. Stella, Giovanni Sartoni, and Bernard Derrida. Unusual universality of branching interfaces in random media. *Phys. Rev. E*, 52:R1269–R1272, Aug 1995.

[35] Jesper Lykke Jacobsen and John Cardy. Critical behaviour of random-bond potts models: a transfer matrix study. *Nuclear Physics B*, 515(3):701 – 742, 1998.

[36] Christophe Chatelain and Bertrand Berche. Finite-size scaling study of the surface and bulk critical behavior in the random-bond eight-state potts model. *Phys. Rev. Lett.*, 80:1670–1673, Feb 1998.

[37] A. Malakis, A. Nihat Berker, I. A. Hadjiagapiou, and N. G. Fytas. Strong violation of critical phenomena universality: Wang-landau study of the two-dimensional blume-capel model under bond randomness. *Phys. Rev. E*, 79:011125, Jan 2009.

[38] A. Malakis, A. Nihat Berker, I. A. Hadjiagapiou, N. G. Fytas, and T. Papakonstantinou. Multicritical points and crossover mediating the strong violation of universality: Wang-landau determinations in the random-bond $d = 2$ blume-capel model. *Phys. Rev. E*, 81:041113, Apr 2010.

[39] Panagiotis E. Theodorakis and Nikolaos G. Fytas. Monte carlo study of the triangular blume-capel model under bond randomness. *Phys. Rev. E*, 86:011140, Jul 2012.

[40] Rafael L. Greenblatt, Michael Aizenman, and Joel L. Lebowitz. Rounding of first order transitions in low-dimensional quantum systems with quenched disorder. *Phys. Rev. Lett.*, 103:197201, Nov 2009.

[41] P. Goswami, D. Schwab, and S. Chakravarty. Rounding by disorder of first-order quantum phase transitions: Emergence of quantum critical points. *Phys. Rev. Lett.*, 100:015703, 2008.

[42] Fawaz Hrahsheh, José A. Hoyos, and Thomas Vojta. Rounding of a first-order quantum phase transition to a strong-coupling critical point. *Phys. Rev. B*, 86:214204, Dec 2012.

[43] Hatem Barghathi, Fawaz Hrahsheh, Jose A. Hoyos, Rajesh Narayanan, and Thomas Vojta. Strong-randomness phenomena in quantum Ashkin-Teller models. *Phys. Scr.*, T165:014040, 2015.

[44] Fawaz Hrahsheh, José A. Hoyos, Rajesh Narayanan, and Thomas Vojta. Strong-randomness infinite-coupling phase in a random quantum spin chain. *Phys. Rev. B*, 89:014401, Jan 2014.

[45] A. Okabe, B. Boots, K. Sugihara, and S.N. Chiu. *Spatial Tessellations: Concepts and Applications of Voronoi Diagrams*. Wiley, Chichester, 2000.

[46] Hatem Barghathi and Thomas Vojta. Phase transitions on random lattices: How random is topological disorder? *Phys. Rev. Lett.*, 113:120602, Sep 2014.

III. MONTE CARLO SIMULATIONS OF THE DISORDERED THREE-COLOR QUANTUM ASHKIN-TELLER CHAIN

Ahmed K. Ibrahim and Thomas Vojta

Department of Physics, Missouri University of Science and Technology, Rolla, MO 65409, USA

ABSTRACT[*]

We investigate the zero-temperature quantum phase transitions of the disordered three-color quantum Ashkin-Teller spin chain by means of large-scale Monte Carlo simulations. We find that the first-order phase transitions of the clean system are rounded by the quenched disorder. For weak inter-color coupling, the resulting emergent quantum critical point between the paramagnetic phase and the magnetically ordered Baxter phase is of infinite-randomness type and belongs to the universality class of the random transverse-field Ising model, as predicted by recent strong-disorder renormalization group calculations. We also find evidence for unconventional critical behavior in the case of strong inter-color coupling, even though an unequivocal determination of the universality class is beyond our numerical capabilities. We compare our results to earlier simulations, and we discuss implications for the classification of phase transitions in the presence of disorder.

[*]Published in Physical Review B 95, 054403 (2017).

1. INTRODUCTION

Zero-temperature quantum phase transitions can be classified into continuous or first-order just as classical thermal phase transitions. First-order quantum phase transitions have gained considerable attention recently, not only because of their fundamental interest but also because experimentally important transitions turn from being continuous at higher temperatures to first-order at lower temperatures. A prominent example of this behavior is the itinerant ferromagnetic transition [1, 2]. (For a recent review of metallic quantum ferromagnets see Ref. [3].)

As real materials always contain a certain amount of vacancies, impurities, or other defects, understanding the influence of such quenched disorder is of both conceptual and practical importance. Theoretical research on continuous quantum phase transitions in the presence of disorder has predicted a number of exotic phenomena such as infinite-randomness critical points [4, 5, 6], quantum Griffiths phases [7, 8], and smeared phase transitions [9]. More recently, several of these phenomena have been observed in experiments [10, 11, 12, 13]. A classification of strong-disorder effects was developed in Ref. [14] and refined in Ref. [15], see also Refs. [16] for reviews.

In contrast, less is known about first-order quantum phase transitions in the presence of disorder. Greenblatt et al. [17] proved a quantum version of the classical Aizenman-Wehr theorem [18, 19, 20] that states that first-order phase transitions cannot exist in disordered systems in $d \leq 2$ space dimensions. (If the disorder breaks a continuous symmetry, the marginal dimension is $d = 4$.) This agrees with a few available explicit results: Senthil and Majumdar [21] predicted that quenched randomness turns the first-order quantum phase transitions of the quantum Potts and clock chains into infinite-randomness critical points in the random transverse-field Ising universality class. The same was found by Goswami et al. [22] for the disordered N-color one-dimensional quantum Ashkin-Teller model [23] in

the weak-coupling regime (weak interactions between the colors). In the strong-coupling regime, the critical point between the paramagnetic and Baxter phases is still of infinite-randomness type, but it is predicted to be in a different universality class [24, 25].

All these results were obtained using versions of the strong-disorder renormalization group [26] which becomes controlled in the limit of infinitely strong disorder. It is therefore highly desirable to verify that the predictions also hold for realistic, weakly or moderately disordered systems. A recent Monte Carlo study of the quantum Ashkin-Teller model [27] provided evidence for the activated scaling expected at an infinite-randomness critical point. However, the authors could not verify the predicted random transverse-field Ising universality class and suggested that the discrepancy stems, perhaps, from the first-order origin of this transition.

To shed some light onto this question, we map the disordered three-color quantum Ashkin-Teller chain onto a $(1+1)$ dimensional classical Hamiltonian with columnar disorder. We investigate this classical model by means of large-scale Monte Carlo simulations for systems with up to 3.6 million lattice sites (10.8 million spins). In the weak-coupling regime, we find universal critical behavior in the random transverse-field Ising universality class, as predicted by the strong-disorder renormalization group. We also perform exploratory simulations in the strong coupling regime that establish the phase diagram and confirm unconventional activated dynamical scaling. However, because the efficient cluster Monte Carlo algorithms we use in the weak-coupling regime are not valid for strong coupling, we can not quantitatively verify the distinct critical behavior predicted in Refs. [24, 25].

The rest of the paper is organized as follows. In Sec. 2, we introduce the quantum Ashkin-Teller chain and the mapping onto a classical Hamiltonian. We also summarize the predictions of the strong-disorder renormalization group calculations. Sec. 3 is devoted to the Monte Carlo simulations and their results. We conclude in Sec. 6.

2. MODEL AND THEORY

2.1. QUANTUM ASHKIN-TELLER CHAIN. The N-color quantum Ashkin-Teller chain [23, 28] is a generalization of the original model suggested by Ashkin and Teller many decades ago [29]. It is made up of N coupled identical transverse-field Ising chains each containing L spins. The quantum Hamiltonian can be expressed as

$$\begin{aligned} H &= -\sum_{\alpha=1}^{N}\sum_{i=1}^{L}\left(J_i\sigma^z_{\alpha,i}\sigma^z_{\alpha,i+1}+h_i\sigma^x_{\alpha,i}\right) \\ &\quad -\sum_{\alpha<\beta}^{N}\sum_{i=1}^{L}\left(K_i\sigma^z_{\alpha,i}\sigma^z_{\alpha,i+1}\sigma^z_{\beta,i}\sigma^z_{\beta,i+1}+g_i\sigma^x_{\alpha,i}\sigma^x_{\beta,i}\right). \end{aligned} \tag{1}$$

Here, σ^x and σ^z are Pauli matrices describing the spin degrees of freedom. i denotes the lattice sites while α and β are color indices. The ratios $\epsilon_{h,i} = g_i/h_i$ and $\epsilon_{J,i} = K_i/J_i$ characterize the strengths of the inter-color coupling. In the following, we are interested in the case of positive interactions J_i, K_i and fields h_i, g_i. Besides its fundamental interest, different versions of the Ashkin-Teller model have been used to describe absorbed atoms on surfaces [30], organic magnets, current loops in high-temperature superconductors [31, 32], as well as the elastic response of DNA molecules [33].

In the clean quantum Ashkin-Teller chain, the interactions $J_i \equiv J$, transverse fields $h_i \equiv h$, as well as the inter-color coupling ratios $\epsilon_{J,i} \equiv \epsilon_J$ and $\epsilon_{h,i} \equiv \epsilon_h$ are uniform in space. The ground state phases of this model are easily understood qualitatively. If the inter-color coupling ratios $\epsilon_J, \epsilon_h \ll 1$, the behavior is dominated by the transverse-field Ising chain terms in the first line of Eq. (1). The system is thus in the paramagnetic phase if the transverse fields are larger than the interactions, $h \gg J$, but in the ordered (Baxter) phase for $h \ll J$. In the Baxter phase, each color orders ferromagnetically but the relative orientation of different colors is arbitrary. An additional phase, the so-called product phase, can appear between the paramagnetic and Baxter phases for strong inter-color coupling, $\epsilon_J, \epsilon_h \gg 1$. In this phase, products $\sigma^z_{\alpha,i}\sigma^z_{\beta,i}$ of two spins of different colors develop long-range order while

the spins $\sigma^z_{\alpha,i}$ themselves remain disordered. (For a qualitative overview of the phases, see Fig. 1 which shows the phase diagram of the disordered Ashkin-Teller model for a particular set of parameters; here the classical temperature T_c encodes the ratio h/J.) For at least three colors, the direct quantum phase transition between the paramagnetic and Baxter phases is known to be of first-order [23, 28, 34]. The quantum Ashkin-Teller chain is therefore a paradigmatic model for studying the effects of disorder on a first-order quantum phase transition.

Note that the form of the Hamiltonian (1) is invariant under the duality transformation $\sigma^z_{\alpha,i}\sigma^z_{\alpha,i+1} \to \tilde{\sigma}^x_{\alpha,i}$, $\sigma^x_{\alpha,i} \to \tilde{\sigma}^z_{\alpha,i}\tilde{\sigma}^z_{\alpha,i+1}$, $J_i \rightleftarrows h_i$, and $\epsilon_{J,i} \rightleftarrows \epsilon_{h,i}$, where $\tilde{\sigma}^x_{\alpha,i}$ and $\tilde{\sigma}^z_{\alpha,i}$ are the dual Pauli matrices [35]. Self-duality therefore requires that a direct transition between the paramagnetic and Baxter phases (for $\epsilon_h = \epsilon_J$) must occur exactly at $h = J$.

2.2. RENORMALIZATION GROUP PREDICTIONS. We now briefly summarize the results of several strong-disorder renormalization group calculations for the N-color random quantum Ashkin-Teller chain. Goswami et al. [22] analyzed the weak-coupling regime and found that the inter-color coupling ratios $\epsilon_{J,i}, \epsilon_{h,i}$ renormalize to zero, and the renormalization group flow becomes asymptotically identical to that of the one-

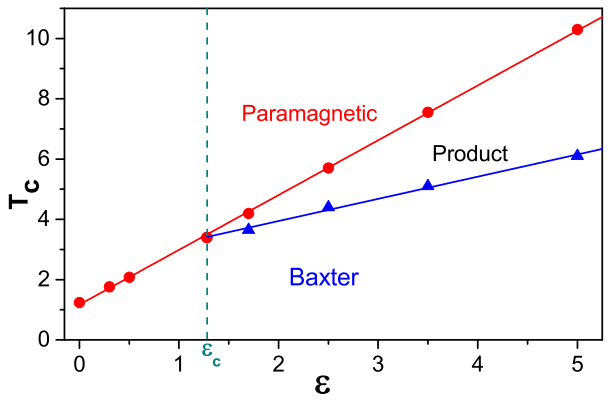

Fig. 1. Phase diagram of the classical Hamiltonian (3) for $N = 3$ colors and disorder distribution (4) with $J_h = 1$, $J_l = 0.25$, and $c = 0.5$. The dots and triangles mark the numerically determined transitions between the Baxter, product, and paramagnetic phases. The solid lines are guides to the eye only. The dashed line marks $\epsilon_c = 1.281$ [see Eq. (2)] which separates the weak and strong coupling regimes in the strong-disorder renormalization group calculations.

dimensional random transverse-field Ising model [4]. More specifically, this happens if all initial (bare) $\epsilon_{J,i}$ and $\epsilon_{h,i}$ are smaller than a critical value

$$\epsilon_c(N) = \frac{2N-5}{2N-2} + \sqrt{\left(\frac{2N-5}{2N-2}\right)^2 + \frac{2}{N-1}}\,. \tag{2}$$

(For three colors, $\epsilon_c \approx 1.281$.) In the weak-coupling regime, the strong disorder renormalization group thus predicts that the first-order quantum phase transition of the clean chain is rounded to a continuous one, with infinite-randomness critical behavior in the random transverse-field Ising universality class [4].

The strong-coupling regime of the random quantum Ashkin-Teller chain was studied in Refs. [24, 25, 36]. Using a different implementation of the strong-disorder renormalization group, these papers demonstrated that the inter-color coupling ratios $\epsilon_{J,i}$ and $\epsilon_{h,i}$ renormalize to infinity if their initial (bare) values are larger than ϵ_c. This implies that the four-spin interactions and the two-spin field terms in the Hamiltonian dominate the behavior of the system.

If $\epsilon_{J,i} = \epsilon_{h,i}$, the model is self-dual at the critical point. In this case and for at least three colors, there is still a direct transition between the paramagnetic and Baxter phases, i.e., spins and products order at the same point. This transition occurs at $J_{\rm typ} = h_{\rm typ}$ where $J_{\rm typ}$ and $h_{\rm typ}$ refer to the typical values (geometric means) of the random interactions and fields. The critical behavior of this transition is of infinite randomness type but it is not in the random transverse Ising universality class because products and spins both contribute to observables [24, 25]. In the general case, $\epsilon_{J,i} \neq \epsilon_{h,i}$, a product phase can appear between the paramagnetic and Baxter phases (this also happens for two colors, even in the self-dual case) [36]. The phase transition between the paramagnetic and product phases as well as the transition between the product and Baxter phases are both expected to belong to the random transverse-field Ising universality class.

2.3. QUANTUM-TO-CLASSICAL MAPPING. To test the renormalization group predictions by Monte Carlo simulations, we now map the random quantum Ashkin-Teller chain onto a (1+1)-dimensional classical Ashkin-Teller model. This can be done using standard methods, e.g., by writing the partition function as a Feynman path integral in imaginary time (see also Ref. [37]). The resulting classical Hamiltonian reads:

$$\begin{aligned} H_{cl} &= -\sum_{\alpha,i,t}\left(J_i^{(s)} S_{i,t}^{\alpha} S_{i+1,t}^{\alpha} + J_i^{(t)} S_{i,t}^{\alpha} S_{i,t+1}^{\alpha}\right) \\ &\quad -\sum_{\alpha<\beta,i,t}\left(\epsilon_i^{(s)} J_i^{(s)} S_{i,t}^{\alpha} S_{i+1,t}^{\alpha} S_{i,t}^{\beta} S_{i+1,t}^{\beta}\right) \\ &\quad -\sum_{\alpha<\beta,i,t}\left(\epsilon_i^{(t)} J_i^{(t)} S_{i,t}^{\alpha} S_{i,t+1}^{\alpha} S_{i,t}^{\beta} S_{i,t+1}^{\beta}\right) . \end{aligned} \tag{3}$$

Here, $S_{i,t}^{\alpha} = \pm 1$ is a classical Ising spin of color α at position i in space and t in (imaginary) time. The classical interactions $J_i^{(s)}$, $J_i^{(t)}$ and inter-color coupling ratios $\epsilon_i^{(s)}$, $\epsilon_i^{(t)}$ as well as the classical temperature T are determined by the parameters of the original quantum Hamiltonian (1). (The classical temperature T does not equal the physical temperature of the quantum system (1) which is encoded in the system size L_t in time direction.) Specifically, the inter-color coupling ratio $\epsilon_i^{(s)}$ is identical to $\epsilon_{J,i}$ of the quantum Hamiltonian but $\epsilon_i^{(t)}$ is *not* identical to $\epsilon_{h,i}$. Instead, it is a complicated function of the transverse field and the two-color field terms. We also note that the quantum-to-classical mapping generates further terms in the classical Hamiltonian in addition to those shown in (3). These extra terms contain higher products of up to N colors.

As we are interested in the critical behavior which is expected to be universal, the precise values of $J_i^{(s)}$, $J_i^{(t)}$, $\epsilon_i^{(s)}$, and $\epsilon_i^{(t)}$ are not important and can be chosen for computational convenience (see Sec. 3). Moreover, we can neglect the terms that contain products of more than two colors [38].

3. MONTE CARLO SIMULATIONS

3.1. OVERVIEW. We perform large-scale Monte Carlo simulations of the classical Hamiltonian (3) for the case of $N = 3$ colors by employing an Ising embedding method similar that used in Ref. [39]. It can be understood as follows. If we fix the values of all spins with color $\alpha \neq 1$, the Hamiltonian (3) acts as an (1+1)-dimensional Ising model for the spins $S^{(1)}_{i,t}$ with effective interaction $J^{\text{eff}}_{ij} = J + \epsilon J(S^{(2)}_i S^{(2)}_j + S^{(3)}_i S^{(3)}_j)$. This embedded Ising model can be simulated by means of any Ising Monte Carlo algorithm. We use a combination of the efficient Swendsen-Wang multicluster algorithm [40] and the Wolff single cluster algorithm [41]. Analogous embedded Ising models can be constructed for the spins $S^{(2)}_{i,t}$ and $S^{(3)}_{i,t}$, and by performing cluster updates for all three embedded Ising models we arrive at a valid and efficient algorithm for the Ashkin-Teller model.

The Swendsen-Wang and Wolff cluster algorithms require all interactions to be nonnegative, $J^{\text{eff}} \geq 0$ [42].

This is only guaranteed if the coupling ratio ϵ does not exceed $1/(N-1) = 1/2$. For larger ϵ, we perform exploratory simulations using the less efficient Metropolis algorithm[43] as well as the Wang-Landau method [44].

By means of these algorithms, we simulate systems with linear sizes $L = 10$ to 60 in space direction and $L_t = 2$ to 60,000 in (imaginary) time direction, using periodic boundary conditions. The largest system had 3.6 million lattice sites, i.e., 10.8 million spins. To implement the quenched disorder, we consider $J^{(s)}_i$ and $J^{(t)}_i$ to be independent random variables drawn from a binary probability distribution

$$W(J) = c\delta(J - J_h) + (1 - c)\delta(J - J_l) \tag{4}$$

where c is the concentration of the higher value J_h of the interaction while $1 - c$ is the concentration of the lower value J_l. The inter-color coupling ratios are uniform, $\epsilon^{(s)}_i = \epsilon^{(t)}_i = \epsilon$ (implying that the disorders in K and g are identical to those in J and h, respectively)

[45]. As $J_i^{(s)}$ and $J_i^{(t)}$ only depend on the space coordinate i but not on the time coordinate t, the resulting disorder is columnar, i.e., perfectly correlated in the time direction. In the simulations, we use $J_h = 1$, $J_l = 0.25$, and $c = 0.5$ while ϵ takes values between 0 and 5. All observables are averaged over 10,000 to 40,000 disorder configurations, unless otherwise noted.

When using cluster algorithms ($\epsilon \leq 0.5$), we equilibrate each sample using 100 full Monte Carlo sweeps. Each full sweep is made up of a Wolff sweep for each color (consisting of a number of single-cluster flips such that the total number of flipped spins equals the number of lattice sites) and a Swendsen-Wang sweep for each color. The Swendsen-Wang sweep aims at equilibrating small clusters of weakly coupled sites that may be missed by the Wolff algorithm. The actual equilibration is significantly faster than 100 sweeps. [46] The measurement period consists of another 100 full Monte Carlo sweeps with a measurement taken after each sweep. To deal with biases introduced by using such short measurement periods, we employ improved estimators [46]. Simulations for $\epsilon > 0.5$ that use the Metropolis and Wang-Landau methods require much longer runs, details will be discussed below.

During the simulation runs, we measure the following observables: energy, specific heat, total magnetization

$$m = \frac{1}{3LL_t} \sum_{\alpha} \left| \sum_{i,t} S_{i,t}^{\alpha} \right| \tag{5}$$

and its susceptibility χ_m. A particularly useful quantity for the finite-size scaling analysis is the Binder cumulant

$$g_{\text{av}} = \left[1 - \frac{\langle m^4 \rangle}{3 \langle m^2 \rangle^2} \right]_{\text{dis}} \tag{6}$$

where $\langle \ldots \rangle$ denotes the thermodynamic (Monte Carlo) average and $[\ldots]_{\text{dis}}$ is the disorder average. In addition, we also measure the product order parameter

$$p = \frac{1}{3LL_t} \sum_{\alpha<\beta} \left| \sum_{i,t} S_{i,t}^{\alpha} S_{i,t}^{\beta} \right| , \tag{7}$$

the corresponding product susceptibility χ_p, and the product Binder cumulant g_p.

The phase diagram of the classical Hamiltonian (3) resulting from these simulations is shown in Fig. 1. In the weak-coupling regime, $\epsilon < \epsilon_c$, we find a direct transition between the magnetically ordered Baxter phase at low temperatures and the paramagnetic high-temperature phase. For strong coupling, $\epsilon > \epsilon_c$, these two phases are separated by a product phase. Interestingly, the value of ϵ_c agrees within the numerical errors with the strong-disorder renormalization group prediction (2) of about 1.281 (even though the disorder is not infinitely strong, and we have modified the classical Hamiltonian as discussed at the end of Sec. 2.3). In the following, we study the critical behaviors of the transitions separating these phases in detail, and we compare them to the renormalization group predictions.

3.2. WEAK COUPLING REGIME. In the weak-coupling regime, $\epsilon < \epsilon_c$, we perform simulations for coupling ratios $\epsilon = 0$, 0.3 and 0.5 employing the Wolff and Swendsen-Wang cluster algorithms as discussed above. Because the disorder breaks the symmetry between the space and (imaginary) time directions in the Hamiltonian (3), the finite-size scaling analysis of the data to find the critical exponents becomes more complicated. This is caused by the fact that the system sizes L and L_t in the space and time directions are expected to have different scaling behavior. Thus, the correct aspect ratios L_t/L of the samples to be used in the simulations are not known a priori.

To overcome this problem we follow the iterative method employed in Refs. [47, 48, 49, 50] which is based on the Binder cumulant. As the renormalization group calculations predict infinite-randomness criticality with activated dynamical scaling, the scaling form of the Binder cumulant (which has scale dimension 0) reads

$$g_{\rm av}(r, L, L_t) = X_g(rL^{1/\nu}, \ln(L_t/L_t^0)/L^{\psi}) \; . \tag{8}$$

Here $r = (T - Tc)/T_c$ denotes the distance from criticality, X_g is a scaling function, and ψ and ν refer to the tunneling and correlation length critical exponents. L_t^0 is a microscopic reference scale. (For conventional power-law scaling, the second argument of the scaling function would read L_t/L^z with z being the dynamical exponent.) For fixed L, $g_{\rm av}$ has a maximum as function of L_t at position $L_t^{\rm max}$ and value $g_{\rm av}^{\rm max}$. The position of the maximum yields the *optimal* sample shape for which the system sizes L and L_t behave as the correlation lengths ξ and ξ_t. At criticality L_t must thus behave as $\ln(L_t^{\rm max}/L_t^0) \sim L^\psi$, fixing the second argument of the scaling function X_g. Consequently, the peak value $g_{\rm av}^{\rm max}$ is independent of L at criticality, and the $g_{\rm av}$ vs. r curves of optimally shaped samples cross at $T = T_c$. Once the optimal sample shapes are found, finite-size scaling proceeds as usual [51, 52].

To test our simulation and data analysis technique, we first consider the case $\epsilon = 0$ for which the quantum Ashkin-Teller model reduces to three decoupled random transverse-field Ising chains whose quantum phase transition is well understood [4]. We perform simulations for sizes $L = 10$ to 50 and $L_t = 2$ to 20000 and find a critical temperature $T_c \approx 1.24$. At this temperature, we confirm the activated scaling (8) of the Binder cumulant with the expected value $\psi = 1/2$. We also confirm the scaling of the magnetization at T_c (for the optimally shaped samples), $m \sim L^{-\beta/\nu}$ with $\beta = 0.382$ and $\nu = 2$.

After this successful test, we now turn to the Ashkin-Teller model proper. We perform two sets of simulations: (i) $\epsilon = 0.5$ using system sizes $L = 10$ to 60, $L_t = 2$ to 60000 and (ii) $\epsilon = 0.3$ with system sizes $L = 10$ to 50, $L_t = 2$ to 40000. In each case, we start from a guess for the optimal shapes and find an approximate value of T_c from the crossing of the $g_{\rm av}$ vs. T curves for different L. We then find the maxima of the $g_{\rm av}$ vs. L_t curves at this temperature which yield improved optimal shapes. After iterating this procedure two or three times, we obtain T_c and the optimal shapes with reasonable precision.

Fig. 2 shows the resulting Binder cumulant $g_{\rm av}$ for $\epsilon = 0.5$ as function of L_t for different L at the approximate critical temperature of $T_c = 2.08(5)$. As expected at T_c, the maxima $g_{\rm av}^{\rm max}$ of these curves are independent of L (the slightly lower values at the

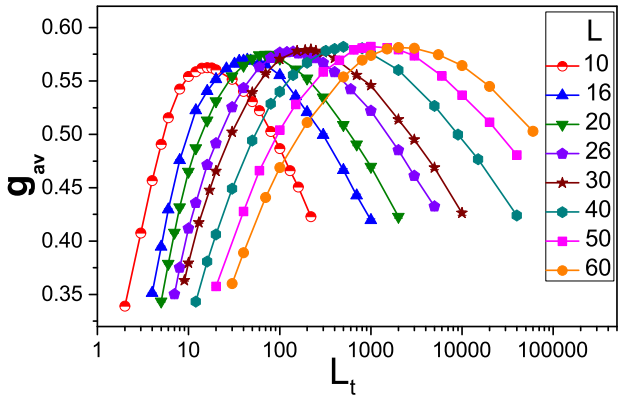

Fig. 2. Binder cumulant $g_{\rm av}$ as a function of L_t for several L at the critical temperature $T_c = 2.08$ for $\epsilon = 0.5$. The statistical error of $g_{\rm av}$ is smaller than the symbol size.

smallest L can be attributed to corrections to scaling). Moreover, the figure shows that the $g_{\rm av}$ vs. L_t domes rapidly become broader with increasing spatial size L, indicating non-power-law scaling. To analyze this quantitatively, we present a scaling plot of these data in Fig. 3. For conventional power-law dynamical scaling, the curves for different L should collapse onto each other when plotted as $g_{\rm av}$ vs. $L_t/L_t^{\rm max}$. The inset of Fig. 3 clearly demonstrates that this is not the case. In contrast, the Binder cumulant scales well when

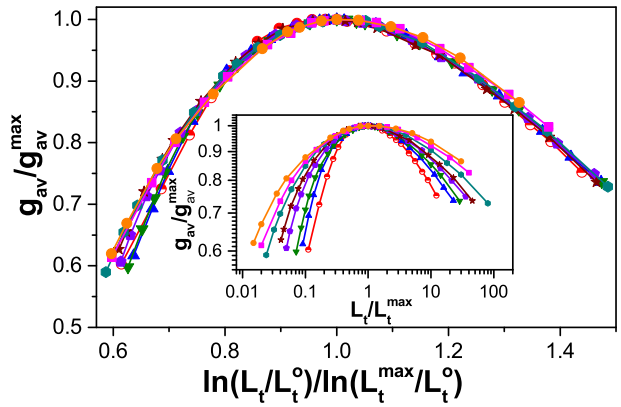

Fig. 3. Scaling plot of the Binder cumulant at $T_c = 2.08$ for $\epsilon = 0.5$. The symbols are the same as in Fig. 2. Main panel: Activated scaling $g_{\rm av}/g_{\rm av}^{\rm max}$ vs. $\ln(L_t/L_t^0)/\ln(L_t^{\rm max}/L_t^0)$ according to Eq. (8). The microscopic scale $L_t^0 = 0.06$. Inset: Power-law scaling $g_{\rm av}/g_{\rm av}^{\rm max}$ vs. $L_t/L_t^{\rm max}$.

plotted versus $\ln(L_t/L_t^0)/\ln(L_t^{\max}/L_t^0)$ as shown in the main panel of the figure. (Here, we treat the microscopic scale L_t^0 as a fit parameter). This behavior is in agreement with the activated scaling form (8).

We perform the same analysis for $\epsilon = 0.3$ at the approximate critical temperature of $T_c = 1.76(3)$, with analogous results. To verify the value of the tunneling exponent ψ, we now analyze the dependence of $L_t^{\max}$ on L. Fig. 4 shows that the data for both $\epsilon = 0.3$ and 0.5 can be well fitted with the relation $\ln(L_t^{\max}/L_t^0) \sim L^{\psi}$ with $\psi = 1/2$ as predicted by the strong-disorder renormalization group. The inset of this figure clearly demonstrates that the relation between $L_t^{\max}$ and L cannot be described by a power law. We can define, however, an effective (scale-dependent) dynamical exponent $z_{\rm eff} = d\ln(L_t^{\max})/d\ln(L)$. For $\epsilon = 0.5$, it increases from about 2 for the smallest system sizes to almost 4 for the largest ones.

We now turn to the critical behavior of magnetization and susceptibility. At the critical temperature, the magnetization of the optimally shaped samples is predicted to show a power-law dependence on the spatial system size, $m \sim L^{-\beta/\nu}$ with $\beta = 2 - \phi \approx 0.382$ and $\nu = 2$. Here, $\phi = (\sqrt{5}+1)/2$ is the golden mean. In the left panel of Fig. 5, we therefore present a double logarithmic plot of m vs. L for $\epsilon = 0.3$ and 0.5. The data for both coupling

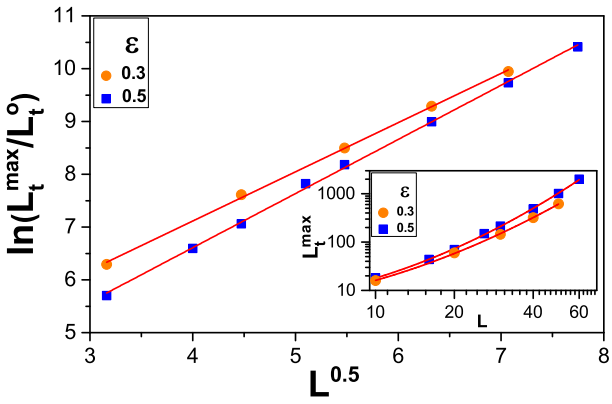

Fig. 4. $\ln(L_t^{\max}/L_t^0)$ vs. $L^{0.5}$ at criticality for $\epsilon = 0.3$ and 0.5. The data for $\epsilon = 0.3$ are shifted upwards by 0.3 for clarity. The solid lines are linear fits. Inset: Double logarithmic plot of $L_t^{\max}$ vs. L.

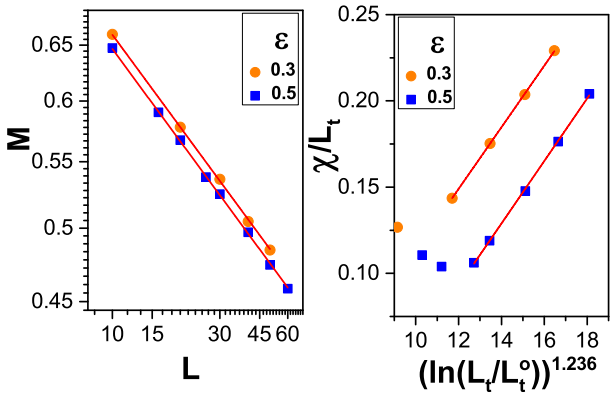

Fig. 5. Left: Double logarithmic plot of m vs. L for optimally shaped samples at criticality for $\epsilon = 0.3$ and 0.5. The solid lines are fits to the predicted power-law $m \sim L^{-\beta/\nu}$ with $\beta/\nu = 0.191$. Right: χ/L_t vs. $[\ln(L_t/L_t^0)]^{2\phi-2}$ for optimally shaped samples at criticality for $\epsilon = 0.3$ and 0.5. The solid lines are linear fits. The statistical errors of the data in both panels are smaller than the symbol size.

ratios can be fitted well with the predicted power law. While the magnetization follows a conventional power law dependence on the system size, the susceptibility is affected by the activated scaling. Its predicted system size dependence at criticality can be expressed in terms of the temporal size L_t as $\chi \sim L_t[\ln(L_t/L_t^0)]^{2\phi-2}$. We test this prediction in the right panel of Fig. 5 by plotting χ/L_t vs. $[\ln(L_t/L_t^0)]^{2\phi-2}$ for the optimally shaped samples. As the leading power law is divided out, this plot provides a sensitive test of the logarithmic corrections. The figure shows that the susceptibility indeed follows the predicted L_t dependence for system sizes $L > 20$. The deviations for the smaller sizes can likely be attributed to corrections to scaling stemming from the crossover between the clean first-order phase transition and the infinite-randomness critical point that governs the asymptotic behavior. The clean first-order phase transition is stronger for $\epsilon = 0.5$ than for 0.3; accordingly, χ shows stronger corrections to scaling for $\epsilon = 0.5$.

Finally, we analyze the slope $dg_{\rm av}/dT$ of the Binder cumulant at criticality. It is expected to vary with system size as $dg_{\rm av}/dT \sim L^{1/\nu}$ with $\nu = 2$. As is shown in Fig. 6, our slopes indeed follow the power-law dependence predicted by the strong-disorder renormalization group for both coupling ratios, $\epsilon = 0.3$ and 0.5.

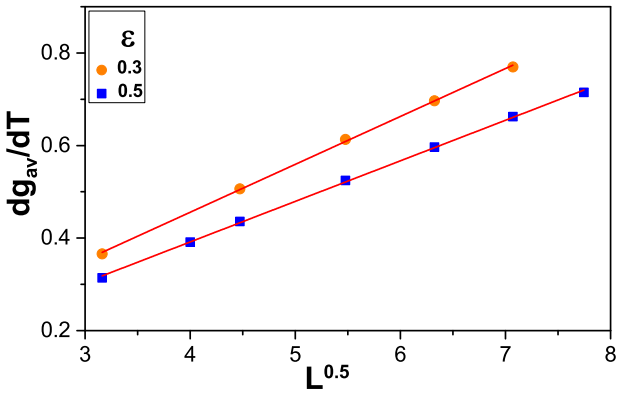

Fig. 6. Slope $dg_{\rm av}/dT$ of the Binder cumulant vs. $L^{0.5}$ at the critical temperature for $\epsilon = 0.3$ and 0.5. The solid lines are linear fits.

3.3. STRONG COUPLING REGIME. In the strong-coupling regime $\epsilon > \epsilon_c \approx 1.281$, we perform simulations for coupling ratios $\epsilon = 1.7, 2.5, 3.5,$ and 5. These simulations greatly suffer from the fact that the embedded Wolff and Swendsen-Wang cluster algorithms are not valid for $\epsilon > 0.5$. We are thus forced to employ the Metropolis single-spin algorithm. In this algorithm, the required equilibration and measurement times increase significantly with system size, reaching several hundred thousand sweeps for moderately large lattices. This severely limits the available sizes and the accuracy of the results. For comparison, we also perform Wang-Landau simulations but the available system sizes are restricted as well.

As the classical Hamiltonian (3) is not self-dual, we can expect a product phase to appear for $\epsilon > \epsilon_c$. Indeed, for all studied ϵ values, we find two distinct phase transitions. (This can already be seen from the specific heat data shown in the left panel of Fig. 7.) The product order parameter p, Eq. (7), develops at a higher temperature T_c^p while the magnetization becomes nonzero only below a lower temperature T_c^m (see phase diagram in Fig. 1). In the following, we look at these two transitions separately.

To analyze the transition between the product and Baxter phases (at which the magnetization becomes critical), we use the same procedure based on the Binder cumulant $g_{\rm av}$ as in Sec. 3.2. The right panel of Fig. 7 shows the Binder cumulant at the estimated

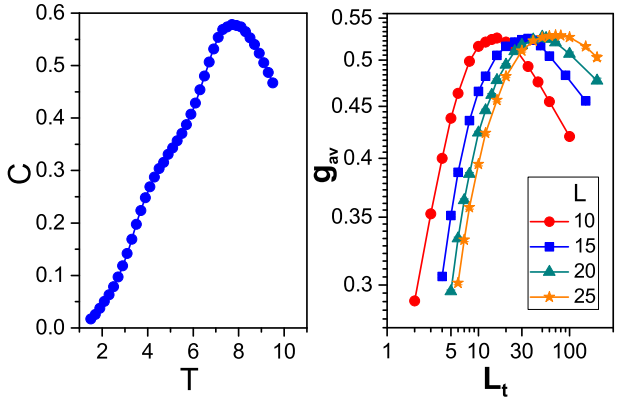

Fig. 7. Left: Specific heat C vs. classical temperature T for $\epsilon = 3.5$, system sizes $L = 10$, $L_t = 100$ and 5000 disorder configurations (using 140,000 Monte Carlo sweeps). Notice two distinct peaks corresponding to two separate phase transitions. Right: Binder cumulant $g_{\rm av}$ as a function of L_t for several L at the critical temperature $T_c = 3.65$ for $\epsilon = 1.7$.

critical temperature $T_c^m = 3.65$ for $\epsilon = 1.7$ as a function of L_t for several L between 10 and 25. As expected at criticality, the maximum value for each of the curves does not depend on L. The figure also shows that the domes become broader with increasing L, indicating non-power-law scaling. The largest spatial system size, $L = 25$ requires an enormous numerical effort, we averaged over 20,000 disorder configurations each using 700,000 Monte Carlo sweeps. Nonetheless the Binder cumulant at the right end of the dome ($L_t = 200$) is not fully equilibrated as its value shifts with increasing number of sweeps. Because of the limited system size range and the equilibration problems for the larger sizes we are not able to quantitatively analyze the critical behavior of this transition.

Similar problems, though slightly less severe, also plague the transition between the paramagnetic and product phases at which the product order parameter p becomes critical. Fig. 8 shows the Binder cumulant g_p for the product order parameter at the estimated critical temperature $T_c^p = 7.55$ and $\epsilon = 3.5$ as a function of L_t. The maxima of the different curves are again independent of L, as expected at the critical temperature. Moreover, the domes broaden with increasing system size. A scaling analysis of these data is presented in Fig. 9. The inset shows that the behavior of g_p is not compatible with

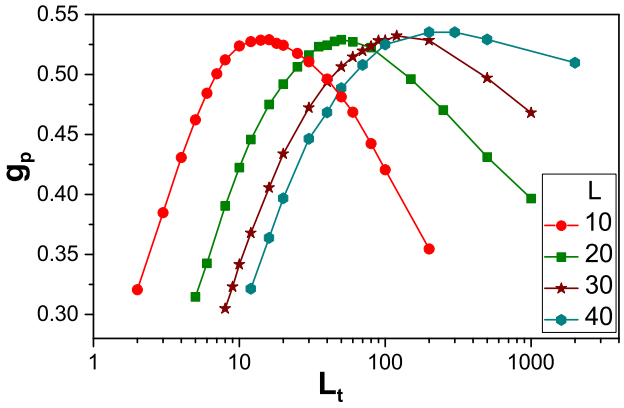

Fig. 8. Product Binder cumulant g_p as a function of L_t for several L at the critical temperature $T_c^p = 7.55$ for $\epsilon = 3.5$.

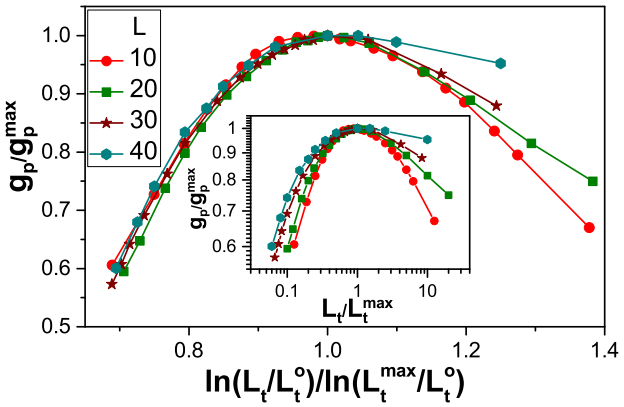

Fig. 9. Scaling plot of the product Binder cumulant g_p at $T_c^p = 7.55$ for $\epsilon = 3.5$. The symbols are the same as in Fig. 8. Main panel: Activated scaling $g_p/g_p^{\max}$ vs. $\ln(L_t/L_t^0)/\ln(L_t^{\max}/L_t^0)$ with $L_t^0 = 0.02$. Inset: Power-law scaling $g_p/g_p^{\max}$ vs. $L_t/L_t^{\max}$.

conventional power-law scaling. In contrast, the data scale reasonably well when plotted versus $\ln(L_t/L_t^0)/\ln(L_t^{\max}/L_t^0)$ as shown in the main panel of the figure. This behavior is in agreement with activated scaling in analogy to Eq. (8) for the Binder cumulant $g_{\rm av}$ of the magnetization. The deviations from data collapse for large L_t (ie., at the right side of the domes) stem from the fact that these systems do not equilibrate properly despite us using up to 500,000 Monte Carlo sweeps for each of the 20,000 disorder configurations (the g_p values still drift with increasing number of sweeps). This also prevents us from studying larger system sizes.

If we ignore the small system size range and the equilibration problems and analyze (along the lines of Sec. 3.2) the system size dependencies of $L_t^{\max}$, the product order parameter p, and its susceptibility χ_p, we obtain critical exponents that are roughly compatible with the random transverse-field Ising universality class (as expected from the strong-disorder renormalization group). We do not believe, however, that this constitutes a quantitative confirmation, and we cannot rule out a different universality class with somewhat different critical exponents.

4. CONCLUSIONS

In summary, we have studied the fate of the first-order quantum phase transition in the three-color quantum Ashkin-Teller spin chain under the influence of quenched disorder. To this end, we have mapped the random quantum Ashkin-Teller Hamiltonian onto a $(1+1)$-dimensional classical Ashkin-Teller model with columnar disorder. We have then performed large-scale Monte Carlo simulations for systems with up to 3.6 million lattice sites (10.8 million spins). In agreement with the quantum version of the Aizenman-Wehr theorem, we have found that the first-order transition of the clean system is rounded to a continuous one in the presence of bond randomness.

For weak inter-color coupling ϵ, efficient cluster Monte Carlo algorithms have allowed us to simulate large systems. Our data for the quantum phase transition are in full agreement with the results of the strong-disorder renormalization group calculation [22] that predicts universal critical behavior in the random transverse-field Ising universality class. Specifically, we have confirmed for two different values of ϵ the activated dynamical scaling with a tunneling exponent $\psi = 1/2$, the correlation length exponent $\nu = 2$, and the order parameter exponent $\beta = 2 - \phi$ with ϕ the golden mean. We have also confirmed the behavior of the magnetic susceptibility.

In contrast, our simulations for large inter-color coupling ϵ have been restricted to smaller system sizes, and they have suffered from equilibration problems because efficient cluster algorithms are not available. Consequently, we have not been able to fully test the renormalization group calculations in this regime. Our numerical data provide evidence for activated dynamical scaling at the quantum phase transitions between the paramagnetic and product phases as well as between the product and Baxter phases. For the latter transition we have also determined rough estimates of the critical exponents and found them compatible with the random transverse-field Ising universality class. However, a quantitative verification of the critical behavior is beyond our current numerical capabilities.

Let us compare our results with earlier simulations. While our critical behavior (in the weak-coupling regime) fully agrees with the random transverse-field Ising universality class, some exponents calculated in Ref. [27] show sizable deviations. This is particularly interesting because the *spatial* system sizes L used in both simulations are comparable (the largest L in Ref. [27] is actually larger than ours). We believe that the results of Ref. [27] do not agree with the renormalization group predictions because the simulations are still crossing over from the clean first-order transition to the disordered critical point, probably because the chosen parameters lead to relatively weak disorder. This would mean that the measured exponent values are effective rather than true asymptotic exponents. Support for this hypothesis can be obtained from comparing the dynamical scaling in the present

paper and in Ref. [27]. An infinite-randomness critical point features activated dynamical scaling, i.e., the temporal system size L_t scales exponentially with the spatial size L via $\ln(L_t) \sim L^{\psi}$. This implies that the conventional dynamical exponent $z = \infty$. The optimal temporal system size (defined, e.g., via the maximum of the Binder cumulant) therefore must increase very rapidly with L. Indeed, the inset of Fig. 4 shows that $L_t^{\max}$ increases from 18 to about 2000 while L varies only from 10 to 60. The corresponding effective (scale-dependent) dynamical exponent $z_{\text{eff}} = d\ln(L_t^{\max})/d\ln(L)$ reaches almost 4 for the largest sizes. In contrast, $L_t^{\max}$ reaches only 224 for $L = 96$ in Ref. [27] and z_{eff} stays below 2, placing the system further away from the asymptotic regime $z_{\text{eff}} \to \infty$.

To conclude, as our numerical results (in the weak-coupling regime) fully agree with the renormalization group predictions, we have not found any indications that the *asymptotic* critical behavior of the disordered system "remembers" the first-order origin of the transition. This supports the expectation that the general classification of disordered critical points developed in Refs. [14, 15, 16] also holds for critical points emerging from the rounding of first-order (quantum) phase transitions. However, the crossover from the clean to the disordered behavior is certainly affected by the first-order nature of the clean transition. The breakup length beyond which phase coexistence is destroyed by domain formation increases with decreasing disorder and may exceed the system size. For sufficiently weak disorder, the true asymptotic behavior is then unobservable in both simulations and experiment. This crossover will be even slower in $(2+1)$-dimensional systems because $d = 2$ is the marginal dimension for the Aizenman-Wehr theorem, suggesting an exponential dependence of the breakup length on the disorder strength [53, 54].

ACKNOWLEDGEMENTS

This work was supported by the NSF under Grants No. DMR-1205803 and No. DMR-1506152. We thank Q. Zhu for sharing his Wang-Landau code.

REFERENCES

[1] D. Belitz, T. R. Kirkpatrick, and T. Vojta. Nonanalytic behavior of the spin susceptibility in clean Fermi systems. *Phys. Rev. B*, 55:9452, 1997; First order transitions in multicritical points in weak itinerant ferromagnets. *Phys. Rev. Lett.*, 82:4707, 1999.

[2] D. Belitz, T. R. Kirkpatrick, and T. Vojta. How generic scale invariance influences quantum and classical phase transitions. *Rev. Mod. Phys.*, 77:579, 2005.

[3] M. Brando, D. Belitz, F. M. Grosche, and T. R. Kirkpatrick. Metallic quantum ferromagnets. *Rev. Mod. Phys.*, 88:025006, May 2016.

[4] D. S. Fisher. Random transverse field Ising spin chains. *Phys. Rev. Lett.*, 69:534, 1992; Critical behavior of random transverse-field Ising spin chains. *Phys. Rev. B*, 51:6411, 1995.

[5] O. Motrunich, S. C. Mau, D. A. Huse, and D. S. Fisher. Infinite-randomness quantum Ising critical fixed points. *Phys. Rev. B*, 61:1160, 2000.

[6] J. A. Hoyos, C. Kotabage, and T. Vojta. Effects of dissipation on a quantum critical point with disorder. *Phys. Rev. Lett.*, 99:230601, 2007; T. Vojta, C. Kotabage, and J. A. Hoyos. Infinite-randomness quantum critical points induced by dissipation. *Phys. Rev. B*, 79:024401, 2009.

[7] M. Thill and D. A. Huse. Equilibrium behaviour of quantum Ising spin glass. *Physica A*, 214:321, 1995.

[8] H. Rieger and A. P. Young. Griffiths singularities in the disordered phase of a quantum ising spin glass. *Phys. Rev. B*, 54:3328, 1996; A. P. Young and H. Rieger. Numerical study of the random transverse-field Ising spin chain. *Phys. Rev. B*, 53:8486, 1996.

[9] T. Vojta. Disorder-induced rounding of certain quantum phase transitions. *Phys. Rev. Lett.*, 90:107202, 2003; J. A. Hoyos and T. Vojta. Theory of smeared quantum phase transitions. *Phys. Rev. Lett.*, 100:240601, 2008.

[10] S. Guo, D. P. Young, R. T. Macaluso, D. A. Browne, N. L. Henderson, J. Y. Chan, L. L. Henry, and J. F. DiTusa. Discovery of the griffiths phase in the itinerant magnetic semiconductor $fe_{1-x}co_xs_2$. *Phys. Rev. Lett.*, 100:017209, Jan 2008; L. L. Henry, and J. F. DiTusa. Magnetic and thermodynamic properties of cobalt-doped iron pyrite: Griffiths phase in a magnetic semiconductor. *Phys. Rev. B*, 81:144423, 2010.

[11] T. Westerkamp, M. Deppe, R. Küchler, M. Brando, C. Geibel, P. Gegenwart, A. P. Pikul, and F. Steglich. Kondo-cluster-glass state near a ferromagnetic quantum phase transition. *Phys. Rev. Lett.*, 102:206404, 2009.

[12] S. Ubaid-Kassis, T. Vojta, and A. Schroeder. Quantum Griffiths phase in the weak itinerant ferromagnetic alloy $Ni_{1-x}V_x$. *Phys. Rev. Lett.*, 104:066402, 2010.

[13] L. Demkó, S. Bordács, T. Vojta, D. Nozadze, F. Hrahsheh, C. Svoboda, B. Dóra, H. Yamada, M. Kawasaki, Y. Tokura, and I. Kézsmárki. Disorder promotes ferromagnetism: Rounding of the quantum phase transition in $Sr_{1-x}Ca_xRuO_3$. *Phys. Rev. Lett.*, 108:185701, May 2012.

[14] T. Vojta and J. Schmalian. Quantum Griffiths effects in itinerant Heisenberg magnets. *Phys. Rev. B*, 72:045438, 2005.

[15] Thomas Vojta and José A. Hoyos. Criticality and quenched disorder: Harris criterion versus rare regions. *Phys. Rev. Lett.*, 112:075702, Feb 2014.

[16] T. Vojta. Rare region effects at classical, quantum, and non-equilibrium phase transitions. *J. Phys. A*, 39:R143, 2006; Quantum Griffiths effects and smeared phase transitions in metals: theory and experiment. *J. Low Temp. Phys.*, 161:299, 2010; Strong-disorder magnetic quantum phase transitions: Status and new developments. *J. Phys. Conf. Series*, 529(1):012016, 2014.

[17] Rafael L. Greenblatt, Michael Aizenman, and Joel L. Lebowitz. Rounding of first order transitions in low-dimensional quantum systems with quenched disorder. *Phys. Rev. Lett.*, 103:197201, Nov 2009; Michael Aizenman, Rafael L. Greenblatt, and Joel L. Lebowitz. Proof of rounding by quenched disorder of first order transitions in low-dimensional quantum systems. *J. Math. Phys.*, 53(2):–, 2012.

[18] Yoseph Imry and Michael Wortis. Influence of quenched impurities on first-order phase transitions. *Phys. Rev. B*, 19:3580–3585, Apr 1979.

[19] Kenneth Hui and A. Nihat Berker. Random-field mechanism in random-bond multicritical systems. *Phys. Rev. Lett.*, 62:2507–2510, May 1989.

[20] Michael Aizenman and Jan Wehr. Rounding of first-order phase transitions in systems with quenched disorder. *Phys. Rev. Lett.*, 62:2503–2506, May 1989.

[21] T. Senthil and S. N. Majumdar. Critical properties of random quantum Potts and clock models. *Phys. Rev. Lett.*, 76:3001, 1996.

[22] P. Goswami, D. Schwab, and S. Chakravarty. Rounding by disorder of first-order quantum phase transitions: Emergence of quantum critical points. *Phys. Rev. Lett.*, 100:015703, 2008.

[23] Eduardo Fradkin. N-color Ashkin-Teller model in two dimensions: Solution in the large-N limit. *Phys. Rev. Lett.*, 53:1967–1970, Nov 1984; R. Shankar. Ashkin-Teller and Gross-Neveu models: New relations and results. *Phys. Rev. Lett.*, 55:453–456, Jul 1985.

[24] Fawaz Hrahsheh, José A. Hoyos, and Thomas Vojta. Rounding of a first-order quantum phase transition to a strong-coupling critical point. *Phys. Rev. B*, 86:214204, Dec 2012.

[25] Hatem Barghathi, Fawaz Hrahsheh, Jose A. Hoyos, Rajesh Narayanan, and Thomas Vojta. Strong-randomness phenomena in quantum Ashkin-Teller models. *Phys. Scr.*, T165:014040, 2015.

[26] F. Igloi and C. Monthus. Strong disorder renormalization group approach of random systems. *Phys. Rep.*, 412:277, 2005.

[27] Arash Bellafard and Sudip Chakravarty. Activated scaling in disorder-rounded first-order quantum phase transitions. *Phys. Rev. B*, 94:094408, Sep 2016.

[28] Gary S. Grest and Michael Widom. N-color Ashkin-Teller model. *Phys. Rev. B*, 24:6508–6515, Dec 1981.

[29] J. Ashkin and E. Teller. Statistics of two-dimensional lattices with four components. *Phys. Rev.*, 64:178–184, Sep 1943.

[30] Per Bak, P. Kleban, W. N. Unertl, J. Ochab, G. Akinci, N. C. Bartelt, and T. L. Einstein. Phase diagram of selenium adsorbed on the ni(100) surface: A physical realization of the ashkin-teller model. *Phys. Rev. Lett.*, 54:1539–1542, Apr 1985.

[31] Vivek Aji and C. M. Varma. Theory of the quantum critical fluctuations in cuprate superconductors. *Phys. Rev. Lett.*, 99:067003, Aug 2007.

[32] Vivek Aji and C. M. Varma. Quantum criticality in dissipative quantum two-dimensional xy and ashkin-teller models: Application to the cuprates. *Phys. Rev. B*, 79:184501, May 2009.

[33] Zhe Chang, Ping Wang, and Ying-Hong Zheng. Ashkin Teller Formalism for Elastic Response of DNA Molecule to External Force and Torque. *Commun. Theor. Phys.*, 49:525–528, 2008.

[34] H.A. Ceccatto. Quantum n-colour ashkin-teller model: exact solution in the large-n limit. *J. Phys. A*, 24:2829, 1991.

[35] R.J. Baxter. *Exactly Solved Models in Statistical Mechanics*. Academic Press, New York, 1982.

[36] Fawaz Hrahsheh, José A. Hoyos, Rajesh Narayanan, and Thomas Vojta. Strong-randomness infinite-coupling phase in a random quantum spin chain. *Phys. Rev. B*, 89:014401, Jan 2014.

[37] S. Sachdev. *Quantum phase transitions*. Cambridge University Press, Cambridge, 1999.

[38] While this does not change the critical behavior, it destroys the self-duality of the Hamiltonian.

[39] Shai Wiseman and Eytan Domany. Critical behavior of the random-bond ashkin-teller model: A monte carlo study. *Phys. Rev. E*, 51:3074–3086, Apr 1995.

[40] Robert H. Swendsen and Jian-Sheng Wang. Nonuniversal critical dynamics in monte carlo simulations. *Phys. Rev. Lett.*, 58:86–88, Jan 1987.

[41] U. Wolff. Collective Monte-Carlo updating for spin systems. *Phys. Rev. Lett.*, 62:361, 1989.

[42] Generalizations of the Swendsen-Wang and Wolff algorithms exist for systems with competing interaction, but they turn out be much less efficient [55, 56].

[43] N. Metropolis, A. Rosenbluth, M. Rosenbluth, and A. Teller. Equation of state calculations by fast computing machines. *J. Chem. Phys.*, 21:1087, 1953.

[44] Fugao Wang and D. P. Landau. Efficient, multiple-range random walk algorithm to calculate the density of states. *Phys. Rev. Lett.*, 86:2050–2053, Mar 2001.

[45] Effects of nonuniform inter-color coupling ratios were worked out in Ref. [36] for two colors and briefly discussed in Ref. [25] for the general N color case. They only affect the multicritical point separating the weak and strong coupling regimes.

[46] Qiong Zhu, Xin Wan, Rajesh Narayanan, José A. Hoyos, and Thomas Vojta. Emerging criticality in the disordered three-color ashkin-teller model. *Phys. Rev. B*, 91:224201, Jun 2015.

[47] M. Guo, R. N. Bhatt, and D. A. Huse. Quantum critical behavior of a three-dimensional Ising spin glass in a transverse magnetic field. *Phys. Rev. Lett.*, 72:4137, 1994.

[48] H. Rieger and A. P. Young. Zero-temperature quantum phase transition of a two-dimensional Ising spin glass. *Phys. Rev. Lett.*, 72:4141, 1994.

[49] R. Sknepnek, T. Vojta, and M. Vojta. Exotic vs. conventional scaling and universality in a disordered bilayer quantum Heisenberg antiferromagnet. *Phys. Rev. Lett.*, 93:097201, 2004; T. Vojta and R. Sknepnek. Quantum phase transitions of the diluted o(3) rotor model. *Phys. Rev. B.*, 74:094415, 2006.

[50] Thomas Vojta, Jack Crewse, Martin Puschmann, Daniel Arovas, and Yury Kiselev. Quantum critical behavior of the superfluid-mott glass transition. *Phys. Rev. B*, 94:134501, Oct 2016.

[51] M. N. Barber. Finite-size scaling. In C. Domb and J. L. Lebowitz, editors, *Phase Transitions and Critical Phenomena*, volume 8, pages 145–266. Academic, New York, 1983.

[52] J. Cardy, editor. *Finite-size scaling*. North Holland, Amsterdam, 1988.

[53] K. Binder. Random-field induced interface widths in ising systems. *Z. Phys. B*, 50:343, 1983.

[54] G. Grinstein and Shang-keng Ma. Surface tension, roughening, and lower critical dimension in the random-field ising model. *Phys. Rev. B*, 28:2588–2601, Sep 1983.

[55] David A. Kessler and Michael Bretz. Unbridled growth of spin-glass clusters. *Phys. Rev. B*, 41:4778–4780, Mar 1990.

[56] Shoudan Liang. Application of cluster algorithms to spin glasses. *Phys. Rev. Lett.*, 69:2145–2148, Oct 1992.

IV. NUMERICAL INVESTIGATION OF A DISORDERED SUPERCONDUCTOR-METAL QUANTUM PHASE TRANSITION

Ahmed K. Ibrahim and Thomas Vojta

Department of Physics, Missouri University of Science and Technology, Rolla, MO 65409, USA

ABSTRACT[*]

We investigate the quantum phase transitions of a disordered nanowire from superconducting to metallic behavior by employing extensive Monte Carlo simulations. To this end, we map the quantum action onto a (1+1)-dimensional classical XY model with long-range interactions in imaginary time. We then analyze the finite-size scaling behavior of the order parameter susceptibility, the correlation time, the superfluid density, and the compressibility. We find that the critical behavior is of infinite-randomness type and belongs to the random transverse-field Ising universality class, as predicted by a strong disorder renormalization group calculation.

[*] All of this section is reproduced from a manuscript in preparation for European Physical Journal B (2018).

1. INTRODUCTION

Investigating the electrical transport in fluctuating superconductors has attracted great interest in experimental studies during the last decades [1]. Recently, many experiments [2, 3, 4, 5, 6] have studied the electrical transport characteristics of one-dimensional ultrathin metallic nanowires. Upon decreasing the temperature, measurements of resistance have demonstrated that thicker wires display a phase transition from a metal to a superconducting state. However, thinner wires do not show superconductivity even at the lowest temperatures T.

The behavior of these experiments can be understood using the concept of a superconductor-metal quantum phase transition in the pair-breaking universality class, as proposed in recent work [7, 8, 9]. A characterization of this transition built on microscopic BCS theory suggests a model of superconducting fluctuations damped by decay into unpaired electrons [10, 11, 12, 13, 14].

Quenched disorder plays a significant role in disordered nanowires due to the random positions of the pair-breaking magnetic moments. The thermodynamics of this disordered superconductor-metal quantum phase transition has been studied analytically via a strong-disorder renormalization group analysis [15] and numerically [9] via a large-N analysis in which the number of order parameter components is generalized from 2 to $N \gg 1$. These methods predict that the behavior is governed by a nonperturbative infinite-randomness critical point in the same universality class as the random transverse-field Ising model. It presents slow activated dynamical scaling rather than conventional (power-law) one, i.e., the correlation time ξ_τ is related to the correlation length ξ as $\ln\xi_\tau \sim \xi^\psi$, where ψ is the tunneling exponent. Observables also show nonconventional scaling behavior. For example, with decreasing temperature, the order parameter susceptibility at criticality diverges as

$$\chi \sim \frac{1}{T}[\ln(1/T)]^{2\phi-d/\psi}, \tag{1}$$

where ϕ is the cluster size exponent.

In this paper, we investigate the effects of disorder on the quantum phase transition between superconductor and metal in thin nanowires by employing a Monte Carlo method. This allows us to test these predictions directly for $N = 2$ order parameter components. Our paper is organized as follows: In Sec. 2, we define the overdamped Cooper pair model and describe the mapping onto a classical XY Hamiltonian. In Sec. 3, we explain the renormalization group predictions. Section 4 is devoted to the Monte Carlo simulations. In Sec. 5, we discuss our results and compare them to the predictions of the strong-disorder renormalization group. We conclude in Sec. 6.

2. THE MODEL

The starting point of our work is a quantum Landau-Ginzburg-Wilson (LGW) free energy functional for an N-component vector order-parameter $\varphi = (\varphi_1, ..., \varphi_N)$ in d space dimensions (for the superconductor-metal transition in nanowires, $d = 1$ and $N = 2$). The action can be derived from a Hamiltonian of disordered electrons by employing standard techniques [16, 17, 18, 19]. In the absence of quenched disorder, the clean LGW action reads [15, 20]

$$S = \int dy dx \varphi(x) \Gamma(x, y) \varphi(y) + \frac{u}{2N} \int dx \varphi^4(x), \tag{2}$$

where $x \equiv (\mathbf{x}, \tau)$ is a vector that includes position $\mathbf{x}$ and imaginary time τ, $\int dx \equiv \int d\mathbf{x} \int_0^{1/T} d\tau$, and u is the standard 4^{th}-order coefficient. $\Gamma(x, y)$ is the bare inverse propagator (two-point vertex) whose Fourier transform reads

$$\Gamma(\mathbf{q}, \omega) = r + \xi_0^2 \mathbf{q}^2 + \gamma_0 |\omega|^{2/z_0}. \tag{3}$$

Here, r is the distance from criticality, ξ_0 is a microscopic length, ω_n is the Matsubara frequency, γ_0 is the damping coefficient, and $z_0 = 2$ for the Ohmic order parameter dynamics caused by the coupling to the conduction electrons.

To inspect the predictions of the strong-disorder renormalization group [15] by means of a Monte Carlo method, we need to map the quantum action (Eq. 2) in d space dimension onto a $(d + 1)$-dimensional classical XY model. This mapping can be accomplished by discretizing space and imaginary time and interpreting imaginary time as another space dimension. As a result, the classical XY Hamiltonian reads:

$$H = -\sum_{i,\tau}(J_i^{(s)} S_{i,\tau} S_{i+1,\tau} + J_i^{(\tau)} S_{i,\tau} S_{i,\tau+1}) - \sum_{i,\tau,\tau'} K_{\tau,\tau'} S_{i,\tau} S_{i,\tau'}. \tag{4}$$

Here, $S_{i,\tau}$ is the XY spin at position i in space and τ in imaginary time, and $J_i^{(s)}$ and $J_i^{(\tau)}$ are the ferromagnetic interactions between nearest neighbor spins in space and time directions, respectively. $K_{\tau,\tau'}$ is the long-range interaction in time that reads

$$K_{\tau,\tau'} = \gamma|\tau - \tau'|^{-\alpha}, \tag{5}$$

where γ is the interaction amplitude while $\alpha = 2$ for Ohmic dissipation. We tune the transition by varying the classical temperature T, while keeping $J_i^{(s)}$, $J_i^{(\tau)}$, and $K_{\tau,\tau'}$ constant.

Under this mapping, the actual temperature T_Q of the quantum system maps on the temporal system size L_τ of the XY model, the superfluid density maps onto the spin-wave stiffness in space direction, and the compressibility maps onto the stiffness in imaginary time direction.

3. THEORY

3.1. RENORMALIZATION GROUP PREDICTIONS. In this section, we briefly summarize the results of a strong-disorder renormalization group [15] of the LGW field theory (Eq. 2) with quenched disorder. Hoyos *et al*. found that Ohmic dissipation leads to a quantum critical point of exotic infinite-randomness type that belongs to the random transverse-field Ising chain universality class [21, 22]. Whereas the dynamical scaling of the clean system is power-law scaling, the disordered system follows the unconventional (activated) scaling.

The strong-disorder renormalization group [15, 22] makes the following predictions for the finite-size scaling behavior of observables (see also Refs. [23, 24]). The order parameter susceptibility χ at criticality is expected to depend on the system size L_τ in imaginary time direction via

$$\chi \sim L_\tau [\ln(L_\tau/b)]^{2\phi-1/\psi}, \tag{6}$$

where $\phi = (1+\sqrt{5})/2$ and $\psi = 1/2$ are the critical exponents of the infinite-randomness critical point, b is arbitrary constant. In the ordered Griffiths phase ($T < T_c$), the susceptibility diverges as

$$\chi \sim L_\tau^{1+1/z}, \tag{7}$$

and in the disordered Griffiths phase ($T > T_c$), it behaves as

$$\chi \sim L_\tau^{1-1/z}. \tag{8}$$

Here, $z > 1$ is the Griffiths dynamical exponent.

The spin-wave stiffness ρ_s of the XY Hamiltonian describes the change in the free-energy density f during a twist of the spins at two opposite boundaries by an angle θ. For small θ and large system size l, the free-energy change reads

$$f(\theta) - f(0) = \frac{\rho_s}{2}\frac{\theta^2}{l^2}. \tag{9}$$

We can distinguish two kinds of stiffnesses, the space-stiffness $\rho_s^{(s)}$, and the time-stiffness $\rho_s^{(\tau)}$. To discuss the space-stiffness $\rho_s^{(s)}$ (which corresponds to the superfluid density of the quantum system), we implement the twist between 0 and L in space direction with $l = L$ in Eq. (9). The theory developd in Refs. [23, 25] implies anomalous behavior of $\rho_s^{(s)}$: Because the distribution of the effective interactions $J_{eff}^{(s)}$ becomes very broad under the renormalization group, the stiffness vanishes for $L \to \infty$ in part of the ordered Griffiths phase between T_c and T^* where T^* is the temperature where the Griffiths dynamical exponent $z = 1$. In this temperature range, it behaves as

$$\rho_s^{(s)} \sim L^{1-z}. \tag{10}$$

Normal behavior with nonzero $\rho_s^{(s)}$ in the thermodynamic limit is restored for $T < T^*$. In contrast, the time-stiffness $\rho_s^{(\tau)}$ (which corresponds to the compressibility of the quantum system) is nonzero everywhere in the ordered phase, and behaves as

$$\rho_s^{(\tau)} \sim |T - T_c|^{\beta}, \tag{11}$$

where β is the exponent of the order parameter.

4. MONTE CARLO SIMULATIONS

To confirm the predictions of the strong-disorder renormalization group given in Sec. 3, we perform extensive Monte Carlo simulations of the (1+1)-dimensional XY Hamiltonian (4) with long-range interactions in time direction.

By means of the Luijten algorithm [26], we simulate systems with linear size $L = 20$ to 160 in space direction and $L_\tau = 2$ to 40000 in (imaginary) time direction. We introduce quenched disorder only in the space direction, this implies that the disorder is perfectly correlated in the imaginary time direction. Specifically, $J_i^{(s)}$ and $J_i^{(\tau)}$ are random variables derived from a binary probability distribution

$$\rho(J) = (1 - c)\delta(J - J_l) + c\delta(J - J_h). \tag{12}$$

Here, J_h is the higher value of the interaction while the lower value is J_l. The concentrations of J_h and J_l are c and $(1 - c)$, respectively. In the simulations, we choose $\gamma = 0.1$, $c = 0.5$, J_h=2 and J_l=0.5 as parameters. For each run we use 100 Monte Carlo sweeps for equilibration and 200 sweeps for measurements. During these simulations, we measure the energy, specific heat, magnetization, susceptibility, correlation function, correlation length, space and time stiffnesses, and Binder cumulant. All observables are averaged over 1000 to 10 000 disorder configurations.

5. THERMODYNAMICS

5.1. CLEAN SYSTEM. To test our simulation method and to make contact with the literature, we first study the clean case with uniform $J_i^{(s)} = J_i^{(\tau)} = 1$. To estimate the location of the critical point, we use the finite-size scaling method [27, 28]. The magnetic

Binder cumulant g [29, 30] has a finite-size scaling form of

$$g(r, L, L_\tau) = \Upsilon_g(rL^{1/\nu}, L_\tau/L^z). \tag{13}$$

Here, $r = (T - T_c)/T_c$ is the distance from the critical point, Υ_g is the scaling function, ν is the correlation length exponent, and z is the dynamical exponent. The Binder cumulant can be calculated from

$$g = 1 - \frac{\langle m^4 \rangle}{3\langle m^2 \rangle^2}, \tag{14}$$

where m is the magnetization (order parameter),

$$m = \frac{1}{LL_\tau} \sum_{i,\tau} S_{i,\tau}. \tag{15}$$

The long-range interactions breaks the symmetry between the space and time-like directions. The value of z is therefore not known at the outset, and we need to perform anisotropic finite-size scaling. We employ the iterative method outlined in Refs. [31, 32, 33, 34]: The Binder cumulant has a maximum as function of L_τ for fixed L. According to (13), the peak position L_τ^{max} must behave as L^z at criticality, and the value g^{max} of the maximum must be L-independent. Fig. 1 shows the behavior of Binder cumulant g as a function of L_τ for several system size L at the estimated critical temperature $T_c = 0.56969(6)$. These curves indeed have identical maximum values that are independent of the system size L (because of corrections to scaling, some deviations occur at small L).

To test the scaling form of the Binder cumulant (13) and measure the dynamical exponent z, we plot the data of the Binder cumulant as a function of L_τ/L^z and vary z until a good collapse is achieved. As shown in Fig. 2, the data collapse onto each other in the conventional power-law dynamical scaling form as expected [35, 36], yielding a dynamical exponent $z = 2.01(6)$.

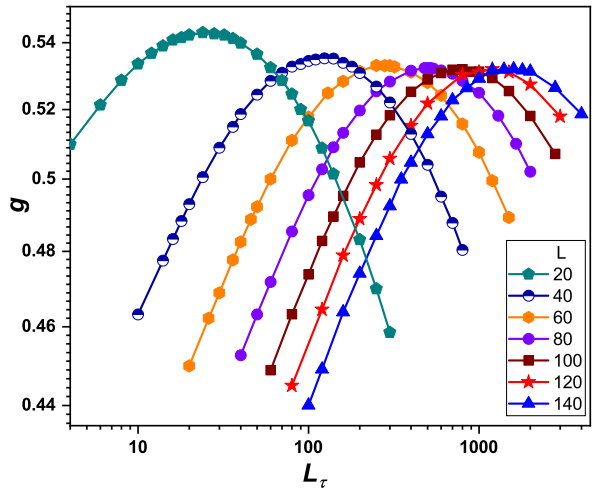

Fig. 1. Binder cumulant g vs. L_τ for different L at the critical temperature $T_c = 0.56969$. The statistical error of g is much smaller than the symbol size.

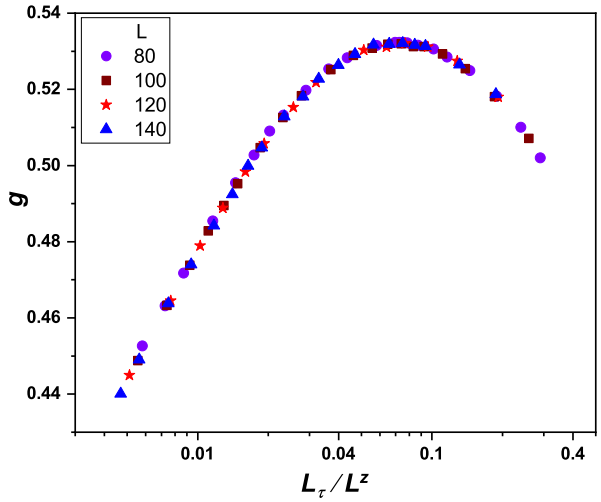

Fig. 2. Scaling plot of the Binder cumulant g as a function of L_τ/L^z for different L at $T_c = 0.56969$. All curves collapse and follow the power-law scaling for $z = 2.01$.

To compute further critical exponents of the system, we analyze the properties of magnetization and susceptibility at the critical point, as well as the slope dg/dT of the Binder cumulant. Correlation length exponent ν can be estimated from slopes of Binder cumulant. Taking the derivative with respect to temperature in (13), it follows that dg/dT at criticality

($r = 0$) behaves as $L^{1/\nu}$ (if evaluated for the optimal sample shapes $L_\tau = L_\tau^{max} \sim L^z$). In Fig. 3 we plot these slopes as a function of system size L, then we determine the critical exponent $\nu = 0.687(9)$ from a power-law fit to $dg/dT \sim L^{1/\nu}$.

We study the scaling behavior of magnetization and susceptibility at criticality. We find that these observables follow power-law scaling, $m \sim L^{-\beta/\nu}$ and $\chi \sim L^{\gamma/\nu}$ as expected [27]. We estimate the critical exponents to be $\beta/\nu = 0.507(5)$ and $\gamma/\nu = 2.03(4)$ (see Fig. 3).

Moreover, we test the hyper scaling relation [37]

$$\frac{2\beta}{\nu} + \frac{\gamma}{\nu} = d + z. \tag{16}$$

We find that our results fulfill the hyper scaling behavior. All clean exponents agree with those found in Ref. [36] within their errorbars.

Note that the correlation length exponent $\nu = 0.687$ violates the Harris criterion $d\nu > 2$ [38], implying that the clean critical behavior will be unstable against disorder.

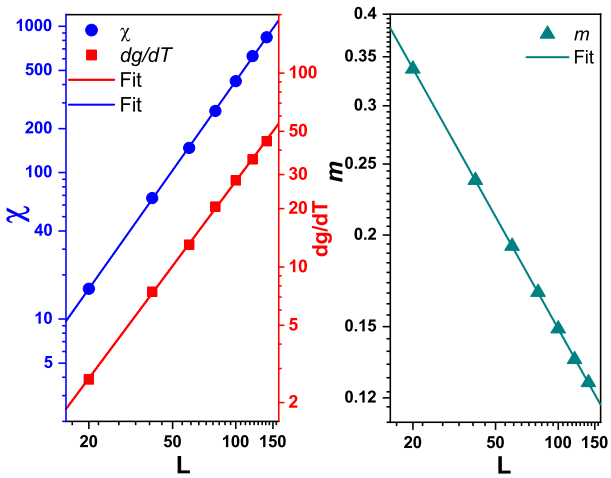

Fig. 3. Left: Double logarithmic plot of susceptibility χ and slope of Binder cumulant dg/dT vs. system size L for optimally shaped samples at criticality. The solid lines are fits to the predicted power laws $\chi \sim L^{\gamma/\nu}$ and $dg/dT \sim L^{1/\nu}$ with $\gamma/\nu = 2.03$ and $1/\nu = 1.454$. Right: Magnetization m as a function of L at criticality. The slope of the fitted line with $m \sim L^{-\beta/\nu}$ gives $\beta/\nu = 0.507$.

5.2. DISORDERED SYSTEM. After studying and analyzing the behavior of the pure critical point, we now apply quenched disorder to the Hamiltonian (4) by making the ferromagnetic interactions $J_i^{(s)}$ and $J_i^{(\tau)}$ random variables with the distribution (12). We have attempted to use the same Binder-cumulant-based finite-size scaling method as in the clean case to find the critical point. Unfortunately, this analysis is hampered by strong corrections to scaling. We have therefore turned to analyzing the dependence of order parameter susceptibility on L_τ (see Eqs. 6, 7 and 8), in analogy to Ref. [24] where similar difficulties were encountered. To test Eqs. (7) and (8), one needs to take samples having effectively infinite size L ($L \gg L_\tau$). We have performed simulations with system size $L = 1000$ and $L_\tau = 10$ to 224. Fig. 4 confirms that the behavior of χ versus L_τ for different temperatures in the Griffiths region agrees with the finite-size power laws (7) and (8) predicted by theory.

To find T_c we employ the behavior of Eqs. (7) and (8) and extract the values of the dynamical exponent z for the ferromagnetic and paramagnetic sides of the Griffiths region. The exponent z is predicted to diverge at the critical point as

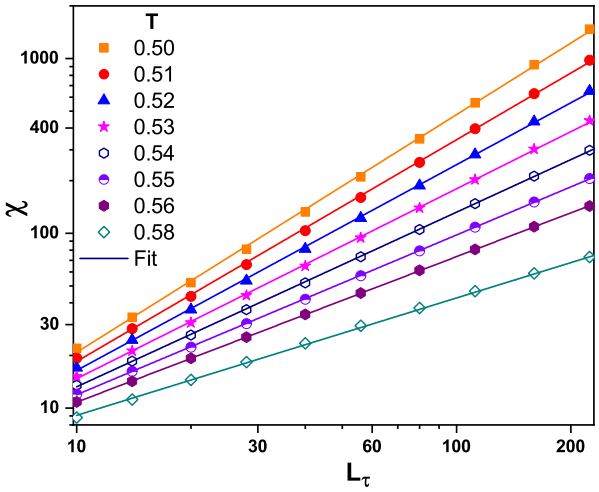

Fig. 4. Susceptibility χ as a function of L_τ for various temperatures in the Griffiths phase. The size in space direction is $L = 1000$. The solid lines are fits to the power laws (7) and (8).

$$z \sim \frac{1}{|T - T_c|}. \tag{17}$$

Fig. 5 shows the values of z in the ordered and disordered Griffiths phase as a function of temperature T. These values are fitted to the power law relation (17) giving an estimated critical temperature of $T_c \approx 0.5398(91)$.

In addition to the order parameter susceptibility, we also investigate the superfluid density and the compressibility of the quantum system. They are represented by the spin-wave stiffness in the space and time directions, respectively.

The spatial stiffness can be computed using the relation [39]

$$\begin{aligned} \rho_s^{(s)} &= \frac{1}{N} \sum_{i,j,\tau,\tau'} J_{i,j,\tau,\tau'} \langle \vec{S}_{i,\tau} \cdot \vec{S}_{j,\tau'} \rangle (i-j)^2 \\ &\quad - \frac{1}{NT} \left\langle \left(\sum_{i,j,\tau,\tau'} J_{i,j,\tau,\tau'} \hat{\mathbf{K}} \cdot (\vec{S}_{i,\tau} \times \vec{S}_{j,\tau'})(i-j) \right)^2 \right\rangle, \end{aligned} \tag{18}$$

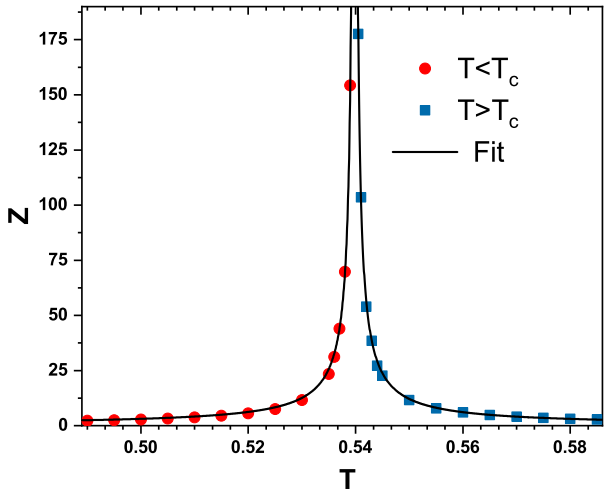

Fig. 5. Dynamical exponent z as a function of classical temperature T in Griffiths regions. The data are extracted from the susceptibility data in Fig. 4. The solid lines are fits of z to Eq. (17).

where

$$J_{i,j,\tau,\tau'} = \begin{cases} J_i^{(s)} & \text{if } j = i \pm 1\,, \quad \tau = \tau' \\ J_i^{(\tau)} & \text{if } i = j \quad , \quad \tau = \tau' \pm 1 \quad , \\ \gamma|\tau - \tau'|^{-\alpha} & \text{if } i = j \quad , \quad \tau \neq \tau', \\ 0 & \text{otherwise} \end{cases}$$

$N = LL_\tau$ is the total number of sites, and $\hat{\mathbf{K}}$ is the unit vector perpendicular to the (i, τ)-plane. For the calculation of $\rho_s^{(\tau)}$, the term $(i - j)$ has to replaced by $(\tau - \tau')$.

The behavior of the spin-wave stiffnesses is illustrated in Fig. 6. It shows the results for the space and time stiffness of a system of size $L = 160$ and $L_\tau = 10000$. Clearly, the two stiffness behave differently. According to Eq. 11, the time stiffness is expected to behave as $|T - T_c|^\beta$. Despite significant finite-size rounding, our data are qualitative compatible with this prediction, giving $T_c \approx 0.54$, in agreement with our earlier estimate of $T_c \approx 0.5398$. In contrast, the space-stiffness $\rho_s^{(s)}$ vanishes at a lower temperature $T \approx 0.503$, giving rise to anomalous elasticity [25] for temperatures between T_c and T^*.

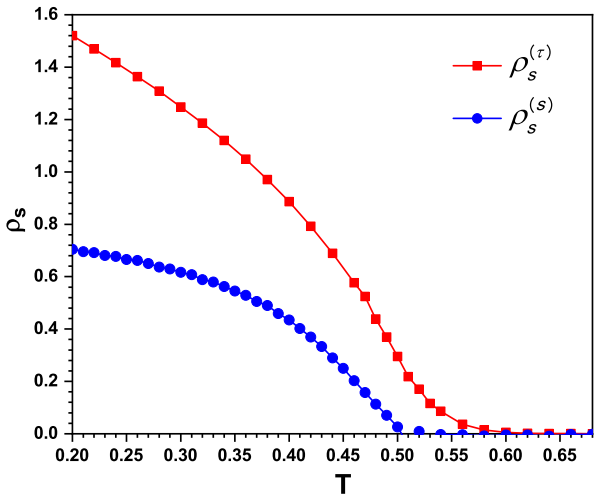

Fig. 6. Spin-wave stiffness in space $\rho_s^{(s)}$ and time $\rho_s^{(\tau)}$ as function of the classical temperature T with system size $L = 160$ and $L_\tau = 10000$. The data for $\rho_s^{(s)}$ are rescaled by 500 for clarity.

In addition, we compute the correlation function G in the space and time directions to determine the correlation length ξ, and then estimate the correlation exponent ν. The correlation functions in space and time directions are defined as

$$G(x) = \frac{1}{N} \sum_{i,j,\tau} \langle \vec{S}_{i,\tau} \cdot \vec{S}_{j,\tau} \rangle \delta(x - |i - j|), \tag{19}$$

$$G(\tau) = \frac{1}{N} \sum_{i,\tau_1,\tau_2} \langle \vec{S}_{i,\tau_1} \cdot \vec{S}_{i,\tau_2} \rangle \delta(\tau - |\tau_1 - \tau_2|). \tag{20}$$

Fig. 7 shows the spatial correlation function (19) for different temperatures in the Griffiths region for system of sizes $L = 80$ and $L_\tau = 1200$.

The strong-disorder renormalization group [22] predicts that the correlation function in space direction x behaves as

$$G(x) \sim \frac{\exp[-(x/\xi) - (27\pi^2/4)^{1/3}(x/\xi)^{1/3}]}{(x/\xi)^{5/6}}. \tag{21}$$

The values of ξ can be extracted by fitting the data of $G(x)$ to Eq. (21) for distances between $x = 3$ and some cutoff at wich the curves start to become noisy. The inset of Fig. 7 shows the relation between the correlation length ξ and the distance from criticality $\delta = |T - T_c|$ which reads [22]

$$\xi \sim |\delta|^{-\nu}. \tag{22}$$

As expected, the data can be fitted to the power law (22), giving a correlation length exponent of $\nu = 1.8(3)$, in reasonable agreement with the renormalization group result $\nu = 2$ [22].

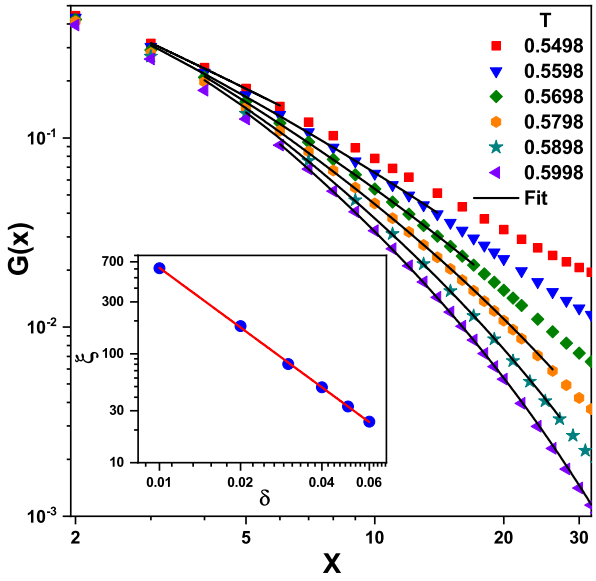

Fig. 7. Space-correlation function $G(x)$ for several temperature in Griffiths phase. The solid lines are fits to Eq. (21). Inset: The space-correlation length ξ obtained by analyzing space-correlation function as a function of distance δ from critical temperature. The solid line is a fit of Eq. (22).

We also analyze the correlation time that we compute from the Fourier transform $\tilde{G}(q)$ of the correlation function:

$$\xi = \left[\frac{\tilde{G}(0) - \tilde{G}(q_{min})}{q_{min}^2 \tilde{G}(q_{min})} \right]^{1/2}. \tag{23}$$

Here, q_{min} is the minimum wave number, $2\pi/L_\tau$ in time direction.

We analyze the behavior of the correlation time ξ_τ in the Griffiths phase by plotting ξ_τ/L_τ as a function of temperature T for several system of size L_τ, as shown in Fig. 8. Clearly, the different curves cross at temperature $T \approx 0.5775$, much higher than our critical temperature $T_c \approx 0.5398$. This indicates that the correlation time ξ_τ diverges in part of the disordered phase. This behavior can be understood by finding the rare region contribution

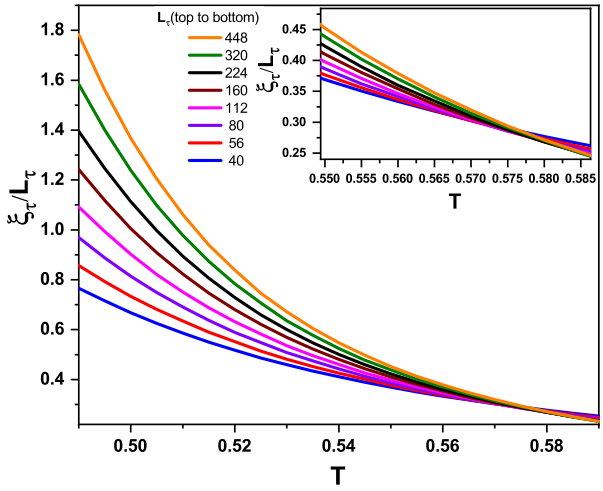

Fig. 8. Scaled correlation time ξ_τ/L_τ versus temperature T for different values of L_τ in the Griffiths region. The system size in space is $L = 1000$; the data are averaged over 2000 disorder configurations. The inset shows a magnification for the crossing point of the curves.

to the correlation time ξ_τ. It can be estimated from [24]

$$\xi_\tau \sim \int_0^{\epsilon_0} d\epsilon\ \epsilon^{1/z-1}\ \frac{1}{\epsilon}, \tag{24}$$

where ϵ is the renormalized distance from criticality of rare region. According to Eq. (24), the integral diverges for $z > 1$ and converges for $z < 1$. Therefore, the correlation time diverges in the disordered Griffiths phase at the temperature at which the Griffiths dynamical exponent is $z = 1$. We estimate this temperature in Fig. 8 to be $T \approx 0.5775$. This value is in a good agreement with our results in Fig. 5.

6. CONCLUSIONS

In summary, we have studied the superconductor to metal quantum phase transition in ultra thin nanowires by performing large-scale Monte Carlo simulations. To this end, we have mapped the quantum action onto a (1+1)-dimensional classical XY Hamiltonian with long-rang interactions.

For clean systems, we have employed finite-size scaling of the Binder cumulant to estimate the critical point and determine the universality class of the phase transition. Our results agree well with earlier Monte-Carlo simulations [36] as well as perturbative renormalization group results [35, 40].

In the presence of quenched disorder, our results provide strong evidence in support of the infinite-randomness behavior that was predicted by the strong-disorder renormalization group approach [15] and the large-N analyses [9]. The critical behavior is in the same universality class as the random transverse-field Ising chain. This may appear surprising at first glance because the random transverse-field Ising model has discrete symmetry and no dissipation while our current problem has continuous XY symmetry and Ohmic dissipation. However, the behavior agrees with the general classification of disordered quantum phase transitions developed in Refs. [41, 42, 43]. In both systems, the rare regions are right at the lower critical dimension of the problem, putting the transitions into class B [43]. Moreover, both clean transitions violate the Harris criterion, implying that the dirty transitions are in subclass $B2$ which features infinite-randomness criticality [43].

Rare regions also lead to unusual properties in the ordered (superconducting) Griffiths phase. Specifically, the superfluid density vanishes in part of the ordered Griffiths phase while the compressibility is already nonzero. In this regime, the system displays anomalous elasticity [25].

Our Monte-Carl simulation can be generalized to compute further observables including the dynamical conductivity in the regime $\omega \gg T$. This remains a task for the future.

ACKNOWLEDGEMENTS

This work was supported by the NSF under Grants No. DMR-1506152 and PHY-1125915. Thomas Vojta is thankful for the hospitality of the Kavli Institute for Theoretical Physics, Santa Barbara, where part of the work was performed.

REFERENCES

[1] W. W. Webb and R. J. Warburton. Intrinsic quantum fluctuations in uniform filamentary superconductors. *Phys. Rev. Lett.*, 20:461–465, Feb 1968.

[2] C. N. Lau, N. Markovic, M. Bockrath, A. Bezryadin, and M. Tinkham. Quantum phase slips in superconducting nanowires. *Phys. Rev. Lett.*, 87:217003, Nov 2001.

[3] G. R. Boogaard, A. H. Verbruggen, W. Belzig, and T. M. Klapwijk. Resistance of superconducting nanowires connected to normal-metal leads. *Phys. Rev. B*, 69:220503, Jun 2004.

[4] A. Rogachev, A. T. Bollinger, and A. Bezryadin. Influence of high magnetic fields on the superconducting transition of one-dimensional nb and moge nanowires. *Phys. Rev. Lett.*, 94:017004, Jan 2005.

[5] Fabio Altomare, A. M. Chang, Michael R. Melloch, Yuguang Hong, and Charles W. Tu. Evidence for macroscopic quantum tunneling of phase slips in long one-dimensional superconducting al wires. *Phys. Rev. Lett.*, 97:017001, Jul 2006.

[6] A. Rogachev, T.-C. Wei, D. Pekker, A. T. Bollinger, P. M. Goldbart, and A. Bezryadin. Magnetic-field enhancement of superconductivity in ultranarrow wires. *Phys. Rev. Lett.*, 97:137001, Sep 2006.

[7] Subir Sachdev, Philipp Werner, and Matthias Troyer. Universal conductance of nanowires near the superconductor-metal quantum transition. *Phys. Rev. Lett.*, 92:237003, Jun 2004.

[8] Adrian Del Maestro, Bernd Rosenow, Nayana Shah, and Subir Sachdev. Universal thermal and electrical transport near the superconductor-metal quantum phase transition in nanowires. *Phys. Rev. B*, 77:180501, May 2008.

[9] Adrian Del Maestro, Bernd Rosenow, Markus Müller, and Subir Sachdev. Infinite randomness fixed point of the superconductor-metal quantum phase transition. *Phys. Rev. Lett.*, 101:035701, Jul 2008.

[10] Igor F. Herbut. Zero-temperature *d*-wave superconducting phase transition. *Phys. Rev. Lett.*, 85:1532–1535, Aug 2000.

[11] A. V. Lopatin, N. Shah, and V. M. Vinokur. Fluctuation conductivity of thin films and nanowires near a parallel-field-tuned superconducting quantum phase transition. *Phys. Rev. Lett.*, 94:037003, Jan 2005.

[12] B. Spivak, A. Zyuzin, and M. Hruska. Quantum superconductor-metal transition. *Phys. Rev. B*, 64:132502, Aug 2001.

[13] M. V. Feigel'man, A. I. Larkin, and M. A. Skvortsov. Quantum superconductor-metal transition in a proximity array. *Phys. Rev. Lett.*, 86:1869–1872, Feb 2001.

[14] Victor Galitski. Nonperturbative microscopic theory of superconducting fluctuations near a quantum critical point. *Phys. Rev. Lett.*, 100:127001, Mar 2008.

[15] J. A. Hoyos, C. Kotabage, and T. Vojta. Effects of dissipation on a quantum critical point with disorder. *Phys. Rev. Lett.*, 99:230601, 2007; T. Vojta, C. Kotabage, and J. A. Hoyos. Infinite-randomness quantum critical points induced by dissipation. *Phys. Rev. B*, 79:024401, 2009.

[16] J. Hertz. Quantum critical phenomena. *Phys. Rev. B*, 14:1165, 1976.

[17] A. J. Millis. Effect of a nonzero temperature on quantum critical points in itinerant fermion systems. *Phys. Rev. B*, 48:7183, 1993.

[18] T. R. Kirkpatrick and D. Belitz. Long-range order versus random-singlet phases in quantum antiferromagnetic systems with quenched disorder. *Phys. Rev. Lett.*, 76:2571, 1996.

[19] D. Belitz, T. R. Kirkpatrick, and T. Vojta. How generic scale invariance influences quantum and classical phase transitions. *Rev. Mod. Phys.*, 77:579, 2005.

[20] Adrian Del Maestro, Bernd Rosenow, José A. Hoyos, and Thomas Vojta. Dynamical conductivity at the dirty superconductor-metal quantum phase transition. *Phys. Rev. Lett.*, 105:145702, Oct 2010.

[21] D. S. Fisher. Random transverse field Ising spin chains. *Phys. Rev. Lett.*, 69:534, 1992.

[22] D. S. Fisher. Critical behavior of random transverse-field Ising spin chains. *Phys. Rev. B*, 51:6411, 1995.

[23] P. Mohan, R. Narayanan, and T. Vojta. Infinite randomness and quantum Griffiths effects in a classical system: the randomly layered Heisenberg magnet. *Phys. Rev. B*, 81:144407, 2010.

[24] Fawaz Hrahsheh, Hatem Barghathi, and Thomas Vojta. Infinite-randomness criticality in a randomly layered heisenberg magnet. *Phys. Rev. B*, 84:184202, Nov 2011.

[25] Priyanka Mohan, Paul M. Goldbart, Rajesh Narayanan, John Toner, and Thomas Vojta. Anomalously elastic intermediate phase in randomly layered superfluids, superconductors, and planar magnets. *Phys. Rev. Lett.*, 105:085301, Aug 2010.

[26] E. Luijten and H. W. J. Blöte. Monte-Carlo method for spin models with long-range interactions. *Int. J. Mod. Phys. C*, 6:359, 1995.

[27] M. N. Barber. Finite-size scaling. In C. Domb and J. L. Lebowitz, editors, *Phase Transitions and Critical Phenomena*, volume 8, pages 145–266. Academic, New York, 1983.

[28] J. Cardy, editor. *Finite-size scaling*. North Holland, Amsterdam, 1988.

[29] K. Binder. Critical properties from monte carlo coarse graining and renormalization. *Phys. Rev. Lett.*, 47:693–696, Aug 1981.

[30] K. Binder and D. P. Landau. Finite-size scaling at first-order phase transitions. *Phys. Rev. B*, 30:1477–1485, Aug 1984.

[31] M. Guo, R. N. Bhatt, and D. A. Huse. Quantum critical behavior of a three-dimensional Ising spin glass in a transverse magnetic field. *Phys. Rev. Lett.*, 72:4137, 1994.

[32] H. Rieger and A. P. Young. Zero-temperature quantum phase transition of a two-dimensional Ising spin glass. *Phys. Rev. Lett.*, 72:4141, 1994.

[33] R. Sknepnek, T. Vojta, and M. Vojta. Exotic vs. conventional scaling and universality in a disordered bilayer quantum Heisenberg antiferromagnet. *Phys. Rev. Lett.*, 93:097201, 2004.

[34] Thomas Vojta, Jack Crewse, Martin Puschmann, Daniel Arovas, and Yury Kiselev. Quantum critical behavior of the superfluid-mott glass transition. *Phys. Rev. B*, 94:134501, Oct 2016.

[35] S. Pankov, S. Florens, A. Georges, G. Kotliar, and S. Sachdev. Non-Fermi-liquid behavior from two-dimensional antiferromagnetic fluctuations: A renormalization-group and large-n analysis. *Phys. Rev. B*, 69:054426, 2004.

[36] Philipp Werner, Matthias Troyer, and Subir Sachdev. Quantum spin chains with site dissipation. *Journal of the Physical Society of Japan*, 74(Suppl):67–70, 2005.

[37] Mucio A. Continentino, Gloria M. Japiassu, and Amós Troper. Critical approach to the coherence transition in kondo lattices. *Phys. Rev. B*, 39:9734–9737, May 1989.

[38] A. B. Harris. Effect of random defects on the critical behaviour of Ising models. *J. Phys. C*, 7:1671, 1974.

[39] S. Teitel and C. Jayaprakash. Phase transtions in frustrated two-dimensional XY models. *Phys. Rev. B*, 27:598–601, Jan 1983.

[40] S. Sachdev, P. Werner, and M. Troyer. Universal conductance of nanowires near the superconductor-metal quantum transition. *Phys. Rev. Lett.*, 92:237003, 2004.

[41] T. Vojta and J. Schmalian. Quantum Griffiths effects in itinerant Heisenberg magnets. *Phys. Rev. B*, 72:045438, 2005.

[42] T. Vojta. Rare region effects at classical, quantum, and non-equilibrium phase transitions. *J. Phys. A*, 39:R143, 2006.

[43] Thomas Vojta and José A. Hoyos. Criticality and quenched disorder: Harris criterion versus rare regions. *Phys. Rev. Lett.*, 112:075702, Feb 2014.

SECTION

2. CONCLUSIONS AND OUTLOOK

This dissertation is an attempt to understand and interpret the effects of randomness on the behavior of several kinds of phase transitions (thermal, quantum and nonequilibrium) by employing large-scale Monte-Carlo simulations.

The first section introduced general and basic concepts of thermal, quantum and nonequilibrium phase transitions as well as critical behavior including order parameters, the scaling hypothesis, and finite-size scaling. Moreover, we explained the stability of phase transitions against disorder based on the Imry-Ma and Harris criteria. In addition, we also introduced the strong-disorder renormalization group which is an important technique to investigate disordered phase transitions. Finally, we gave an explanation of rare-region and Griffiths effects on phase transitions and criticality.

The rest of this dissertation consisted of reprints of three published refereed papers and one manuscript. In Paper I, we studied the effects of long-range correlated spatial disorder on the nonequilibrium phase transition in the contact process. These long-range correlations increase the probability for finding rare active regions which leads to enhanced Griffiths singularities with non-power-law Griffiths behavior. Our theory is also applicable to classical and quantum equilibrium systems such as the quantum phase transition in random transverse-field Ising model.

In Paper II, the two-dimensional four-color Ashkin-Teller model was investigated by Monte Carlo simulations to analyze the effects of quenched disorder on its first-order phase transitions. The randomness destroys the first-order phase transition and turns it into a continuous one. We found that the emerging critical behavior of the disordered Ashkin-

Teller model is compatible with the critical behavior in the clean two-dimensional Ising universality class with universal logarithmic corrections. This concurs with perturbative renormalization-group predictions.

Paper III studied the influence of quenched disorder on the quantum phase transitions in the two-dimensional three-color quantum Ashkin-Teller model by Monte Carlo simulations. We have found that in the weak-coupling regime the quenched disorder rounds the first-order quantum phase transition to a second-order one which features infinite-randomness critical behavior. This agrees with the predictions of a strong-disorder renormalization group analysis. However, in the strong-coupling regime there are two distinct quantum phase transitions separating the paramagnetic, product and Baxter (ferromagnetic) phases.

In Paper IV, we investigated the superconductor to metal quantum phase transition in ultra-thin metallic nanowires by employing large-scale Monte Carlo simulations. We studied the critical behavior of pure and disordered systems. The results of the disordered case provide strong evidence in support of infinite-randomness critical behavior and agree with strong-disorder renormalization group predictions.

In summary, we have explained how quenched disorder can change and modify phase transitions and the critical behavior in different systems (classical and quantum equilibrium as well as nonequilibrium). This gave us an opportunity to understand more deeply the interplay between such impurities (randomness) and phase transitions. Most of this work focuses on the thermodynamic behavior. However, our methods can also be applied to study real-time dynamics and transport properties. This remains a task for the future.

REFERENCES

[1] N. Goldenfeld. *Lectures on phase transitions and the renormalization group*. Addison-Wesley, Reading, 1992.

[2] L. D. Landau. *Phys. Z. Sowjetunion*, 11:26, 1937.

[3] L. D. Landau. *Zh. Eksp. Teor. Fiz.*, 7:19, 1937.

[4] L. D. Landau. *Phys. Z. Sowjetunion*, 11:545, 1937.

[5] L. D. Landau. *Zh. Eksp. Teor. Fiz.*, 7:627, 1937.

[6] J. D. van der Waals. *On the continuity of the gas and liquid state*. PhD thesis, University of Leiden, 1873.

[7] P. Weiss. *J. Phys. Theor. Appl. (Paris)*, 6:661, 1907.

[8] L. P. Kadanoff et. Static phenomena near critical points: Theory and experiment. *Rev. Mod. Phys.*, 39:395–431, Apr 1967.

[9] B. Widom. Surface tension and molecular correlations near the critical point. *J. Chem. Phys.*, 43:3892, 1965.

[10] Michael E. Fisher. Rigorous inequalities for critical-point correlation exponents. *Phys. Rev.*, 180:594–600, Apr 1969.

[11] B D Josephson. Inequality for the specific heat: I. derivation. *Proceedings of the Physical Society*, 92(2):269, 1967.

[12] G. S. Rushbrooke. On the thermodynamics of the critical region for the ising problem. *The Journal of Chemical Physics*, 39(3):842–843, 1963.

[13] Kenneth G. Wilson. Renormalization group and critical phenomena. i. renormalization group and the kadanoff scaling picture. *Phys. Rev. B*, 4:3174–3183, Nov 1971.

[14] Kenneth G. Wilson. Renormalization group and critical phenomena. ii. phase-space cell analysis of critical behavior. *Phys. Rev. B*, 4:3184–3205, Nov 1971.

[15] J. Hertz. Quantum critical phenomena. *Phys. Rev. B*, 14:1165, 1976.

[16] S. Sachdev. *Quantum phase transitions*. Cambridge University Press, Cambridge, 1999.

[17] H. F. Trotter. On the product of semi-groups of operators. *Proc. American Math. Soc.*, 10:545, 1959.

[18] R. P. Feynman and A. R. Hibbs. *Quantum Mechanics and Path Integrals*. McGraw-Hill, New York, 1965.

[19] Lars Onsager. Crystal statistics. i. a two-dimensional model with an order-disorder transition. *Phys. Rev.*, 65:117–149, Feb 1944.

[20] T. Vojta. Rare region effects at classical, quantum, and non-equilibrium phase transitions. *J. Phys. A*, 39:R143, 2006.

[21] G. Odor. Universality classes in nonequilibrium lattice systems. *Rev. Mod. Phys.*, 76:663, 2004.

[22] H. Hinrichsen. Nonequilibrium critical phenomena and phase transitions into absorbing states. *Adv. Phys.*, 49:815, 2000.

[23] T. E. Harris. Contact interactions on a lattice. *Ann. Prob.*, 2:969, 1974.

[24] A. A. Markov. *Theory of Algoriths*. Academy of Sciences of the USSR, 1954.

[25] H. K. Janssen. *Z. Phys. B*, 42:151, 1981.

[26] P. Grassberger. *Z. Phys. B*, 47:365, 1982.

[27] M. E. Fisher and M. N. Barber. Scaling theory for finite-size effects in the critical region. *Phys. Rev. Lett*, 28:1516, 1972.

[28] M. N. Barber. Finite-size scaling. In C. Domb and J. L. Lebowitz, editors, *Phase Transitions and Critical Phenomena*, volume 8, pages 145–266. Academic, New York, 1983.

[29] J. Cardy, editor. *Finite-size scaling*. North Holland, Amsterdam, 1988.

[30] J. Cardy. *Scaling and renormalization in statistical physics*. Cambridge University Press, Cambridge, 1996.

[31] G. Grinstein. Phases and phase transitions of quneched disordered systems. In E. G. D. Cohen, editor, *Fundamental Problems in Statistical Mechanics VI*, page 147. Elsevier, New York, 1985.

[32] Curtis A. Doty and Daniel S. Fisher. Effects of quenched disorder on spin-1/2 quantum *XXZ* chains. *Phys. Rev. B*, 45:2167–2179, Feb 1992.

[33] T. Vojta. Phases and phase transitions in disordered quantum systems. In A. Avella and F. Mancini, editors, *Lectures On The Physics Of Strongly Correlated Systems XVII*, pages 188–247. AIP Publishing, Melville, 2013.

[34] Yoseph Imry and Shang-keng Ma. Random-field instability of the ordered state of continuous symmetry. *Phys. Rev. Lett.*, 35:1399–1401, Nov 1975.

[35] Yoseph Imry and Michael Wortis. Influence of quenched impurities on first-order phase transitions. *Phys. Rev. B*, 19:3580–3585, Apr 1979.

[36] Michael Aizenman and Jan Wehr. Rounding of first-order phase transitions in systems with quenched disorder. *Phys. Rev. Lett.*, 62:2503–2506, May 1989.

[37] A. B. Harris. Effect of random defects on the critical behaviour of Ising models. *J. Phys. C*, 7:1671, 1974.

[38] S. K. Ma, C. Dasgupta, and C. K. Hu. Random antiferomagnetic chain. *Phys. Rev. Lett.*, 43:1434, 1979.

[39] C. Dasgupta and S.-K. Ma. Low-temperature properties of the random Heisenberg antiferromagnetic chain. *Phys. Rev. B*, 22:1305, 1980.

[40] F. Igloi and C. Monthus. Strong disorder renormalization group approach of random systems. *Phys. Rep.*, 412:277, 2005.

[41] D. S. Fisher. Random transverse field Ising spin chains. *Phys. Rev. Lett.*, 69:534, 1992.

[42] D. S. Fisher. Critical behavior of random transverse-field Ising spin chains. *Phys. Rev. B*, 51:6411, 1995.

[43] P. Pfeuty. An exact result for the 1d random Ising model in a transverse field. *Phys. Lett. A*, 72:245, 1979.

[44] R. B. Griffiths. Nonanalytic behavior above the critical point in a random Ising ferromagnet. *Phys. Rev. Lett.*, 23:17, 1969.

[45] M. Randeria, J. P. Sethna, and R. G. Palmer. Low-frequency relaxation in Ising spin-glasses. *Phys. Rev. Lett.*, 54:1321, 1985.

[46] T. Vojta and J. Schmalian. Quantum Griffiths effects in itinerant Heisenberg magnets. *Phys. Rev. B*, 72:045438, 2005.

[47] T. Vojta. Quantum Griffiths effects and smeared phase transitions in metals: theory and experiment. *J. Low Temp. Phys.*, 161:299, 2010.

[48] M. Wortis. Griffiths singularities in the randomly dilute one-dimensional Ising model. *Phys. Rev. B*, 10:4665, 1974.

[49] A. B. Harris. Nature of the Griffiths singularity in dilute magnets. *Phys. Rev. B*, 12:203, 1975.

[50] Y. Imry. Griffiths singularity in finite macroscopically large dilute Ising models. *Phys. Rev. B*, 15:4448, 1977.

VITA

Ahmed Khalil Ibrahim was born on November 22, 1977 in Ramadi, Anbar, Iraq. He received his B.S. in Physics from the college of science at the University of Anbar, Anbar, Iraq in 2002. After two years of working as a research assistant in the college of medicine at the University of Anbar, he joined to the college of science at the University of Anbar as a graduate student in the physics department. In March 2009, he received his M.S. in Physics from the college of science at the University of Anbar, Iraq .

In 2013, he joined the group of Dr. Thomas Vojta at the Missouri University of Science and Technology in Rolla, Missouri, USA. In 2014, he became a member of the American Physical Society (APS). In May 2017, he received his 2^{nd} M.S. in Physics and in May 2018, he received his Ph.D. in Physics from the Missouri University of Science and Technology, Rolla, Missouri, USA.